

# Functional Model of the Middle Ear

A Major Qualifying Project



Submitted to the Faculty of Worcester Polytechnic Institute  
In partial fulfillment of the requirements for the  
Degree in Bachelor of Science  
In Mechanical Engineering/Biomedical Engineering

By:

Thomas Ciolfi  
Ryan Hawkins  
Tara Haymon  
Gabrielle Rosales

Advisors:

Professor Sarah Wodin-Schwartz  
Professor Zoe Reidinger

Submitted on: October 13, 2022

*This report represents the work of WPI undergraduate students submitted to the faculty as evidence of a degree requirement. WPI routinely publishes these reports on its website without editorial or peer review. For more information about the projects program at WPI, see <http://www.wpi.edu/Academics/Projects>.*

# Table of Contents

<b>List of Figures</b>	<b>4</b>
<b>List of Tables</b>	<b>6</b>
<b>Acknowledgements</b>	<b>7</b>
<b>Abstract</b>	<b>8</b>
<b>1.0 Introduction</b>	<b>9</b>
<b>2.0 Background</b>	<b>10</b>
2.1 The Human Ear	10
2.2 The Middle Ear	11
2.2.4 Problems of the Middle Ear	12
2.2.4.1 Ossicular Fixation	12
2.2.4.2 Otosclerosis	13
2.3 Functionality of the Middle Ear with Sound Mechanics	13
2.3.1 Sound as a Wave	13
2.4 Current Research and Modeling of the Middle Ear in Academia	14
2.4.1 Trends of the Middle Ear	14
2.4.2 Middle Ear Modeling Techniques and Challenges	16
2.4.3 Medical Application of Silicone	16
2.5 Previous Projects	17
2.5.1 Design and Simulation of a Middle Ear Model to Aid with Otological Studies (2020)	18
2.5.2 Middle Ear Replication for Otological Studies (March 2022)	18
<b>3.0 Project Strategy</b>	<b>21</b>
3.1 Client Statement	21
3.2 Project Goal & Objectives	21
3.3 Design Requirements	22
3.3.1 Objective 1 Design Requirements	22
3.3.2 Objective 2 Design Requirements	22
3.3.2 Objective 3 Design Requirements	22
3.3.4 Objective 4 Design Requirements	22
3.4 Design Constraints	23
3.5 Project Management	23
<b>4.0 Design Process</b>	<b>24</b>
4.1 Model Support Structure	24

4.1.1 Model Base Structure	24
4.1.2 Ligament Attachment Points	28
4.2 Ossicle Connection Material Selection	29
4.2.1 Ossicle Connection Decision Matrices	29
4.3 Ligament Material Selection	31
4.3.1 Ligament Decision Matrices	31
4.4 Incudomalleolar Joint Design	34
4.4.1 IMJ Decision Matrices	35
4.4.1.1 Materials Requiring Molds	36
4.4.2 IMJ Mold Decision Matrices	38
4.5 Incudostapedial Joint Design	41
4.6 IMJ CAD Design	47
4.6.1 IMJ Software Exploration	48
4.6.2 Molding Original IMJ Geometry	48
4.6.3 IMJ Model Simplification	50
4.6.4 Molding of Simplified IMJ	52
<b>5.0 Final Design Verification</b>	<b>54</b>
5.1 Mold Creation	54
5.1.1 Mold Testing	54
5.1.2 Final 3D Printed Mold Designs	57
5.2 Silicone Stiffness Procedure	58
5.3 Vibration Testing	58
5.3.1 Calibration of Accelerometers	59
5.3.2 Test Procedure	59
5.3.3 Results	63
5.4 System Stiffness Testing	65
5.4.1 Calibration of Cameras	65
5.4.2 Test Procedure	65
5.4.3 Results	71
5.4.3.1 IMJ Stiffness Results	71
5.4.3.2 Ligament Stiffness Results	72
<b>6.0 Final Design Validation</b>	<b>74</b>
6.1 Digital Modeling and Design	74
6.2 Physical Modeling and Testing	76
<b>7.0 Discussion</b>	<b>78</b>
7.1 Support Structure Accomplishments and Limitations	78
7.2 Varying Stiffnesses of IMJ Accomplishments and Limitations	78

7.3 Stiffness Testing Accomplishments and Limitations	78
7.4 Ligament and Muscle Material Accomplishments and Limitations	78
7.5 Digital Model Accomplishments and Limitations	79
<b>8.0 Conclusions and Recommendations</b>	<b>80</b>
8.1 Future Recommendations	80
8.1.1 Instructional Page	80
8.1.2 Functional model capable of showing trends	80
8.1.3 3-Axis Accelerometer Data	80
8.1.4 Ligament Stiffness	81
8.2 Broader Impacts	81
8.2.1 Environmental Impacts	81
8.2.2 Societal Influence	81
8.2.3 Ethical Concerns	81
8.2.4 Health and Safety Issues	81
8.2.5 Manufacturability	82
8.2.6 Sustainability	82
<b>References</b>	<b>83</b>
<b>Appendix A – Weeks 1-3 of Team Gantt Chart</b>	<b>90</b>
<b>Appendix B – Calibration of Accelerometers</b>	<b>91</b>
<b>Appendix C – Justification of Accelerometer Calibration Methods</b>	<b>97</b>
<b>Appendix D - Graph of Accelerometer Correction Factors</b>	<b>99</b>
<b>Appendix E - Matlab Code for Data Acquisition and Analysis</b>	<b>101</b>
<b>Appendix F - Calibration of Camera System</b>	<b>107</b>



## List of Figures

2.1	Anterior View of the Anatomy of the Human Ear ( <i>How Do We Hear?</i> , 2022).	10
2.2	Sectioned View of the Middle Ear (Gassler, 2019).	12
2.3	Positive Pressure Effect on Flexible IMJ (Warnholtz et al., 2021).	14
2.4	Positive Pressure Effect on Fixed IMJ (Warnholtz et al., 2021).	15
2.5	Middle Ear Stiffness with Drying (Dobrev et al., 2018).	15
2.6	PDMS, a Commonly Used Silicone ( <i>Properties of Silicones</i> , n.d.).	17
2.7	2020 WPI MQP Team's Model (Tanner et al., 2021).	18
2.8	March 2022 WPI MQP Team's Static Model (Scrivanich et al., 2022).	19
2.9	March 2022 WPI MQP Team's Dynamic Model (Scrivanich et al., 2022).	20
4.1	Structural Support Setup including ThorLabs Pieces.	27
4.2	March 2022 Group's Modeling of the Incus Stapes Connection.	41
4.3	ISJ Design Option A.	42
4.4	ISJ Design Option B.	43
4.5	ISJ Design Option C.	44
4.6	ISJ Molded Design Option C.	45
4.7	ISJ Mold Exterior.	45
4.8	Sliced ISJ Example (Three Slices Eight Pieces).	46
4.9	Sliced ISJ Mold Exterior.	47
4.10	Sliced ISJ Mold Interior.	47
4.11	Original IMJ Design.	47
4.12	Cutting of IMJ out of Half Cube Mold (Blender).	48
4.13	IMJ Cut out of Half Cube Mold (Blender).	49
4.14	IMJ Cut out of Eighth Cube Mold (Blender).	49
4.15	Simplified IMJ with Incus and Malleus.	50
4.16	IMJ Simplification Process in Geomagic.	51
4.17	Simplified IMJ Design vs. Original IMJ Design.	51
4.18	First Molding Attempt with Simplified IMJ.	52
4.19	Final IMJ Mold Design.	53
5.1	Final 3D Printed ISJ Mold Exterior and Interior	57
5.2	Final 3D Printed IMJ Mold.	57
5.3	Wiring Diagram of Accelerometer Test Setup.	59
5.4	Mechanical Actuation of the Model.	60
5.5	Accelerometer Placement on Oval Window.	61
5.6	APX Settings for Calibration of Accelerometer.	61
5.7	APX Settling Settings for Calibration of Accelerometer.	62
5.8	Sweeps of each IMJ.	64
5.9	IMJ 1 Load Application Results.	64
5.10	IMJ 5 Load Application Results.	65

5.11	Stiffness Testing Setup. . . . .	.66
5.12	Top Camera View of Magnets at Oval Window. . . . .	.67
5.13	Top Camera View with Ruler. . . . .	.67
5.14	Using the Set Scale Tool in ImageJ. . . . .	.68
5.15	Line Measurement From One Microbead to End of Frame. . . . .	.69
5.16	Angle (degrees) and Length (mm) of Line. . . . .	.69
5.17	Force Displacement Graph of Middle Ear Model with No IMJ Inserted. . . . .	.70
5.18	Average Stiffness of Model with No IMJ Inserted. . . . .	.71
5.19a	Average Model Stiffness for IMJ. . . . .	.71
5.19b	Average Stiffness for IMJ 5. . . . .	.71
5.20	Average Model Stiffness per IMJ. . . . .	.72
5.21a	Model Stiffness with 2mm Elastic Bands as Ligaments. . . . .	.73
5.21b	Model Stiffness with 1mm Elastic Bands as Ligaments. . . . .	.73
6.1	Adjustability of Eye Hooks on ThorLabs Pieces. . . . .	.74
6.2	Before and After Oval Window 3D Printed Design. . . . .	.75
6.3	Final Molded ISJ. . . . .	.75
6.4	Final Molded IMJ. . . . .	.76
6.5	Material Used to Replicate Ligament in the Model. . . . .	.77
6.6	The Completed Mode. . . . .	.77
7.1	Final Solidworks Model Excluding Ligament Connections . . . . .	.79

## List of Tables

2.1	Elastic Modulus of PDMS with Different Amount of Crosslinking(Wang et al., 2014).	17
4.1	Pairwise Comparison Chart for Structural Support Design Objectives.	24
4.2	Structural Support Objectives Ranking.	25
4.3	Structural Support Options and Descriptions.	26
4.4	Pugh decision matrix for Structural Support Choices.	27
4.5	Ligament Attachment Point Possibilities.	28
4.6	Pugh Decision Matrix for Ligament Attachment Point Options.	29
4.7	Pairwise Comparison Chart for Material Objectives.	29
4.8	Material Objectives Ranking.	30
4.9	Potential Ossicle Connection Materials and Information.	30
4.10	Pugh Decision Matrix for Ossicle Connection Materials.	31
4.11	Pairwise Comparison Chart for Material Objectives.	31
4.12	Material Objectives Ranking.	32
4.13	Potential Ligament Materials and Information.	33
4.14	Pugh Decision Matrix for Ligament Materials	34
4.15	Pairwise Comparison Chart for IMJ Design Objectives.	35
4.16	IMJ Objectives Ranking.	36
4.17	Potential IMJ Materials and Information.	37
4.18	Pugh Decision Matrix for Molded IMJ Materials.	38
4.19	Pairwise Comparison Chart for Mold Design Objectives.	38
4.20	Mold Objectives Ranking.	39
4.21	Potential Mold Materials and Information.	40
4.22	Pugh Decision Matrix for Mold Materials.	41
4.23	Pros and Cons of ISJ Design Option A.	42
4.24	Pros and Cons of ISJ Design Option B.	43
4.25	Pros and Cons of ISJ Design Option C.	44
5.1	Testing of Different Material Molding Options	55
5.2	Qualitative Data and Observations on Different Material Molds.	56
5.3	Amounts of Elastomer Base and Crosslinker Used to Create 5 IMJs	58
5.4	Initial Data Collection.	69
5.5	Displacement Data in Millimeters.	70
5.6	Displacement Data in Meters.	70

## Acknowledgements

Thank you to project sponsor, Dr. Ivo Dobrev, and project advisors Professor Sarah Wodin-Schwartz and Professor Zoe Reidinger for giving their time, knowledge, and guidance over the course of the project.

Additionally, thank you to the Universitätsspital Zürich Department of Otorhinolaryngology for hosting and supporting the project.

# Abstract

This project sought to improve a functioning model of the middle ear, in conjunction with Dr. Ivo Dobrev and the Universitätsspital Zürich Department of Otorhinolaryngology. This model is intended to educate students about middle ear anatomy, physiology, and pathology. After improving the durability and adaptability of the model, the project team performed force-displacement and vibration testing to show the model's capability of demonstrating how stiffening of the incudomalleolar joint affects sound transmission in the system. The model displayed meaningful trends when a load was applied, but it did not match the trends of the actual middle ear. The project team created a 3D assembly of the model in Solidworks, to allow future teams to perform virtual analysis on the design.

# 1.0 Introduction

The ear is a complex organ responsible for our ability to hear. Its main function is to gather sound waves from the surrounding environment and convert them into signals that can be interpreted by the brain. Research into the anatomy, physiology, and pathology of the ear is ongoing, with much that is still unknown.

The Department of Otorhinolaryngology (ORL) at the Universitätsspital Zürich, a research hospital in Zürich, Switzerland, specializes in research of the anatomy and physiology of the middle ear and treatments, such as cochlear implants, for diseases of the middle ear. The ORL has an established academic partnership with Worcester Polytechnic Institute (WPI) through a WPI alumnus, Dr. Ivo Dobrev, who is currently working on postdoctoral research there. Through Dr. Dobrev, WPI has conducted two previous Major Qualifying Projects (MQP) with the goal of developing a dynamic functional model of the middle ear to be used in educational settings. Currently, a physical model that combines accurate anatomy and functionality does not exist, so the development of such a model would greatly benefit the teaching of both undergraduate and graduate students at the university. The model would allow instructors, such as Dr. Dobrev, to demonstrate how the middle ear looks and works and allow students to manipulate the model and have hands-on experience in the classroom.

At the completion of the previous team's MQP, the model had reached a point where many of the components were justified and finalized. This included the material choices that were made as well as the geometry and size of each component in order to create an anatomically accurate ratio to that of middle ear. The team was also able to collect preliminary data in relation to the functionality of the middle ear in . However, due to time constraints, there was much research and testing that still needed to be done to complete the design and model trends seen in the middle ear.

The goal of this project was to further improve and develop the model to demonstrate a desired trend of sound transmission through the middle ear. The trend that the team chose to focus on was how stiffening of the middle ear, which is a common pathological issue, affects sound transmission. This was done by analyzing how changing the stiffness of the IMJ in the model affected the system as a whole. In addition to modeling this trend, the team worked to update and improve the functionality of the model through the selection and justification of new materials and design changes.

## 2.0 Background

This section provides information on the scope of this project and background information necessary for understanding the remainder of this report.

### 2.1 The Human Ear

The human ear is the organ responsible for hearing. The ear is commonly divided into the outer, middle, and inner sections. The distinctions are displayed in Figure 2.1. All three sections play a role in processing sound. When sound waves and vibrations occur outside of the ear, they travel through the external auditory canal and cause the tympanic membrane, commonly referred to as the eardrum, to vibrate. These vibrations then pass into the middle ear and through three small auditory bones known as ossicles. These ossicles are the malleus, incus and stapes. The ossicles amplify the sound waves and send them to the cochlea, a fluid filled hearing organ, in the inner ear. The hair cells within the cochlear fluid convert the sound waves into electrochemical signals. The auditory nerve then sends these electrical impulses to the brain and translates them as sound. (*How Do We Hear?*, 2022)

The human ear is capable of detecting frequencies from 20Hz to 20kHz and sounds starting at 0 decibels. Decibels (dB) are the unit at which sound is measured. The sound of breathing is approximately 10 dB while a motorcycle is approximately 95 dB. Prolonged exposure to sounds over 70 dB can result in damage to the ear and hearing loss. Sounds that are above 120 dB can result in immediate damage to the ears. (*What Noises Cause Hearing Loss?*, 2019)

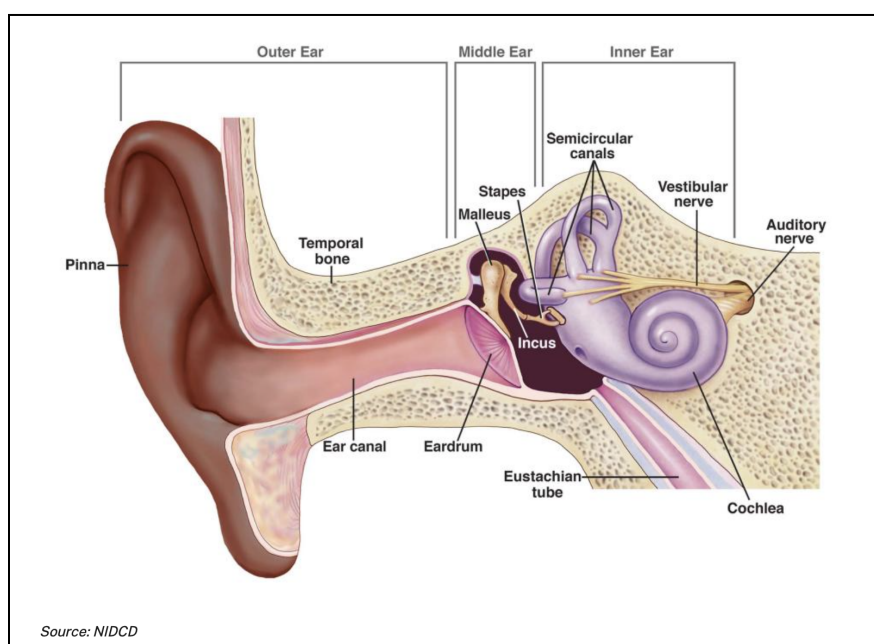


Figure 2.1: Anterior View of the Anatomy of the Human Ear (*How Do We Hear?*, 2022)

## 2.2 The Middle Ear

The anatomy of the middle ear is complex and its function is not fully explored. Figure 2.2 shows the middle ear consisting of the tympanic membrane, the ossicular chain, and the oval window. The primary function of the middle ear is to transmit sound from the outer ear to the inner ear. It also protects the cochlea by filtering dangerously loud vibrations traveling through the outer ear (I. Dobrev, personal communication, August 31, 2022; Gil-Loyzaga, 2016).

The first component of the middle ear is the tympanic membrane. The tympanic membrane consists of the pars tensa and the tympanic annulus. The pars tensa is a multilayered, fibrous membrane which is stiff, yet has a low mass (I. Dobrev, personal communication, August 31, 2022; Rensink, 2011). Within the center of the pars tensa lies the umbo, which is connected to the first part of the ossicular chain and is responsible for the transfer of vibrations. The tympanic annulus is the support structure of the membrane in the form of a ring of cartilage which connects the tympanic membrane to the temporal bone. When the tympanic membrane is struck with sound waves the pars tensa mechanically vibrates and the umbo transfers these vibrations to the ossicular chain. (Dancer & Rebillard, 2018; I. Dobrev, personal communication, August 31, 2022)

The ossicular chain stretches from the tympanic membrane to the oval window and is composed of 3 primary auditory bone structures: the incus, the malleus and the stapes. The ossicular chain includes both bone and flexible connective tissues in order to keep the mechanical system both connected and fluid in sound-induced motion (Puria et al., 2013a). The ossicular chain is supported by ligaments, attaching the ossicles to the surrounding tissue (Dancer & Rebillard, 2018).

The malleus is the first auditory bone of the ossicular chain to vibrate from an external stimulus. It is connected to the second bone structure, the incus, through the incudomalleolar joint (IMJ) which is composed of connective tissue. The incus then connects to the stapes through the incudostapedial joint (ISJ). While these joints are not labeled in Figure 2.2, they are located at the interface between the bones referenced in their names. The ossicles are supported by a series of ligaments, attaching to a variety of locations on surrounding tissue (I. Dobrev, personal communication, August 31, 2022). After the vibrations flow through this chain, they reach the tympanostapedial syndesmosis, which is a cartilage based connection that connects the stapes footplate to the oval window. This connection allows for the membrane to vibrate at the oval window and transmit the waves into the cochlear fluid in the inner ear (Osika, 2022).



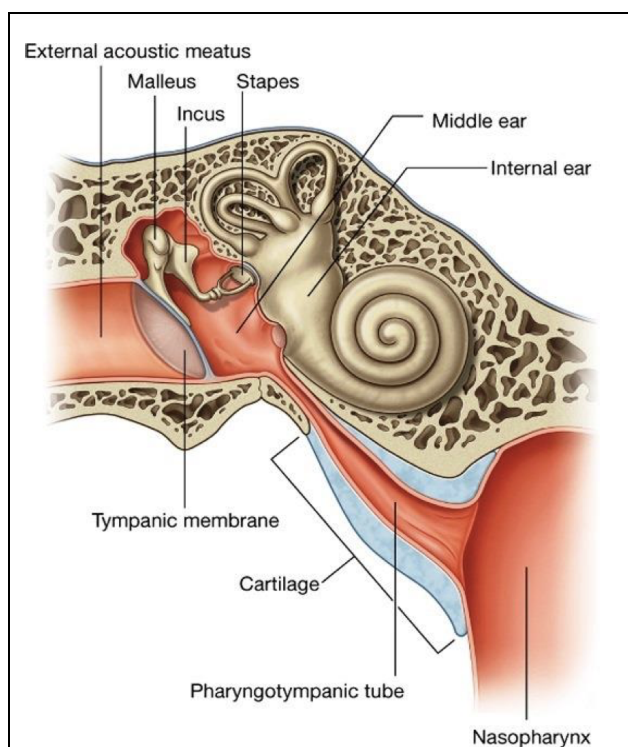


Figure 2.2: Sectioned View of the Middle Ear (Gassler, 2019).

## 2.2.4 Problems of the Middle Ear

Hearing loss that occurs in the middle ear is known as conductive hearing loss (“Types, Causes and Treatments of Hearing Loss,” n.d.). There are numerous causes of conductive hearing loss that are a result of damage or loss of function to the components of the middle ear.

### 2.2.4.1 Ossicular Fixation

Ossicular fixation is a condition where the ossicles of the middle ear become fused in place either during development in the womb or due to chronic ear infections (“Ossicular Fixation,” n.d.). Chronic inflammation will gradually stiffen the ligaments supporting the ossicles, and eventually the ligaments will transition to bone causing the ossicles to fuse in place (“Ossicular Fixation,” n.d.). This type of ossicular fixation is called postinflammatory ossicular fixation and can take form in three different ways (Swartz et al., 1985). These are chronic adhesive otitis media, the fixation or fusing of fibrous tissue due to chronic inflammation; tympanosclerosis, the scarring or death of tissue in the ear drum (*Tympanosclerosis*, n.d.); and fibro-osseous sclerosis (or otosclerosis), the formation or growth of bone within the middle ear (Swartz et al., 1985). Ossicular fixation prevents the ossicles from vibrating and transmitting sound properly, resulting in diminished or lost hearing (“Ossicular Fixation,” n.d.). This can usually be treated with the use of a hearing aid; in more extreme cases ossiculoplasty can be performed (“Ossicular Fixation,” n.d.). Ossiculoplasty is a surgery where the damaged ossicles

are replaced by prosthetic devices that mimic the mechanics of the healthy ossicular chain, returning some level of hearing ability (Mudhol et al., 2013).

#### 2.2.4.2 Otosclerosis

Otosclerosis is a condition of the middle ear where abnormal bone growth occurs, causing stiffening and loss of motion of the ossicles (*Otosclerosis*, 2019). The hardening of an ossicle like the stapes limits the ability of the middle ear to vibrate properly, resulting in hearing impairment and loss (*Otosclerosis*, 2022). There is no known cause of otosclerosis; however, it seems to be hereditary and white, middle-aged women are the most at risk (*Otosclerosis*, 2022). Otosclerosis is usually treated with the use of hearing aids for mild cases and a surgery called a stapedectomy when the hardening becomes too great (*Otosclerosis*, 2022). In a stapedectomy, the hardened stapes is partially removed and then bypassed by a prosthetic device that then takes up the responsibility of transmitting vibrations to the inner ear (*Otosclerosis*, 2019).

### 2.3 Functionality of the Middle Ear with Sound Mechanics

The middle ear's purpose is to transmit sound waves from the tympanic membrane into fluid vibrations to the inner ear (Sunil Puria et al., 2007). The ossicles within the middle ear move conjunctively in all three dimensions to transmit these vibrations (Sunil Puria et al., 2007). Sound waves cause the eardrum to push against the malleus, which in turn moves the incus. The incus connects to the stapes, which imparts vibrations on the oval window. Through this sequence, vibrations travel from the tympanic membrane to the oval window. The difference in size between the tympanic membrane and oval window results in an increase in the strength of the vibration as it passes through the middle ear (Dancer & Rebillard, 2018). Although it is understood that the ossicular chain works as a system to transmit sound, the functionality of each component in the chain still remains unknown. To gather more information about the individual components, experimentation with stimulation and vibrometry are still being researched.

#### 2.3.1 Sound as a Wave

Sound is the compression and expansion of a medium in the form of a mechanical wave ("Sound and Hearing," 2019). This motion creates longitudinal waves, which can be modeled as a combination of sinusoidal waves. In this application, sine waves have 3 parameters; amplitude, frequency and phase shift (Gerig, 2015). The amplitude represents the magnitude of the wave, the frequency is the number of cycles per second, generally labeled Hertz (Hz), and a phase shift represents how far the wave is offset from a reference time, which becomes relevant when considering the superposition of waves (Gerig, 2015). The following equation demonstrates how amplitude, frequency, and phase shift are mathematically modeled in a sine wave.

$$y(t) = a * \sin(2 * \Pi * f * t + p)$$

a = Amplitude

f = Frequency

t = Time

p = Phase shift in radians

Sound can propagate through all elastic media, including gasses, liquids, and solids (“Sound and Hearing,” 2019). The amplitude can be measured in terms of pressure variations or displacement. When measured in terms of displacement, the amplitude of the sound wave is proportional to the distance a particular point in space moves over each wavelength. The greater the movement, the greater the amplitude of the wave.

## 2.4 Current Research and Modeling of the Middle Ear in Academia

This section discusses trends that occur in the middle ear and modeling techniques that were relevant in the completion of this project.

### 2.4.1 Trends of the Middle Ear

One trend in the middle ear that has been explored by professionals is the middle ear’s response when there is a load applied in addition to a stimulus. One study showed that when a positive pressure is present in the ear canal, there is an effect on the first natural frequency of the system. This study demonstrated that with a healthy IMJ, the first natural frequency shifts up, and it has a smaller magnitude when this positive pressure is present. A graph of this trend is shown in Figure 2.3. Figure 2.4 shows the trend that arises when this positive pressure is applied in the ear canal of an ear with a fixed IMJ. The same study found that there was a similar shift up in first natural frequency. Comparison of Figures 2.3 and 2.4 clearly illuminates that the reduction in magnitude is much greater for the fixed IMJ. (Warnholtz et al., 2021)

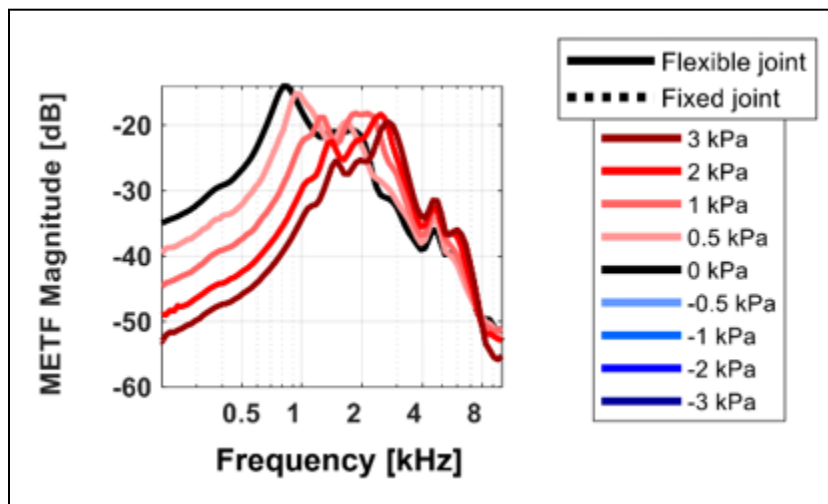


Figure 2.3: Positive Pressure Effect on Flexible IMJ (Warnholtz et al., 2021)

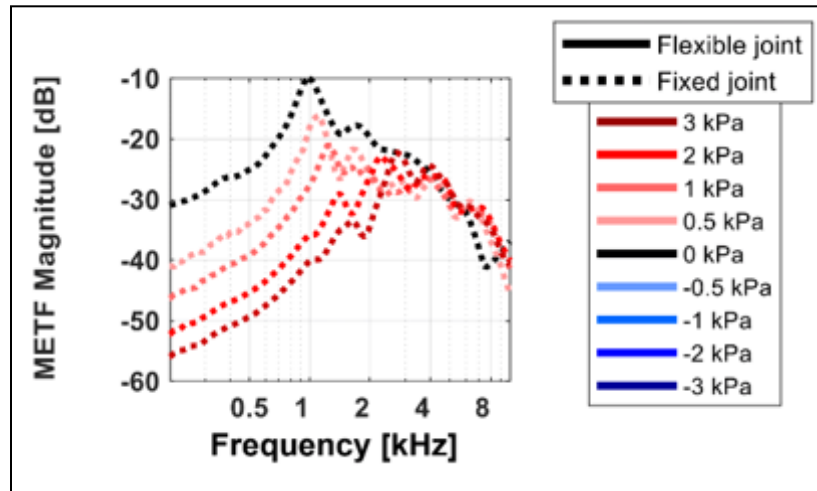


Figure 2.4: Positive Pressure Effect on Fixed IMJ (Warnholtz et al., 2021)

Another trend that has been explored by researchers is how the stiffness of the middle ear affects sound transmission. The stiffness of the middle ear refers to the displacement of the ossicular chain when a given acoustically induced force is applied. These displacements fall around 100 nm and the forces around 100  $\mu$ N. A healthy middle ear has a static stiffness of around 200 to 500 N/m while a middle ear of someone experiencing conductive hearing loss has a stiffness of around 1000-2500 N/m (Figure 2.5). These numbers were determined by taking a healthy middle ear and allowing it to dry to replicate pathological stiffening. When the middle ear was dried, which simulated ossicular fixation, it was found that the middle ear's ability to respond to frequencies lower than 1 kHz decreases while its ability to respond to frequencies higher than 1 kHz increases. This shows that the stiffness of the middle ear affects how sound is transmitted through the ear. (Dobrev et al., 2018)

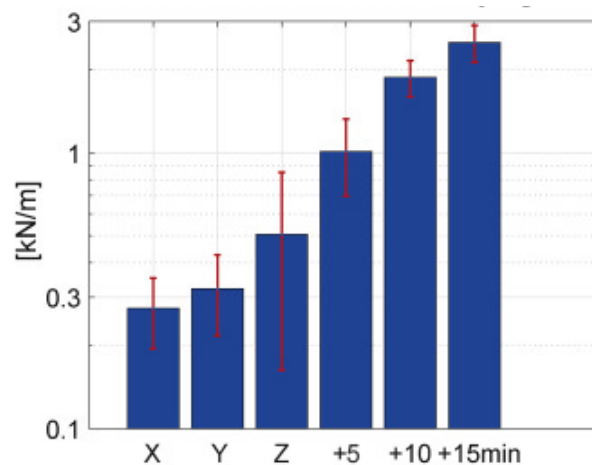


Figure 2.5: Middle Ear Stiffness with Drying (Dobrev et al., 2018)

### 2.4.2 Middle Ear Modeling Techniques and Challenges

There are many challenges associated with creating a model of the middle ear. To start, the middle ear is a very small system, with measurements on the order of micro- or nano- meters, Newtons, or seconds. Creating a model that is the actual size of the middle ear would likely not be useful for educational purposes to better understand the middle ear and its function. Educators and researchers would need a model scaled to a size that would allow for easy viewing and manipulation. Because of this, models must be scaled to a size that is useful but does not change the functionality of the model. Current industry modeling techniques must then take into account a variety of factors, including mechanical and physiological properties, that determine this accuracy and ensure that the anatomy and physiology of the model is a scaled match to that of the middle ear. (Puria et al., 2013b)

Additionally, gathering and interpreting the data required to understand the geometry and variation in the middle ear is complex. Tools such as light and electron microscopy, X-rays, computerized tomography (CT) scans, magnetic resonance imaging (MRI) scans, and ultrasound can be used to map out the parts of the middle ear. However, each of these techniques have their limitations that prevent researchers from modeling exact replicas of the minute yet complex parts of the middle ear. Once the data required for designing the model is obtained, the relationship between parts and how they connect must be analyzed to properly compile the model. Because the middle ear is complex and contains many different types of tissue, researchers modeling the middle ear must understand how each of these parts interact with each other in order to function as a whole. This includes understanding both the functionality of each part and the material properties of each part. Materials need to be selected based on the known properties of the middle ear components. Not all properties will scale identically from true anatomy to model, and details can be lost if the data is simplified. (Puria et al., 2013b)

### 2.4.3 Medical Application of Silicone

Silicone is a common material used in medical applications. Silicone is a synthetic polymer made up of polydimethylsiloxane chains. Dimethylsiloxane refers to a molecule made up of two methane molecules, a silicon atom, and two oxygen atoms (Figure 2.6). These molecules form chains when the hydrogen atoms at the end of the chain (see Figure 2.6) are pulled away in a process called crosslinking. A crosslinker is a water based material that, when mixed with the dimethylsiloxane base, allows the chains to form. The amount of crosslinker added determines the length of the chain. (*Properties of Silicones*, n.d.)

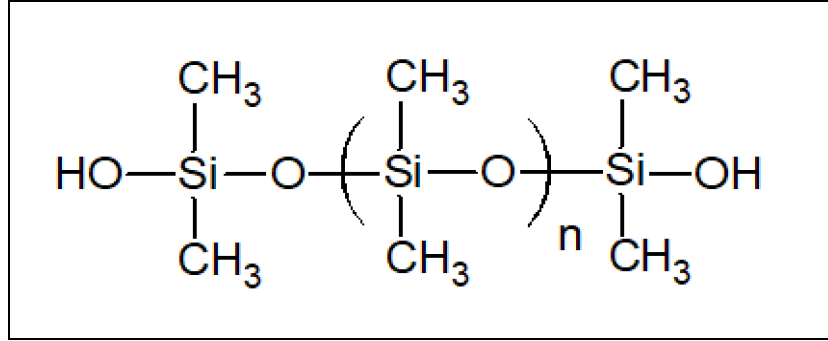


Figure 2.6: PDMS, a Commonly Used Silicone (*Properties of Silicones*, n.d.)

The ability to vary the length of the polydimethylsiloxane chains makes it possible to vary the properties of silicone. Table 2.1 shows an example of how the elastic modulus changes depending on the ratio of base to crosslinker of PDMS, a commonly used silicone. As more crosslinker is added, the resulting silicone becomes more stiff. Because of this, silicone can vary from being a gel-like texture to a hard yet flexible rubber.

Silicone can be used in countless medical applications as an elastomer, adhesive, or gel (Zare et al., 2021). This is due to its biocompatibility to the human body, but also its ability to mimic the native tissue (Zare et al., 2021). For example, PDMS and liquid silicone rubbers are two favored materials used in cochlear implants due to their flexibility, biocompatibility, stability, and physical and chemical purity (Yilmaz-Bayraktar et al., 2022). Some other examples of how silicone is used in the human body include heart shunts and valve replacements, membranes, joint and cartilage implants, and ear and nose prostheses (Zare et al., 2021).

Table 2.1: Elastic Modulus of PDMS with Different Amount of Crosslinking (Wang et al., 2014)

Sample	4 mm diameter		3 mm diameter		$E_{\text{ave}}$ (MPa)
	$E_1$ (MPa)	$E_2$ (MPa)	$E_3$ (MPa)	$E_4$ (MPa)	
PDMS 5 : 1	3.584	3.728	3.458	3.582	$3.59 \pm 0.11$
PDMS 7 : 1	2.950	2.924	2.867	2.894	$2.91 \pm 0.036$
PDMS 10 : 1	2.605	2.633	2.587	2.630	$2.61 \pm 0.021$
PDMS 16.7 : 1	1.109	1.234	1.265	1.227	$1.21 \pm 0.069$
PDMS 25 : 1	0.954	-	1.006	-	$0.98 \pm 0.037$
PDMS 33 : 1	0.548	0.577	-	-	$0.56 \pm 0.021$

## 2.5 Previous Projects

This project is a continuation of two previous MQPs that worked toward developing a functional model of the middle ear. The following section will give a brief overview of the two projects, their accomplishments and limitations, and any recommendations made for future teams.

### 2.5.1 Design and Simulation of a Middle Ear Model to Aid with Otological Studies (2020)

The first iteration of this project was conducted in the fall of 2020 by a previous MQP team at Worcester Polytechnic Institute (WPI). They worked at the Universitätsspital Zürich with Dr. Ivo Dobrev and created a dynamic model of the middle ear. The functional model was created on a 15 to 1 scale and was interchangeably assembled to display the middle ear at healthy and diseased tissue states. The model was able to measure resultant vibrations of the middle ear at these different states. The model is shown in Figure 2.7.

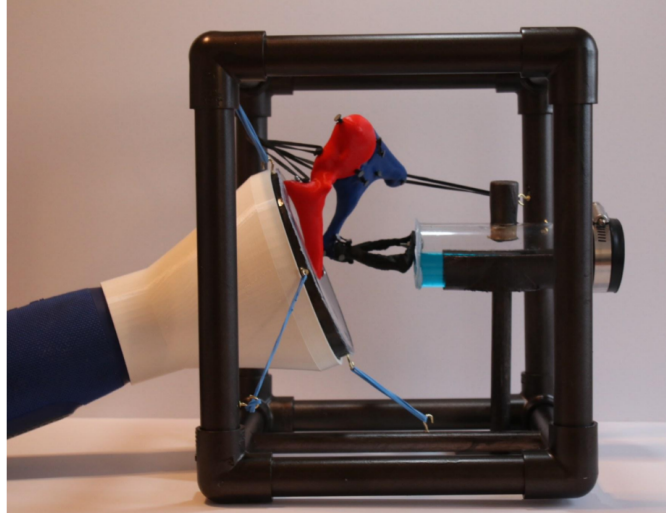


Figure 2.7: 2020 WPI MQP Team's Model (Tanner et al., 2021)

This group fabricated a majority of the ossicular chain and tympanic membrane by utilizing Fused Deposition Modeling (FDM) printing techniques accompanied with a variety of other structural hardware. This project focused on different 3D printing settings accompanied with material research to accurately model the bones of the ossicular chain; however, time constraints prevented them from completing their testing of different materials and print settings. Ultimately, the final model utilized thermoplastics to model the bones in the ossicular chain and used elastomers to model the muscles, tendons, and ligaments that support the ossicles. One major limitation of this project is that its assembly does not allow for easy interchangeability of materials. Another major limitation is that it has significantly physically degraded over time, ultimately becoming unusable by August of 2022.

### 2.5.2 Middle Ear Replication for Otological Studies (March 2022)

The second rendition of this project was conducted by another WPI team in March 2022. These students also worked with Dr. Dobrev at the Universitätsspital Zürich. This team worked to enhance the previous design of the 2020 team's model. They created an interchangeable,

functional model of the middle ear along with a corresponding static model. The static model is shown in Figure 2.8, and the functional model is shown in Figure 2.9.

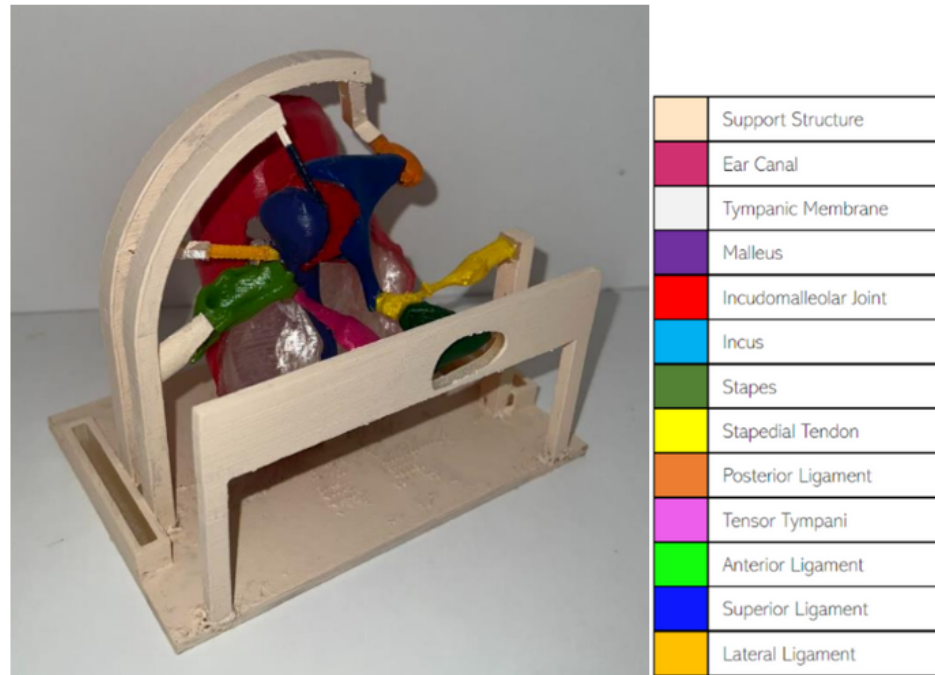


Figure 2.8: March 2022 WPI MQP Team's Static Model (Scrivanich et al., 2022)

The static model is realistic and displays a healthy middle ear with relatively accurate geometric proportions. This model was FDM printed as one continuous piece of PLA with a 10:1 scale, making it smaller than the functional model. It excels in accurately detailing the ligaments, tendons, and joints that suspend the ossicular chain. This model is accompanied by a surgical view cover, which allows the model to show the view a surgeon would see during surgery. However because this model was a singular 3D print, it caused many of the components of the model to become warped, making the final model lack a refined surface finish.



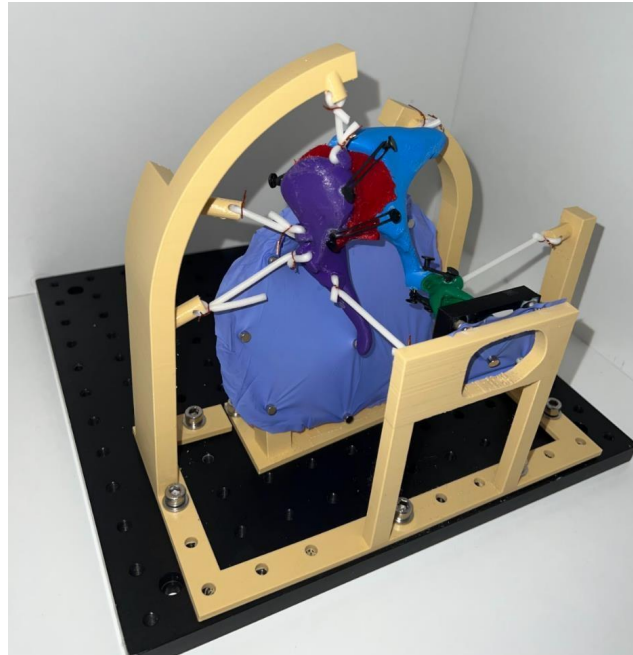


Figure 2.9: March 2022 WPI MQP Team's Dynamic Model (Scrivanich et al., 2022)

The dynamic model created by this group prioritized functionality over anatomical correctness to show the vibrational patterns of the middle ear. The model consisted of a variety of 3D printed parts, screw hardware, magnets, silicone bands. This model expanded on the 2020 version by increasing the interchangeability of the design, allowing for easier disassembly and reassembly. This team focused on a model of healthy tissue, but because of the model's interchangeability and simple assembly, there was future potential for replacing particular components of the model to represent diseased tissue within the middle ear. A focus was put on modeling the auditory bones of the ossicular chain and their connections to the eardrum and oval window. The team sacrificed anatomical detail of the ligaments and tendons in order to allow for dynamic motion. The model was designed for testing, but the team was unable to complete acoustic testing of the model due to time limitations.

This dynamic model has numerous limitations. The entirely 3D printed assembly was very expensive due to the cost of FDM printing in Switzerland. The design also contained complicated geometry making it difficult to fabricate effectively and efficiently through FDM printing, and the model was not structurally sound and could be broken through repetitive use. The silicone used to model the ligaments supporting the ossicular chain was also a limited solution. Its properties were not justified, and it was prone to plastic deformation and breaking.

## 3.0 Project Strategy

This section establishes the overall strategy for the project, which consists of the client statement, project goal and objectives, and a detailed schedule for project management.

### 3.1 Client Statement

The March 2022 MQP dynamic and static models of the middle ear various areas for improvement and development. The client determined the focus for this year's advancements to be based on the dynamic model because of its potential for classroom instruction.

Dr. Ivo Dobrev expressed interest in the following areas to explore for improvement of the previous dynamic model:

1. Improve the durability of the model support structure.
2. Improve the adjustability of the model support structure.
3. Include the ability to measure how the model responds to a stimulus.
4. Demonstrate trends in the model that are similar to how the biological middle ear behaves.
5. Implement a realistic interface for current “bone on bone” contact points in the model.
6. Select and justify the use of a material modeling the support ligaments and muscles that suspend the middle ear assembly.
7. Add a function to the model demonstrating varying stages of pathological hearing loss due to the stiffening of the incudomalleolar joint.

After taking Dr. Dobrev's interests for the project into consideration, the feasibility of the requests were analyzed in order to determine realistic objectives for the scope of the project.

### 3.2 Project Goal & Objectives

The following project goal and objectives were formulated from the above client statement:

**Goal:** Enhance an existing instructional model of the middle ear in order to mimic the pathological stiffening of the incudomalleolar joint.

**Objective 1:** Improve the durability and adjustability of the support structure of the model.

**Objective 2:** Demonstrate the varying stages of pathological hearing loss due to the stiffening of the incudomalleolar joint and its effect on sound transmission.

**Objective 3:** Select and justify the use of a material modeling the support ligaments and muscles that suspend the middle ear assembly.

**Objective 4:** Implement a realistic interface for current “bone on bone” contact points in the model, namely the incudostapedial joint.

### 3.3 Design Requirements

Each of the project objectives can be broken down into the following design requirements.

#### 3.3.1 Objective 1 Design Requirements

The main design requirement for Objective 1 was to improve the supportive materials of the model structure and the connection points in order to create a more secure and adjustable base for the model. Ideal materials for this design requirement would be those that are resistant to damage when regularly handled, and able to be quickly adjusted back and forth between set parameters. This would include designing structural aspects to tighten or loosen the ligaments and muscles to represent different variations of stiffnesses without having to fully disassemble the model.

#### 3.3.2 Objective 2 Design Requirements

The main design requirement for Objective 2 was to create a system that would mimic the stiffening of the IMJ's mechanical properties when it becomes diseased. A model that fulfills this requirement would be one that has a way to easily change the stiffness of the IMJ in a classroom setting while also being able to display in real time the quantitative changes that occur when a part of the system is altered. This would be in the form of graphical data displayed on a computer that illustrates how different stiffnesses change how sound travels through the middle ear. Additionally, exploring different material options for the IMJ was required in order to identify a material that closely mimics the native tissue.

#### 3.3.2 Objective 3 Design Requirements

The main design requirement for Objective 3 was to select materials that are comparable to the properties of the actual middle ear. Specifically, the current model's ligaments and tympanic membrane are made of materials that were not clearly justified. Determining whether or not these materials are comparable to the middle ear's actual structure and function and, if need be, selecting better materials would make the model more realistic.

#### 3.3.4 Objective 4 Design Requirements

The main design requirement for Objective 4 was to determine a way to mitigate the bone on bone contact point at the incus and stapes by adding a new part to mimic the ISJ. This joint should be of similar material to the IMJ and not inhibit the function of the model.

### 3.4 Design Constraints

The two main design constraints facing this project were the limitations of time and money. The project was given a budget of 400 Swiss Francs. This limited the choices when looking for materials used for molding, and how to obtain the required large 3D printed parts. In Switzerland, ordering 3D prints is more difficult and far more expensive compared to the United States – about 10x the price compared to the WPI Rapid Prototyping Lab. This makes iterative design difficult for these 3D printed parts because each will be very expensive to print in Switzerland. Another option was to have the parts shipped from WPI. The one-term nature of this MQP made shipping packages from WPI difficult, because of the long shipping times.

### 3.5 Project Management

The project team utilized a gantt chart to ensure completion of objectives and deliverables within the project time span; a portion of this organizational tool is displayed in Appendix A. Considerations including lead and shipping times for materials, work hours required for each deliverable, and time spent calibrating instrumentation were included in the creation of the gantt chart. The gantt chart displays project tasks and their corresponding dates throughout the 9-week project life cycle.

Alongside the gantt chart, the team also used a website, Trello. Trello is a website that enables the creation of a task board for project teams to track specific tasks and due dates. Project members can assign tasks to individuals as well as mark them complete.

## 4.0 Design Process

Decision making tools were used throughout the design process to help the team make choices with a logic-based process. Pairwise comparison charts and Pugh decision matrices were used to determine design objectives for the support structures, the model IMJ and the molds to create the IMJ, and the model ligaments and muscles. The different requirements selected cover the factors that determined the best material to use. Once these desired design parameters were selected, the ranking process for the pairwise comparison chart was completed to determine the weight of each factor and the numerical ranking of the design objectives. The ranking of the design objectives goes from most important, or greatest weight, to least important, or smallest weight.

After the ranking process for the design requirements was completed, materials were then selected based on the parameters outlined in the pairwise comparison chart. A Pugh decision matrix was then created to determine whether the materials fulfilled the chosen design objectives. The completed Pugh decision matrix then showed numerically which materials best matched the parameters and would be chosen for the final design.

### 4.1 Model Support Structure

This section includes how the support structure of the model was improved throughout the course of this project.

#### 4.1.1 Model Base Structure

The project team improved the base model structure by looking at different structural support options and comparing their viability for future use. Table 4.1 is a pairwise comparison chart calculating the weight of each parameter chosen.

Table 4.1: Pairwise Comparison Chart for Structural Support Design Objectives

	Structural Stability	Adjust.	Inter-change.	Easily Obtainable	Cost Effective	Ability to Replicate	Degrad.	Total
Structural Stability		1	1	1	1	1	1	6
Adjustability	0		1	1	1	1	0	4
Ease of Interchangeability	0	0		0	0	1	0	1
Easily Obtainable	0	0	1		0	1	0	2
Cost Effective	0	0	1	1		1	0	3
Ability to Replicate Coordinates and Angles	0	0	0	0	0		0	0
Degradability	0	1	1	1	1	1		5

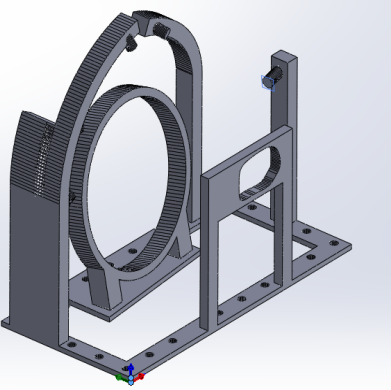

Once these desired design parameters were selected, the ranking process for the pairwise comparison chart was completed to determine the weight of each factor and the numerical ranking of the nine design objectives. Table 4.2 shows the ordered ranking of the design objectives from most important, or greatest weight, to least important, or smallest weight.

Table 4.2: Structural Support Objectives Ranking

Structural Stability	7
Degradability	6
Adjustability	5
Cost Effective	4
Easily Obtainable	3
Ease of Interchangeability	2
Ability to Replicate Coordinates and Angles	1

Once the ranking of design parameters was completed, three structural support choices were analyzed then selected to be tested. A brief overview of each option is included in Table 4.3. These options were either directly available to us in the lab or were able to be fabricated and delivered to us through visitors from WPI.

Table 4.3: Structural Support Options and Descriptions

Structural Support Options	Images	Information
3D Printed Support		<p>This was the support choice used by the March 2022 group. It was printed in PLA at 30% infill. A variety of support beams were needed for the print due to the complex geometry and overhangs used in the design.</p>
ThorLabs	 <p>(Thorlabs, n.d.)</p>	<p>ThorLabs is a company that offers a variety of structural support and connector pieces that can be used in a multitude of situations including modeling. The Thorlabs pieces that were available in the lab consisted of adjustable bases that could easily be connected to the mounting platform using varying length connection rods, and a variety of adjustable adaptors that could easily be mounted on the connection rods. With all of these pieces, many different types of adaptable and adjustable supports could be fabricated.</p>
MakerBeam	 <p>(MakerBeam, n.d.)</p>	<p>MakerBeam is a company that offers T-slot technology structural beams. The beams have a hollow core and have threaded holes at each end and are available in a multitude of different sizes. These beams are primarily used to set up support structures at 90 degree angles. With the pieces that were available in the lab a cube shaped structural support fitted with adaptors to hold hardware could be fabricated.</p>

The chosen structural support options were put into a Pugh decision matrix to determine which structural supports best fulfilled the selected design objectives (Table 4.4). From the Pugh chart, it was determined that the ThorLabs Pieces were best at supporting our model.

Table 4.4: Pugh decision matrix for Structural Support Choices

	Weight	Baseline	ThorLabs	MakerBeam	3D Print
Structural Stability	7	0	1(7)	1(7)	1(7)
Adjustability	5	0	1(5)	-1(5)	-1(5)
Ease of Interchangeability	2	0	1(2)	1(2)	-1(2)
Easily Obtainable	3	0	1(3)	1(3)	1(3)
Cost Effective	4	0	0(4)	0(4)	-1(4)
Ability to Replicate Coordinates and Angles	1	0	1(1)	-1(1)	1(1)
Degradability	6	0	1(6)	1(6)	-1(6)
<b>Score</b>		<b>0</b>	<b>22</b>	<b>12</b>	<b>-6</b>

ThorLabs parts were chosen for their ability to easily fulfill the selected design objectives. However, not all of the 3D printed parts will be replaced by the Thorlabs pieces. This is because the oval window and eardrum geometry are complicated and difficult to replicate without the use of 3D printing. Therefore 3D printing these components is easier and more viable than using ThorLabs pieces. In Figure 4.1 the combination of the selected 3D printed parts and the ThorLabs pieces can be seen.

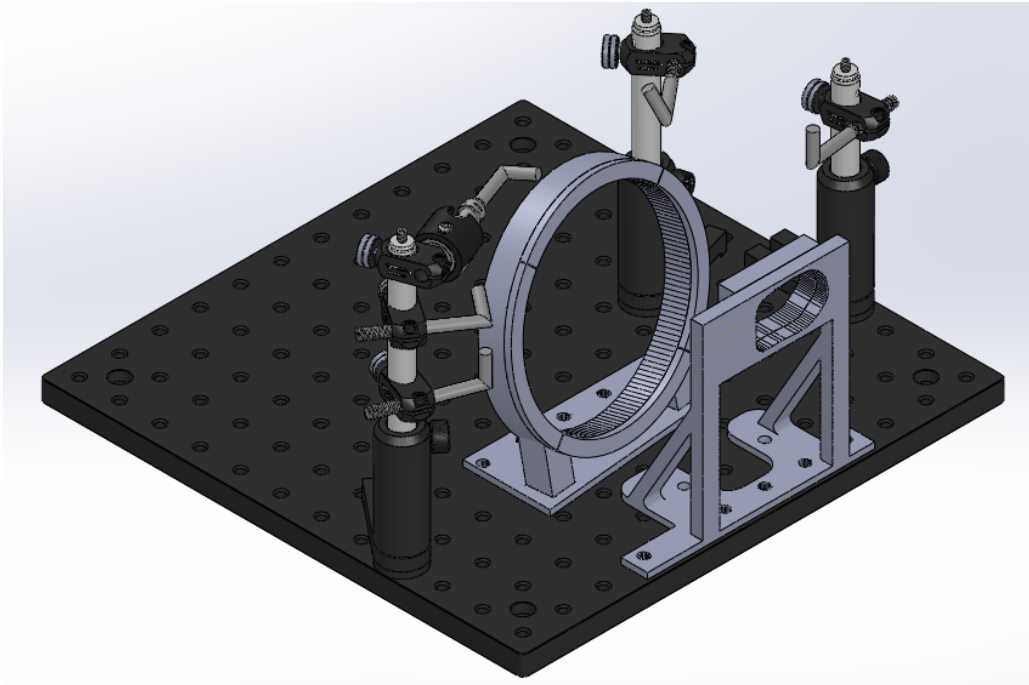


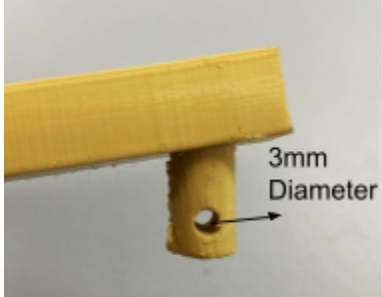


Figure 4.1: Structural Support Setup including ThorLabs Pieces



### 4.1.2 Ligament Attachment Points

Another decision point in the improvement of the model support structure was ligament attachment points. This was pursuant to Objective 1, increasing the durability and adjustability of the model. The original model used 3D printed pegs with through holes, with the ligaments looped through the hole and secured using wire. The two alternative designs the project team considered were eye-hooks and L-hooks. Table 4.5 displays a photo of each attachment method.

Table 4.5: Ligament Attachment Point Possibilities

Attachment Method Options	Image	Information
3D-Printed		March 2022 Model PLA
Eye-Hook	 (Hillman Steel Screw Eye Hook in the Hooks Department at Lowes.Com, n.d.)	Steel Price: 1.48 USD
L-Hook	 (Overstock, n.d.)	1.3" length Price: ~1 CHF

The parameters of interest for attachment points include adjustability and ease of attachment. Adjustability is a function of being able to adjust the position of the point of attachment, and ease of attachment is a function of the ease of removing and reattaching the

ligament to the support structure. Adjustability and ease of attachment are equally weighted parameters.

The three ligament attachment options were put into a Pugh decision matrix to determine which best fulfilled the selected design objectives (Table 4.6). From the Pugh chart, it was determined that the L-hook was the best option for attaching ligaments. The L-hook allows for both adjustability and ease of attachment.

Table 4.6: Pugh Decision Matrix for Ligament Attachment Point Options

	Weight	Baseline	3D Print	Eye-Hook	L-Hook
Adjustability	2	0	-1(2)	1(2)	1(2)
Ease of Interchangeability	1	0	-1(1)	-1(1)	1(1)
<b>Score</b>		<b>0</b>	<b>-3</b>	<b>1</b>	<b>3</b>

## 4.2 Ossicle Connection Material Selection

This section includes selecting a suitable material for the ossicle connectors in order to keep the ossicles secure and correctly linked together.

### 4.2.1 Ossicle Connection Decision Matrices

A pairwise comparison chart was created for determining the desired factors for the materials to be used to represent the ossicle connections. The six design parameters chosen for the ossicles connection selection were degradability, adjustability, tension, cost, accessibility, and ease of use (Table 4.7).

Table 4.7: Pairwise Comparison Chart for Material Objectives

	Degradability	Adjustability	Tension	Cost Effective	Accessibility	Ease of Use	Total
Degradation		1	1	1	0	1	4
Adjustability	0		1	1	0	1	3
Tension	0	0		1	0	1	2
Cost Effective	0	0	0		0	1	1
Accessibility	1	1	1	1		1	5
Ease of use	0	0	0	0	0		0




The six requirements were then scored to determine the ranking. Table 4.8 shows the ranking of the six design objectives with the highest numbers representing the greatest weight and lowest numbers representing the least weight.

Table 4.8: Material Objectives Ranking

Accessibility	6
Degradation	5
Adjustability	4
Tension	3
Cost	2
Ease of use	1

Once the ranking of design parameters was completed, three materials were selected to be tested. These materials were chosen based on their ability to keep the ossicles secure and correctly linked together, as well as accessibility within our project site. The three materials listed in Table 4.9 were found at a nearby craft and hardware store.

Table 4.9: Potential Ossicle Connection Materials and Information

Ossicle Connection Material Options	Image	Information
Rubber O-rings	 <p><i>(Kinzo - O-Ringe, n.d.)</i></p>	Varying diameters and thicknesses Price: 2.95 CHF
Elastic Hair Bands	 <p><i>(Daily Go Mini-Haargummi, n.d.)</i></p>	15 mm band diameter Silicone hair bands Price: 5.95 CHF
Cloth Elastic Hair Bands	 <p><i>(DailyGo Mini (Hair Tie), n.d.)</i></p>	15 mm band diameter Price: 6.85 CHF

The chosen materials were then put into a Pugh decision matrix to determine which material best fulfilled the selected design objectives (Table 4.10). It was determined that either the 1mm or 2mm cloth elastic cord was the best material for the ligaments.

Table 4.10: Pugh Decision Matrix for Ossicle Connection Materials

	Weight	Baseline	Rubber O-rings	Elastics Bands	Cloth Bands
Accessibility	6	0	1(6)	1(6)	1(6)
Degradation	5	0	-1(5)	-1(5)	1(5)
Adjustability	4	0	-1(4)	1(4)	1(4)
Tension	3	0	1(3)	1(3)	1(3)
Cost	2	0	1(2)	1(2)	1(2)
Ease of use	1	0	1(1)	-1(1)	-1(1)
<b>Score</b>		<b>0</b>	<b>3</b>	<b>9</b>	<b>19</b>

### 4.3 Ligament Material Selection

Finding a suitable material for the ligaments was important in order to keep the structure stable and to create a closer sense of anatomical accuracy.

#### 4.3.1 Ligament Decision Matrices

A pairwise comparison chart was created for determining the desired factors for the materials to be used to represent the ligaments. The six design parameters chosen for the ligaments selection were tension, degradability, durability, cost, accessibility, and ease of use (Table 4.11).

Table 4.11: Pairwise Comparison Chart for Material Objectives

	Degradability.	Adjustability.	Tension	Cost Effective	Accessibility	Ease of Use	Total
Degradability		1	1	1	0	1	4
Adjustability	0		1	1	0	1	3
Tension	0	0		1	0	1	2
Cost Effective	0	0	0		0	1	1
Accessibility	1	1	1	1		1	5
Ease of Use	0	0	0	0	0		0

The six requirements were then scored to determine their ranking. Table 4.12 shows the ranking of the six design objectives with the highest numbers representing the greatest weight and lowest numbers representing the least weight.

Table 4.12: Material Objectives Ranking

Accessibility	6
Degradability	5
Adjustability	4
Tension	3
Cost Effective	2
Ease of use	1

Once the ranking of design parameters was completed, five materials were selected to be tested. These materials were chosen based on their ability to keep the model structurally stable while allowing a small range of motion, as well as accessibility to the particular material. The materials listed in Table 4.13 were found at a nearby craft and hardware store.

Table 4.13: Potential Ligament Materials and Information

Ligament Material Options	Image	Information
Silicone Cord	 <p>(50 SHA VMQ Silicone O-Ring Cord Ø3.00 Mm, n.d.), (Thomann Silicone Cord Ø=5mm x L=100mm, n.d.)</p>	<p>VMQ 3mm diameter O-ring cord Price: ~1.85 CHF</p>
Rubber Elastic Cord	 <p>(Suki Fliesenlegergummischnur Kaufen Bei JUMBO, n.d.)</p>	<p>&lt;1mm diameter Price: 2.95 CHF</p>
Cloth Elastic Cord	 <p>(Glorex Gummibänder, 4x3m; Ø 1mm beige/grau/braun/schwarz, n.d.)</p>	<p>1mm diameter Cloth wrapped rubber Price: 4.95 CHF</p>
Cloth Elastic Cord	 <p>(Glorex Gummibänder, 4x3m; Ø 2mm beige/grau/braun/schwarz, n.d.)</p>	<p>2mm diameter Cloth wrapped rubber Price: 3.70 CHF</p>
Cloth Elastic Cord	 <p>(ELASTISCHE KORDEL kaufen bei JUMBO, n.d.)</p>	<p>2.8mm diameter 25 kg weight max Polyester and rubber Price: 13.95 CHF</p>

The chosen materials were then put into a Pugh decision matrix to determine which material best fulfilled the selected design objectives (Table 4.14). From the Pugh matrix, it was determined that either the 1 mm or 2 mm cloth elastic cord was the best material for the ligaments. The 1 mm cloth elastic cord was ultimately chosen as the final design choice after initial stiffness testing showed that the 2 mm made the model system much stiffer than the pursued stiffness.

Table 4.14: Pugh Decision Matrix for Ligament Materials

	Weight	Baseline	Silicone Cord	Rubber Elastic	1 mm Elastic String	2mm Elastic String	2.8 mm Elastic String
Accessibility	6	0	-1(6)	1(6)	1(6)	1(6)	1(6)
Degradation	5	0	-1(5)	-1(5)	1(5)	1(5)	1(5)
Adjustability	4	0	-1(4)	1(4)	1(4)	1(4)	1(4)
Tension	3	0	1(3)	-1(3)	1(3)	1(3)	-1(3)
Cost	2	0	1(2)	1(2)	1(2)	1(2)	-1(2)
Ease of use	1	0	-1(1)	1(1)	1(1)	1(1)	1(1)
<b>Score</b>		<b>0</b>	<b>-11</b>	<b>5</b>	<b>21</b>	<b>21</b>	<b>11</b>

#### 4.4 Incudomalleolar Joint Design

Objective 1 requires that the materials in the dynamic model are durable, yet anatomically representative to mimic the mechanics of native tissue. One of the design objectives for this project was to improve material choice for the dynamic model. In particular, the IMJ was the main aspect of the model that failed to mimic the mechanical properties of the native tissue. The March 2022 MQP team modeled the IMJ using Thermoplastic Polyurethane Elastomer (TPU), a hard plastic that was able to be 3D printed. One of the benefits of using TPU for the main components of the middle ear was the 3D printer's ability to replicate the detailed geometries of the ossicles. The TPU also had the strength to withstand forces acting on the dynamic model without plastic deformation. The main drawback of using TPU was its rigid properties and stiffness that do not accurately represent the joints in the middle ear. The new material selected for the IMJ needed to be less stiff than TPU. Another benefit of selecting a new material was the ability to create five IMJs with varying stiffnesses. The ability to interchange the IMJ with various stiffnesses allows the model to more easily mimic stiffening of the IMJ, another project objective. The materials chosen to investigate were based on research of the mechanical properties such as tensile strength, density, and stiffness. The materials the team chose to investigate are indicated within Table 2.1 of the background.

#### 4.4.1 IMJ Decision Matrices

Nine different parameters were assessed to determine the best material to construct the IMJ, shown in the pairwise comparison chart in Table 4.15. The material used must be resistant to deformation since the IMJ will be regularly changed out and manipulated by users of the model. Additionally, the model IMJ must mimic the actual material properties and stiffening of the IMJ. Ideally, the selected material would have a range of stiffnesses to allow for multiple copies of the same material with incrementally increasing stiffnesses. The most pliable of these stiffnesses should result in the model stiffness falling within 200 to 500 N/m, which would represent a healthy middle ear (Dobrev et al., 2018).

In addition to material properties, factors relating to the fabrication of the IMJ were also included in the pairwise comparison chart. For materials that would be formed in a mold, factors such as low viscosity, drying time, and compatibility to the mold material were utilized as selection criteria. An ideal material would start at a low viscosity to allow for easy pouring into a mold, be able to dry or harden quickly and without special curing techniques, and be easily removed from the mold. Logistical factors, such as ease of use, accessibility, and cost were also added to the pairwise comparison chart to take into account the feasibility of obtaining materials.

Table 4.15: Pairwise Comparison Chart for IMJ Design Objectives

	Deform.	Stiff	Stiff Variability	Low Vis.	Drying Time	Compat.	Use	Access.	Cost	Total
Resistance to Deformation		1	1	1	1	1	1	1	1	8
Stiffness 200-300 N/m	0		1	1	1	0	0	0	0	3
Ability to Vary Stiffness	0	0		1	1	0	0	0	0	2
Low viscosity (for pouring)	0	0	0		1	0	0	0	0	1
Drying time	0	0	0	0		0	0	0	0	0
Compatibility to mold	0	1	1	1	1		1	0	0	5
Ease of use	0	1	1	1	1	0		0	0	4
Accessibility	0	1	1	1	1	1	1		1	7
Cost Effective	0	1	1	1	1	1	1	0		6

Once these desired design parameters were selected, the ranking process for the pairwise comparison chart was completed to determine the weight of each factor and the numerical ranking of the nine design objectives. Table 4.16 shows the ordered ranking of the design objectives from most important, or greatest weight, to least important, or smallest weight.



Table 4.16: IMJ Objectives Ranking






Resistance to deformation	9
Accessibility	8
Cost Effective	7
Compatibility to Mold	6
Ease of Use	5
Stiffness 200-300 N/m	4
Able to vary stiffness	3
Low viscosity (for pouring)	2
Drying time	1

After the ranking process for the design requirements was completed, the materials for the IMJ were selected. The materials were split into two categories: flexible 3D printed materials and molding materials. Initially, 3D printing was the selected route for the fabrication of the IMJ. However, due to the time and budget constraints related to obtaining printed models, the team chose to establish a second option, molding.

#### 4.4.1.1 Materials Requiring Molds

For molding materials, the initial material selected was PDMS. However, obtaining the type of PDMS chosen would have been costly and time consuming, so other materials that were easily accessible and comparable to PDMS were evaluated. Two silicones, one latex, and one gel from a local craft and hardware store were compared to PDMS and tested against the IMJ design objectives (Table 4.17).

Table 4.17: Potential IMJ Materials and Information

IMJ Material Options (Molding)	Image	Information
Silicone HB with catalyst	 <p>(Rayher, n.d.-g)</p>	1 kg, 10 mL catalyst/ crosslinker Heat resistant Firm and rigid 1-3 hours to harden Price: 90 CHF
Silicone NV with catalyst	 <p>(Rayher, n.d.-h)</p>	1 kg, 10 mL catalyst/ crosslinker Low viscosity, free flowing Medium soft 1-3 hours to harden Price: 90 CHF
Latex Emulsion	 <p>(Rayher, n.d.-d)</p>	500 mL Free flowing Stretch resistance Tear proof Price: 40 CHF
Candle Gel	 <p>(Rayher, n.d.-a)</p>	365 mL, 300 g Easily deformed Heated in water bath Price: 13 CHF
SYLGARD 184 Silicone Elastomer (PDMS)	 <p>(Dow, n.d.)</p>	0.5 kg Two part, curing agent Heat Cured Medium stiffness (20A-50A on Shore Hardness Scale) Price: 168.25 USD

These materials were then evaluated in the Pugh decision matrix to determine the best choice (Table 4.18). It was found that the Silicone NV was the most comparable to PDMS while being both accessible and cost efficient.

Table 4.18: Pugh Decision Matrix for Molded IMJ Materials

	Weight	Baseline	PDMS	Silicone HB	Silicone NV	Latex	Candle Gel
Resistance to Deformation	9	0	1(9)	1(9)	1(9)	1(9)	-1(9)
Stiffness 200-300 N/m	4	0	1(4)	-1(4)	1(4)	-1(4)	-1(4)
Able to Vary Stiffness	3	0	1(3)	1(3)	1(3)	-1(3)	-1(3)
Low Viscosity (For Pouring)	2	0	1(2)	1(2)	1(2)	1(2)	1(2)
Drying time	1	0	-1(1)	1(1)	1(1)	1(1)	1(1)
Compatibility to Mold	6	0	1(6)	1(6)	1(6)	1(6)	-1(6)
Ease of Use	5	0	1(5)	1(5)	1(5)	1(5)	1(5)
Accessibility	8	0	-1(8)	1(8)	1(8)	1(8)	1(8)
Cost	7	0	-1(7)	1(7)	1(7)	1(7)	1(7)
<b>Score</b>		<b>0</b>	<b>13</b>	<b>37</b>	<b>45</b>	<b>31</b>	<b>1</b>

#### 4.4.2 IMJ Mold Decision Matrices

A pairwise comparison chart was created for determining the desired factors for the mold of the IMJ. The six design parameters chosen for the mold design were compatibility to the IMJ material, drying time, ability to air dry, cost, accessibility, and ease of use (Table 4.19).

Table 4.19: Pairwise Comparison Chart for Mold Design Objectives

	Compatibility	Drying time	Air Dry	Cost Effective	Accessibility	Ease of Use	Total
Compatibility		1	1	1	0	1	4
Drying time	0		0	0	0	0	0
Ability to Air Dry	0	1		0	0	0	1
Cost Effective	0	1	1		0	0	2
Accessibility	1	1	1	1		1	5
Ease of Use	0	1	1	1	0		3






The six requirements were then scored to determine their ranking. Table 4.20 shows the ranking of the six design objectives with the highest numbers representing the greatest weight and lowest numbers representing the least weight.

Table 4.20: Mold Objectives Ranking

Accessibility	6
Compatibility	5
Ease of Use	4
Cost Effective	3
Ability to Air Dry	2
Drying time	1

Once the ranking of design parameters was completed, six materials were selected to be tested. These materials were chosen based on their feasibility to be used as molds and proximity to the project site. The five materials listed in Table 4.21 were found at a nearby craft and hardware store and were materials that would be used to make molds by hand. The sixth material chosen was resin, which was the lab printer material.

Table 4.21: Potential Mold Materials and Information

Mold Material Options	Image	Information
Casting Powder Raysin 200	 (Rayher, n.d.-b)	Extra Strong, 400 g, Strength: 200N/sqm Air-drying Compatible with latex & silicone 2-8 days to fully dry Can be removed from mold after 30 min Price: 7.50 CHF
Creative Cement	 (Rayher, n.d.-c)	1 kg Air-drying Compatible with acrylic and plastic molds Price: 15 CHF
Wax Lenses/ Candle Wax	 (Rayher, n.d.-i)	800 g Needs to be heated in water bath at 60 C 1-2 hours to harden Price: 19 CHF
Modeling Clay	 (Rayher, n.d.-e)	1 kg Air-drying Price: 13 CHF
Porcelain Clay	 (Rayher, n.d.-f)	400 kg Air-drying Price: 13 CHF

The chosen materials were then put into a Pugh decision matrix to determine which material best fulfilled the selected design objectives (Table 4.22). From the matrix, it was determined that the wax and 3D printed resin were the best materials to make molds out of.

Table 4.22: Pugh Decision Matrix for Mold Materials

	Weight	Baseline	White Casting Powder	Creative Cement	Wax	Modeling Clay	Porcelain Clay	Resin
Compatibility	5	0	1(5)	-1(5)	1(5)	-1(5)	-1(5)	1(5)
Drying time	1	0	1(1)	-1(1)	1(1)	1(1)	1(1)	1(1)
Ability to Air Dry	2	0	1(2)	1(2)	1(2)	1(2)	1(2)	1(2)
Cost Effective	3	0	1(3)	1(3)	1(3)	1(3)	1(3)	1(3)
Accessibility	6	0	1(6)	1(6)	1(6)	1(6)	1(6)	1(6)
Ease of Use	4	0	-1(4)	-1(4)	1(4)	1(4)	1(4)	1(4)
<b>Score</b>		<b>0</b>	<b>13</b>	<b>1</b>	<b>21</b>	<b>11</b>	<b>11</b>	<b>21</b>

## 4.5 Incudostapedial Joint Design

The previous model presented by the March 2022 project team did not contain an Incudostapedial Joint in the design. However, it is an essential part of the improved dynamic model for anatomical accuracy as well as functionality when stimulated with vibrations. The previous model, as shown below, had an incorrect direct connection between the Stapes and Incus (Figure 4.2).



Figure 4.2: March 2022 Group's Modeling of the Incus Stapes Connection

Not only is this connection inaccurate for the exclusion of the ISJ, but also because this absence causes the Incus to slip underneath the Stapes. To circumvent this problem, the team designed an ISJ out of silicon to accurately connect these two bones together. A variety of design

possibilities were created. These designs are displayed in Figures 4.3, 4.4, and 4.5. Corresponding pro and con lists are present in Tables 4.23, 4.24, and 4.25.

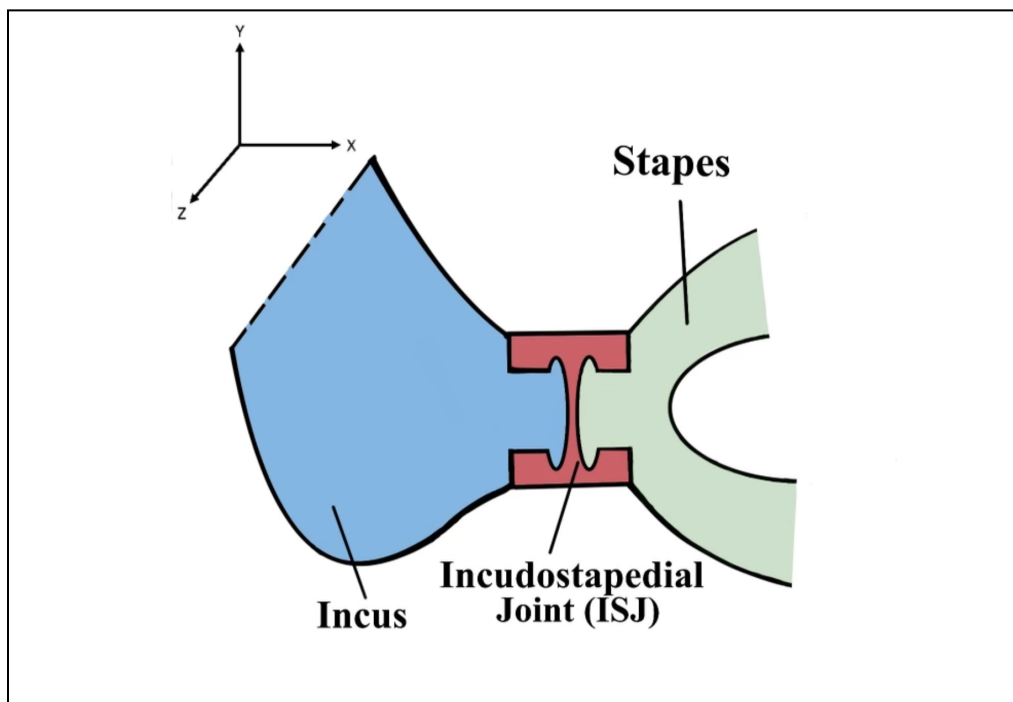


Figure 4.3: ISJ Design Option A

Table 4.23: Pros and Cons of ISJ Design Option A

Pros	Cons
<ul style="list-style-type: none"> <li>• Tight fit of silicon allows for the joint to stay snugly in place.</li> <li>• Connection points are rounded allowing for some rotational movement.</li> </ul>	<ul style="list-style-type: none"> <li>• Thin connection surface which could easily tear during assembly</li> <li>• Tight fit of silicon could inhibit realistic motion of Incus and Stapes</li> </ul>

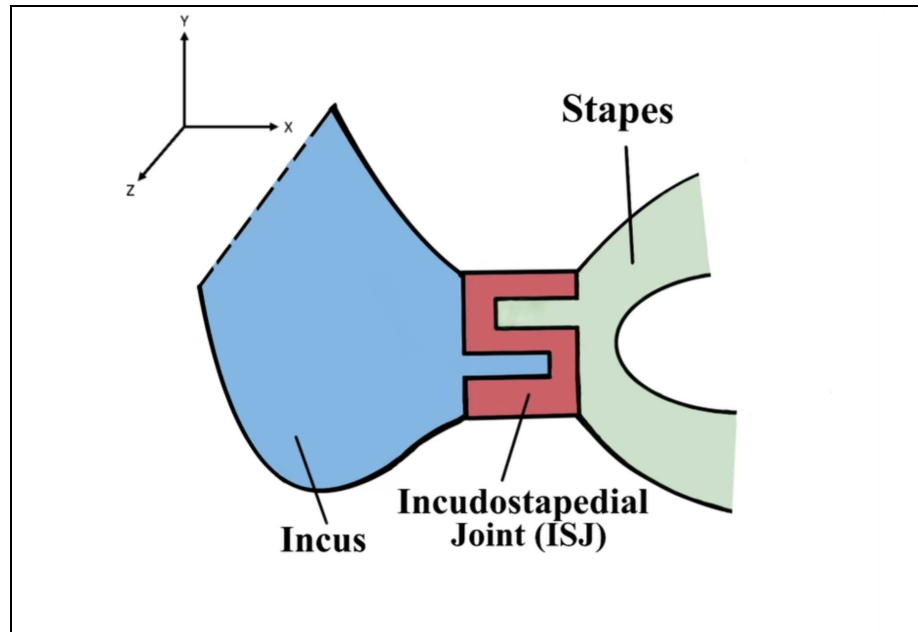


Figure 4.4: ISJ Design Option B

Table 4.24: Pros and Cons of ISJ Design Option B

Pros	Cons
<ul style="list-style-type: none"> <li>• Deep connection points into the molded ISJ from Incus and Stapes</li> <li>• Looser mold that will allow for some freedom of translation in the X and Z axis from Incus and Stapes</li> </ul>	<ul style="list-style-type: none"> <li>• Connection extrusions from Stapes and Incus are offset which could affect accurate transmission through joint when vibrations occur</li> <li>• Many thin silicone walls in the molded piece which could easily tear during assembly</li> </ul>



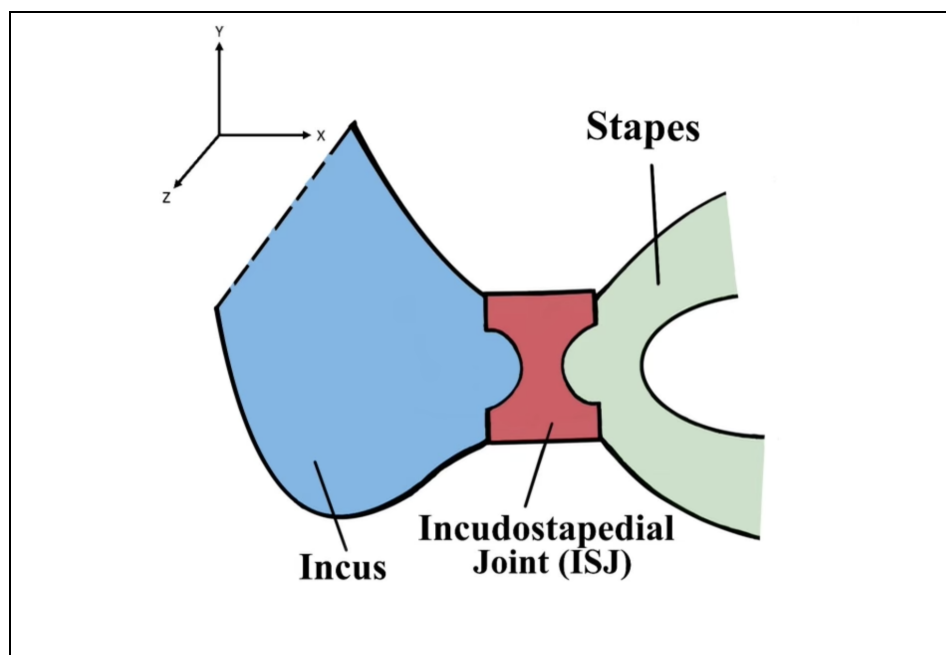


Figure 4.5: ISJ Design Option C

Table 4.25: Pros and Cons of ISJ Design Option C

Pros	Cons
<ul style="list-style-type: none"> <li>• No alterations to the Stapes or Incus necessary</li> <li>• Loose connection surfaces Incus and Stapes to show more realistic motion.</li> </ul>	<ul style="list-style-type: none"> <li>• Connection geometry between joint and ossicles are looser which could cause the Incus to slip into incorrect positioning similar to March 2022 model</li> </ul>

The final design that was pursued was option C due to its ability to more realistically represent the ossicles motion. The next challenge consisted of creating a mold to fabricate the ISJ out of the desired silicon material. In order to quickly iterate through design choices, the lab's Anycubic Photon Mono was utilized. This printer had Anycubic basic resin which once UV cured, offers a very hard mold material. There were two mold type options: reusable and disposable. Reusable molds allow for many molded bodies to be fabricated from a single mold while disposable molds are usually destroyed in order to get the molded part out. The chosen ISJ design had a relatively simple geometry which is why a reusable design was used. Figure 4.6 shows the design option C modeled in Solidworks. The 3D design consists of two rectangular prisms with two different sized spherical shapes cut into them that were measured to fit onto the geometry of the Incus and Stapes.

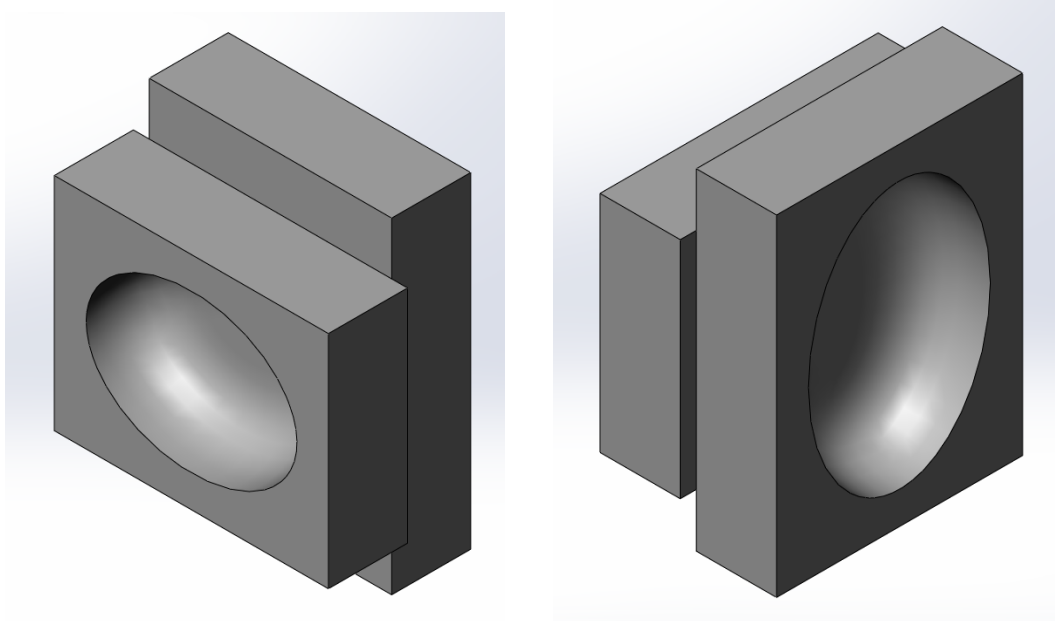


Figure 4.6: ISJ Molded Design Option C

From here an exterior mold was created around the design. A wall thickness of 4mm from outer mold to inner mold was used in order to ensure mold durability. A fill hole designed to have a diameter of 5mm so that a plastic squeeze nozzle could easily be placed in for filling was added. This design can be seen in Figure 4.7.

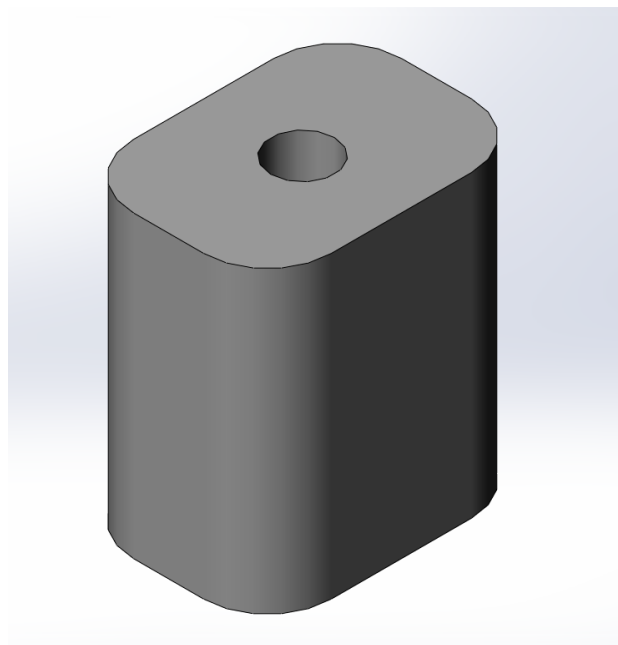


Figure 4.7: ISJ Mold Exterior

To make the mold reusable, it needed to be divided into separate pieces so that it could be disassembled to remove the molded part. This mold design is a rectangular prism with filleted edges. To divide the mold into equal rectangular prism pieces, there are three slices that can be made which are along the top, front and right planes. This means up to eight pieces can easily be created if the mold is sliced three times (Figure 4.8).

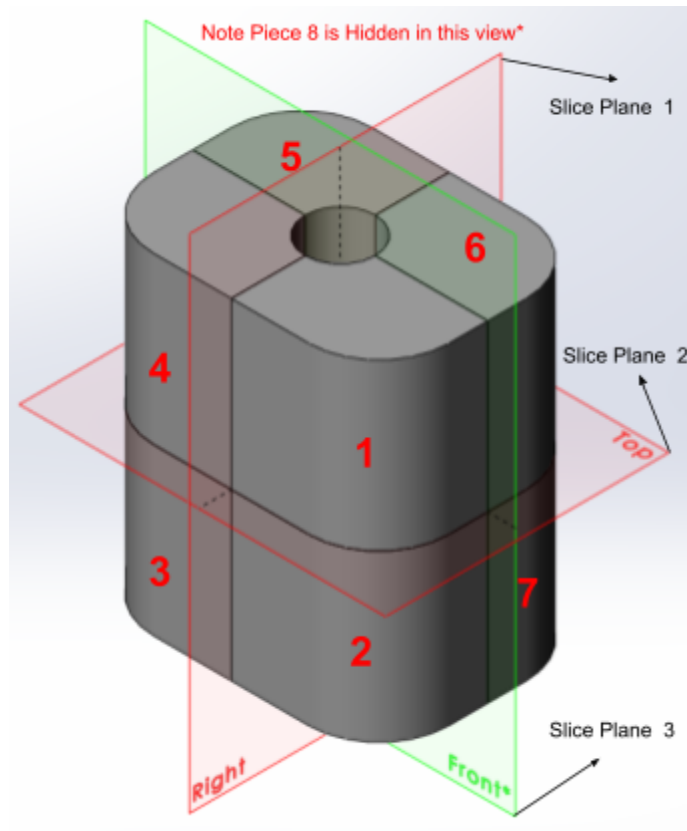


Figure 4.8: Sliced ISJ Example (Three Slices Eight Pieces)

Although possible, It is simpler if only one or two slices are made dividing the mold into two or four parts respectively. After analyzing the mold geometry it was recognized that an easy division could be made along the front plane (Figure 4.9 and 4.10) which allows the molded part to easily be removed. Basic recognizing features were also added in order to help the mold more easily fit together.

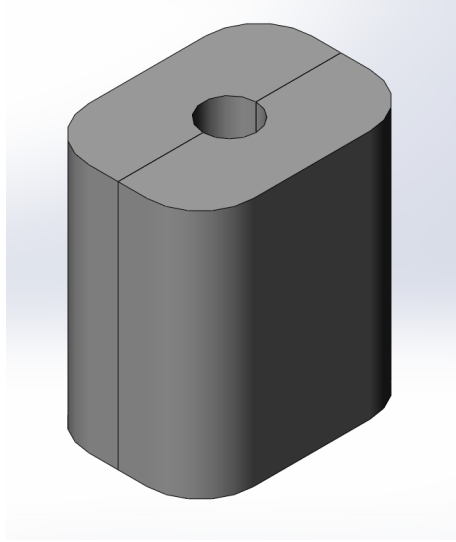


Figure 4.9: Sliced ISJ Mold Exterior

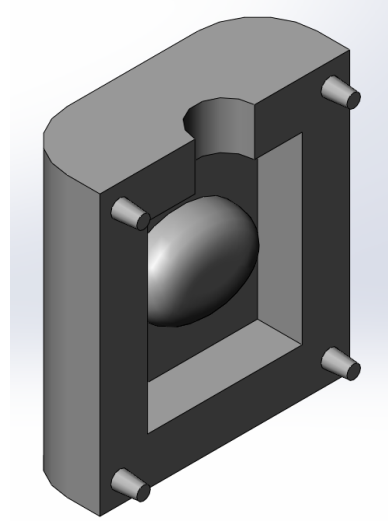


Figure 4.10: Sliced ISJ Mold Interior

## 4.6 IMJ CAD Design

Molding the IMJ was more complicated than molding the ISJ. Unlike the simplistic design of the ISJ, the IMJ model was initially created from a point cloud from a CT scan. The data was transferred into the Geomagic software and then converted into an .stl file type, storing the IMJ in basic points, lines, and simple geometry as seen in Figure 4.11.

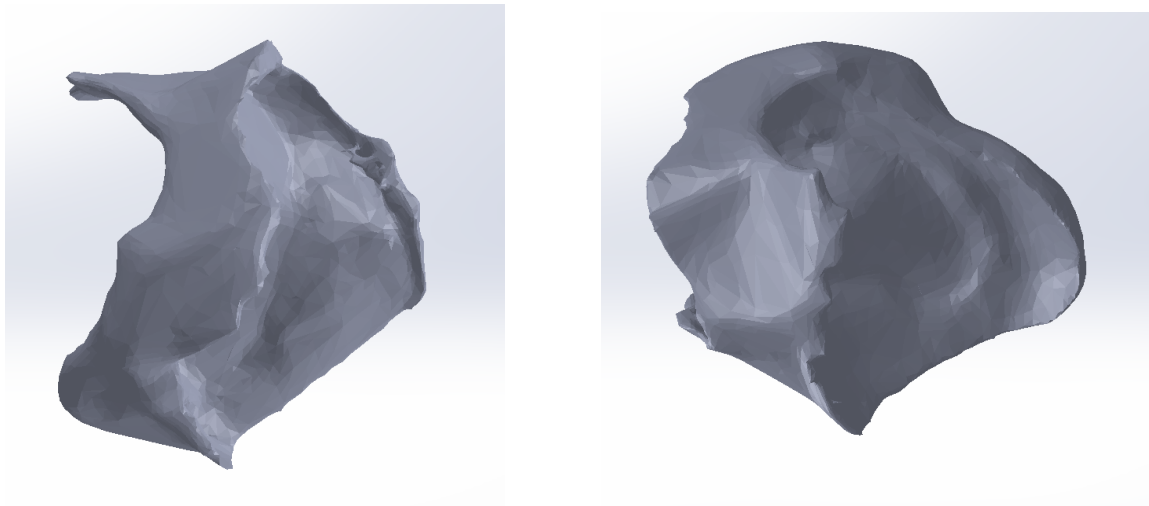


Figure 4.11: Original IMJ Design

The initial approach pursued mold creation by converting the .stl into a Solidworks part file. The model could be used to hollow out a cube or cylinder to create the mold design. The

slicing feature would be utilized in order to divide the mold into pieces, similar to the ISJ. Due to the geometry of the IMJ, deciding where to create these slices was much more difficult, needing to be sliced in locations that would allow for the complex molded piece to be easily removed. The first major problem that was noticed in this process was that when the .stl file was imported into Solidworks, the file was transferred into a surface instead of a solid body, meaning the model was hollow and unable to be used to easily create a mold. Different trajectories emerged in how to solve this problem.

#### 4.6.1 IMJ Software Exploration

Although Solidworks is a great parametric modeling tool, one limitation is its ability to recognize and process advanced files. Therefore for the IMJ mold, other softwares were explored for their ability to process advanced geometry and surfaces. Two softwares that were looked at were Geomagic and Blender. Geomagic is a software focused on computer-aided design, with an emphasis on 3D scanning. This software was used to create the .stl files for the realistic ossicles that were 3D printed in the model. Geomagic is proficient at allowing the user to simplify and edit surfaces of 3D bodies. The Blender software was also explored for its ability to work with surfaces, and its wide range of design options and tools that can be tailored towards this problem.

#### 4.6.2 Molding Original IMJ Geometry

An attempt was made to make a reusable mold out of the March 2022 groups IMJ design. In Blender, the IMJ design was placed overlaying a cube (Figure 4.12) and overlapping material was removed, shown in Figure 4.13.

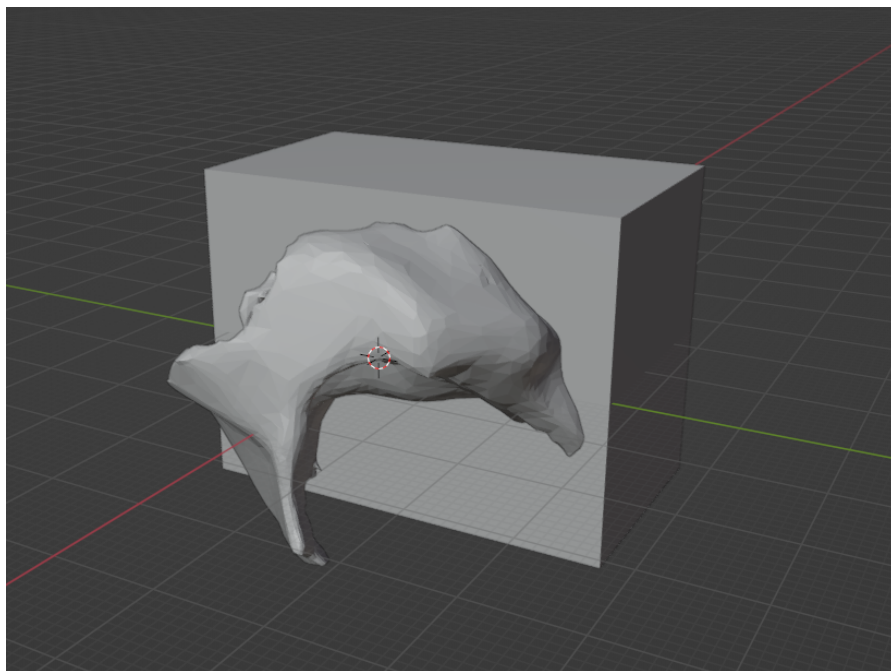


Figure 4.12: Cutting of IMJ out of Half Cube Mold (Blender)

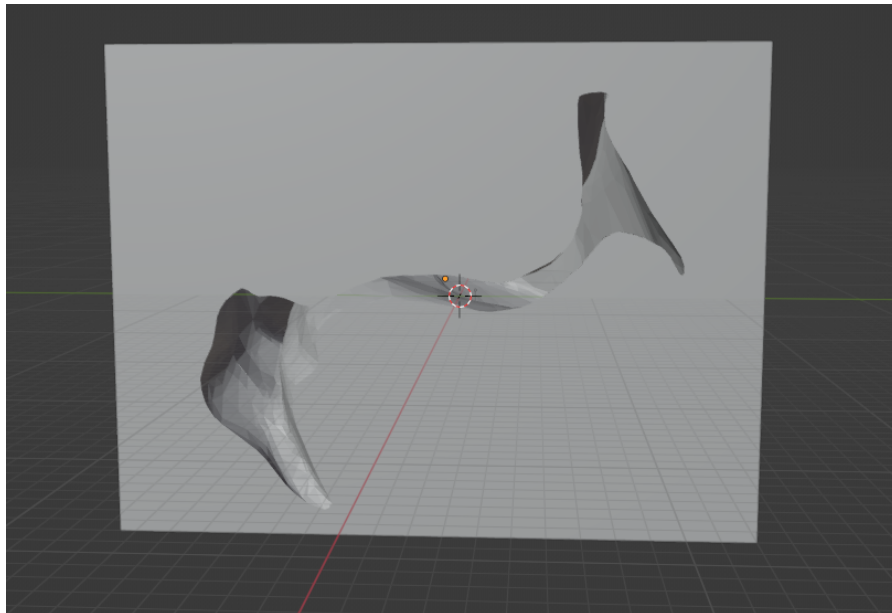


Figure 4.13: IMJ Cut out of Half Cube Mold (Blender)

In Figure 4.13, it becomes clear that the molded IMJ would be very thin in some sections and would be prone to tearing. The geometry of the molded IMJ also twists deep within the mold making removal of the molded piece without destruction of the mold difficult. Attempts were made to divide the mold in four and eight sections. (Figure 4.14).

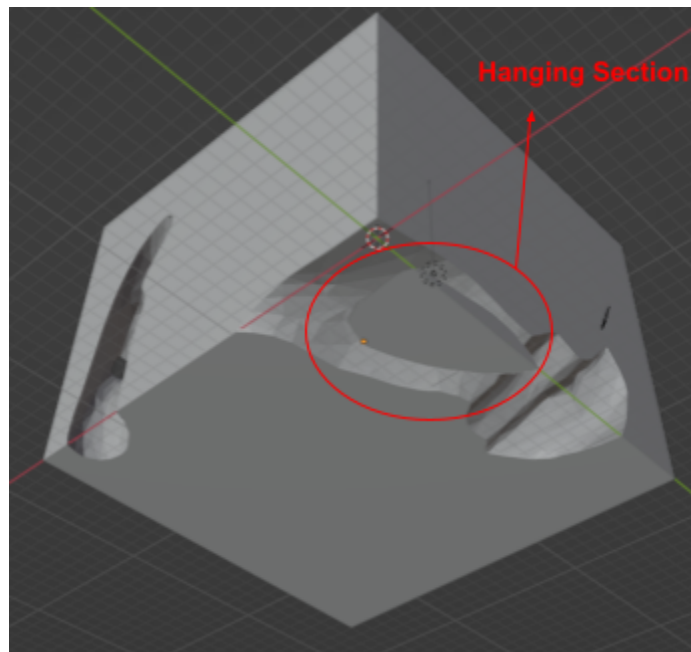


Figure 4.14: IMJ Cut out of Eighth Cube Mold (Blender)

Some sections of the molded part were still not removable. Simplifying the geometry of the IMJ was explored further as molding with the current IMJ design was not a viable solution.

#### 4.6.3 IMJ Model Simplification

The goal of not simplifying the March 2022 IMJ design came from the notion that keeping the CT scanned IMJ data would provide the most anatomically correct IMJ for the model. Yet, after a discussion with Dr. Dobrev, it came to light that the current IMJ model provided by the March 2022 group was not very anatomically accurate. This is because when a CT scan taken of the middle ear occurs, it has difficulty distinguishing between the soft tissues due to their similar densities. This causes the ligaments connected near the IMJ to mesh into the joint on the CT scan. This enlarges the scanned image of the IMJ, making it less accurate. As a result, the IMJ used by the March 2022 project team was simplified.

This simplification took place in the Geomagic software for a variety of reasons. First before the IMJ was converted into an .stl file, it was a Geomagic file that also contained the Incus and Malleus. This helped the simplification process as it allowed for the Incus and Malleus to be references to where the cuts in the IMJ should be made (Figure 4.15).

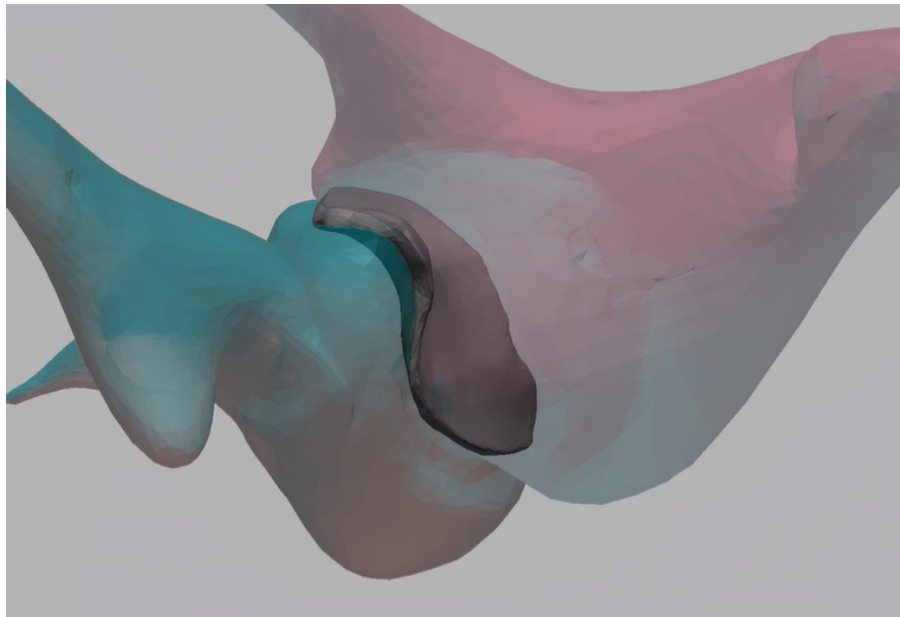


Figure 4.15: Simplified IMJ with Incus and Malleus

From here superfluous material was selected and deleted, demonstrated in Figure 4.16.

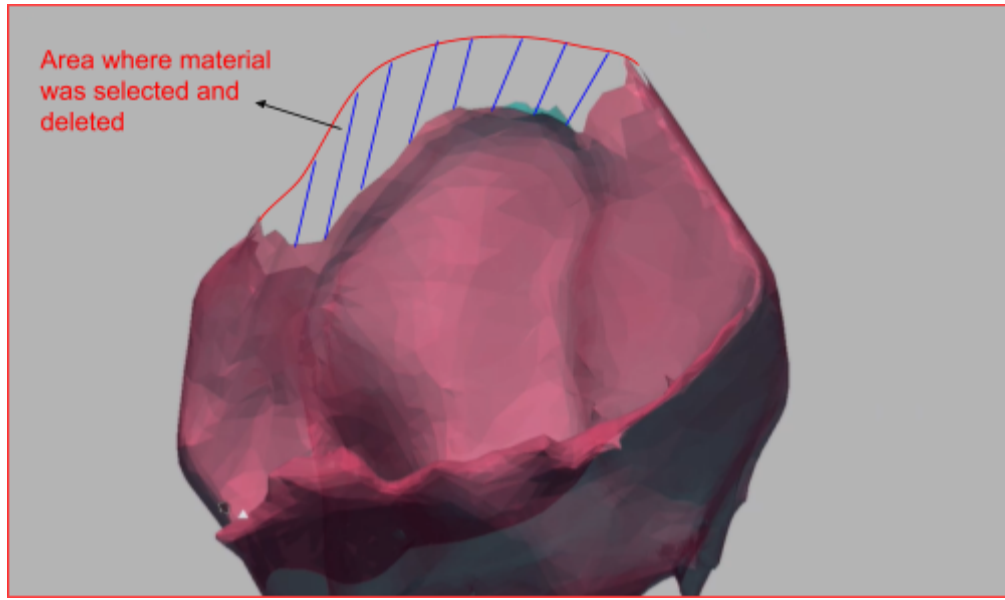


Figure 4.16: IMJ Simplification Process in Geomagic

This model is only a surface and not a solid body, so when these material removals are done, a void is left behind. These voids were filled by selecting both edges of the IMJ left after the material removal and a bridging feature to recreate a closed surface. Finally after this procedure was done around the entire edge of the IMJ, a smoothing feature was used where the bridges were created to smooth and simplify the IMJ mesh. Figure 4.17 shows the simplified IMJ compared to the original.

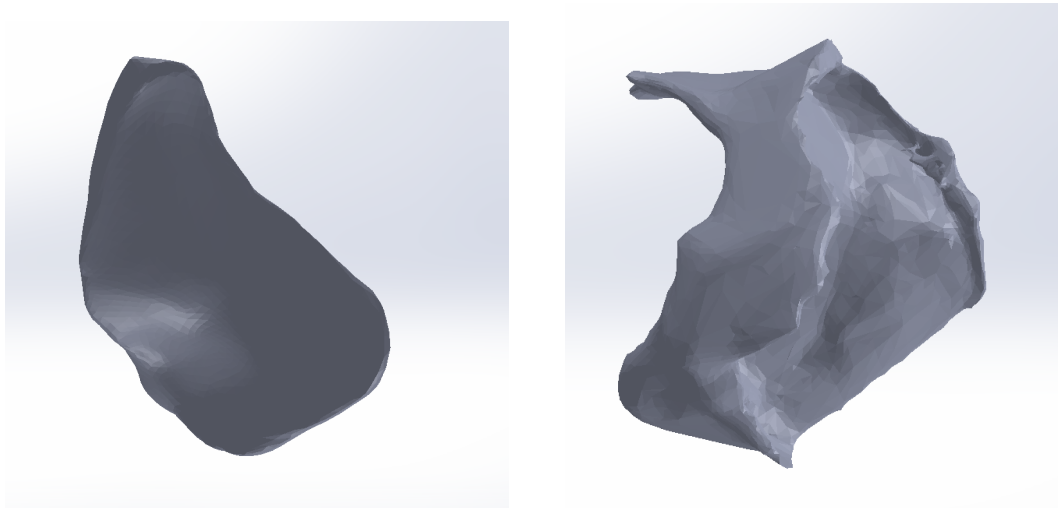


Figure 4.17: Simplified IMJ Design vs. Original IMJ Design



#### 4.6.4 Molding of Simplified IMJ

One of the benefits of the simplified IMJ is its decreased geometric complexity. The new IMJ design was turned into a mold similar to the method used on the previous design. Figure 4.18 shows the resulting design.

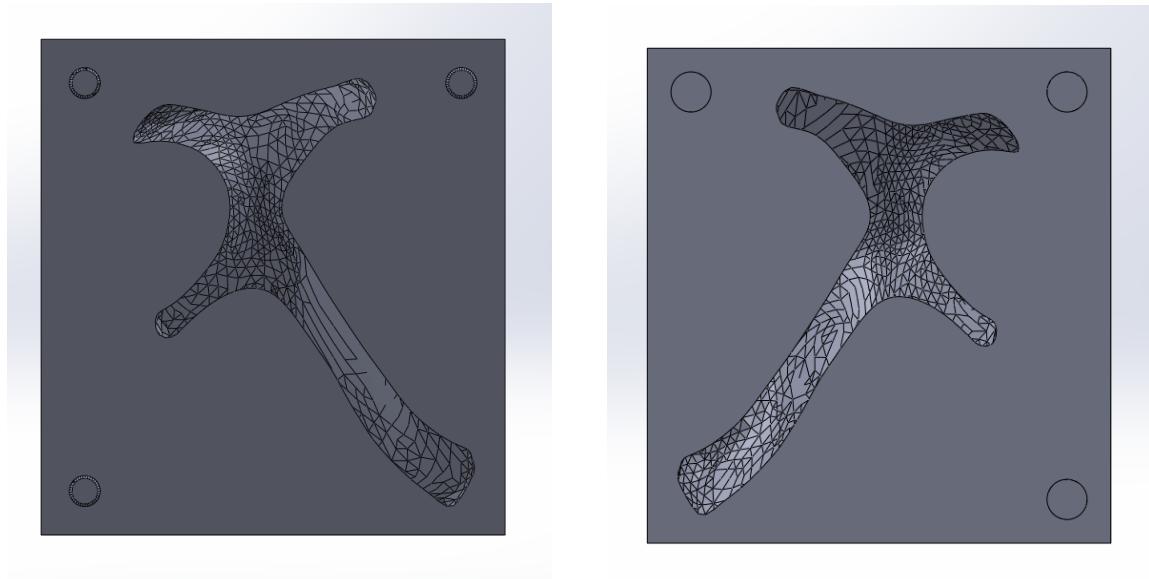


Figure 4.18: First Molding Attempt with Simplified IMJ

One problem with this mold was that sections of the molded part were still difficult to remove due to the mold being sliced on a flat plane. An approach was taken attempting to cut the new IMJ design along the bridged surface created during the simplification process. One of the benefits of the simplified IMJ mold was that the bridged surface created around the edge of the IMJ was primarily flat. This meant that if the mold was sliced along this edge, both halves of the mold should be open allowing for the molded part to be removed easily. This allowed for development of the IMJ mold that would be used for the rest of the project (Figure 4.19).

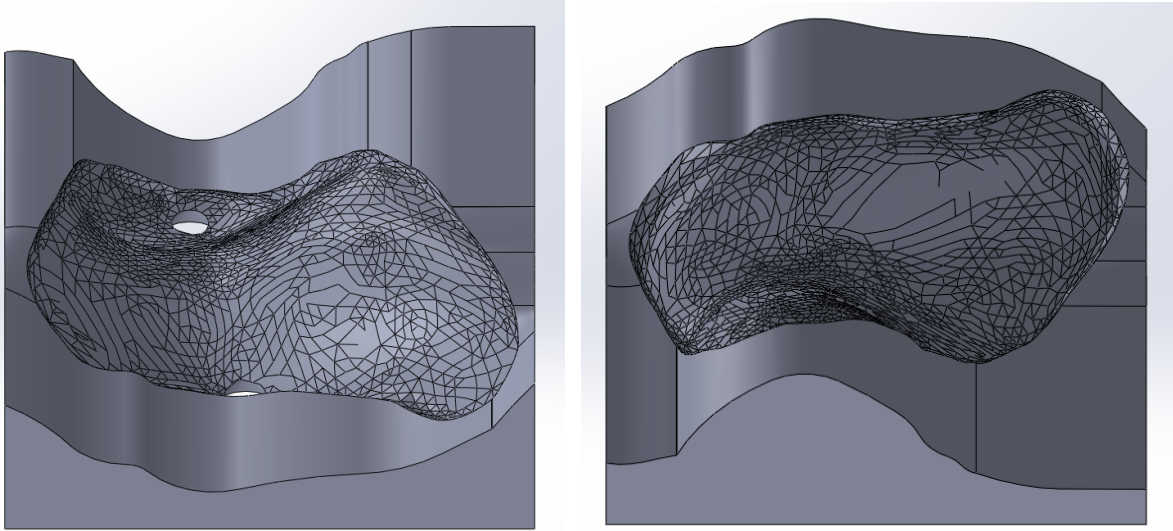


Figure 4.19: Final IMJ Mold Design

## 5.0 Final Design Verification

This section includes a description of mold creation, silicone molding process, vibration testing, and system stiffness testing.

### 5.1 Mold Creation

The team tested multiple mold options for the silicone joints in the model. This section includes the different options that were explored during this process.

#### 5.1.1 Mold Testing

The team experimented with multiple molding options to create the silicone IMJ and ISJ. The best option for molding a specific geometry was using a 3D printed resin on the lab SLA printer. The feasibility of 3D printing a reusable mold with the complex geometry of the IMJ was not trivial. While developing the 3D printing mold, the team also experimented with other molding options. These options were weighed within the Pugh decision matrix in Section 4.4.2.

White casting powder, wax, modeling clay, and porcelain clay were deemed the best suited options for the mold. As shown in Table 5.1, each material was spread onto a petri dish and objects were pressed into it to imprint the material. Objects were selected to encompass a variety of surface finishes and geometry. The objects chosen were: a chapstick cap, a quarter, a Thorlabs clamp, and a small resin 3D printed IMJ. After leaving the objects overnight for the material to solidify, the objects were carefully withdrawn from the material and the imprints were evaluated. After this initial assessment, the molds were filled with silicone in order to evaluate their compatibility with the silicone material and how well the details transferred from the mold to the silicone.

Mold assessments prior to adding silicone were based on the following factors; ability to mold detail, ability to withdraw objects without breaking the mold, and ease of use. Ability to mold details was assessed by collecting qualitative data on how well the small objects left imprints within the molding material. The ability to withdraw the object was evaluated by testing how much force was needed to withdraw the objects being imprinted without destroying the mold or the details imprinted. The ease of use was assessed by how easy it was for the material to be molded to create a specific imprint.

Mold assessments after molding with silicone were based on the following factors; compatibility with silicone, the ability to transfer details to silicone, and ease of use. Compatibility with silicone was assessed by how difficult it was to remove the silicone from the mold and if the material left residue. The ability to transfer detail was assessed by the amount of detail shown in the silicone. The ease of use was evaluated by determining how difficult it was to create the mold and withdraw the objects from the material.

The four different molding materials are shown in the table below along with the objects being molded, the molds after the objects were withdrawn, and the silicone that was created from

the molds. Qualitative data is also included from the factors evaluated. Both the porcelain and modeling clay were not well-suited based on their compatibility with silicone. The porcelain clay left debris on any surface it came in contact with and the modeling clay was too dense to capture the intricate details of the mold. Therefore, only the Thorlabs clamp was tested in porcelain and modeling clay.

Table 5.1: Testing of Different Material Molding Options

Type of Mold	Mold with Objects	Imprint Left by Objects	Silicone Molded
Wax			
Casting Powder			
Modeling Clay			
Porcelain Clay			

Qualitative data and observations were taken on a scale from 1-5, and are displayed in Table 5.2. One being the least favorable, and five being the most favorable.

Table 5.2: Qualitative Data and Observations on Different Material Molds

Type of Mold	Qualitative Data	Observations
Wax	Ease of Use: 4/5 Compatibility with Silicone: 5/5 Ability to Show Details: 4/5 Transfer of Details to Silicone: 5/5 Withdrawal of Silicone from Mold: 4/5	<ul style="list-style-type: none"> <li>• Took a long time to heat up</li> <li>• Need to use glass petri dishes because of the heat</li> <li>• Easy to mold objects</li> <li>• Quickly dried around the objects</li> <li>• Showed great detail of the objects</li> <li>• No wax was transferred when removing the silicone</li> <li>• Silicone was easy to remove with simple geometric objects</li> <li>• The mold was not reusable when the shape geometry was complex</li> </ul>
Plaster	Ease of Use: 4/5 Compatibility with Silicone: 5/5 Ability to Show Details: 3/5 Transfer of Details to Silicone: 4/5 Withdrawal of Silicone from Mold: 4/5	<ul style="list-style-type: none"> <li>• Easy to mold objects in it</li> <li>• Showed great detail of the objects</li> <li>• No plaster was transferred when removing the silicone</li> <li>• Silicone was easy to remove with simple geometric objects</li> </ul>
Modeling Clay	Ease of Use: 3/5 Compatibility with Silicone: 1/5 Ability to Show Details: 3/5 Transfer of Details to Silicone: 3/5 Withdrawal of Silicone from Mold: 2/5	<ul style="list-style-type: none"> <li>• Was very dense</li> <li>• Difficult to imprint small details on objects</li> <li>• Removing the silicone while wet transferred clay onto the silicone</li> <li>• Removing the silicone when fully dry cracked the clay</li> </ul>
Porcelain Clay	Ease of Use: 4/5 Compatibility with Silicone: 2/5 Ability to Show Details: 2/5 Transfer of Details to Silicone: 3/5 Withdrawal of Silicone from Mold: 1/5	<ul style="list-style-type: none"> <li>• Porcelain clay was less dense than modeling clay</li> <li>• Left residue on objects while creating the mold</li> <li>• Removing the silicone while wet transferred clay onto the silicone</li> <li>• Removing the silicone when fully dry cracked the clay</li> </ul>



### 5.1.2 Final 3D Printed Mold Designs

Although a variety of mold testing was conducted in the previous section, the final molds were 3D printed using the Anycubic Photon Mono. The creation of these molds were documented in sections 4.5 and 4.6. The final molds were reusable and utilized recognizing features and fill holes for the silicon material. The final 3D printed molds for the ISJ can be seen in Figure 5.1, and the final 3D printed mold for the IMJ can be seen in Figure 5.2.

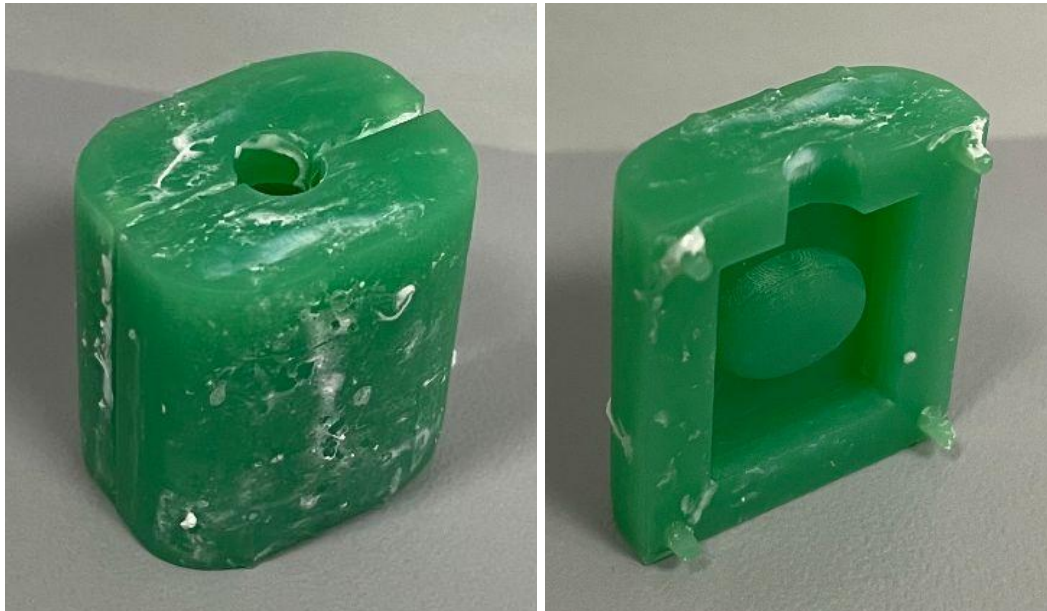


Figure 5.1: Final 3D Printed ISJ Mold Exterior and Interior



Figure 5.2: Final 3D Printed IMJ Mold

## 5.2 Silicone Stiffness Procedure

Silicone is created by adding a crosslinker to an elastomer base. Changing the amount of crosslinker changes the stiffness of the resulting silicone. A lower percentage of crosslinker will result in a lower stiffness and a higher percentage of crosslinker will result in a higher stiffness in the sample (Wang et al., 2014). Table 5.3 shows the amounts of elastomer base and crosslinker used to create the IMJs.

Table 5.3: Amounts of Elastomer Base and Crosslinker Used to Create 5 IMJs

Variation of Stiffness (1-5)	Elastomer Base	Crosslinker
1	9.85g	0.15g
2	9.75g	0.25g
3	9.65g	0.35g
4	9.55g	0.45g
5	9.45g	0.55g

### Materials:

- Silicone NV
- Plastic Stirrers
- Plastic Beaker
- IMJ Molds

### Procedure for Each Silicone IMJ:

1. The scale was zeroed
2. The plastic beaker was weighed on the scale and zeroed
3. The specified amount of silicone without crosslinker was poured into the beaker on the scale to measure out the exact amount
4. The specified amount of crosslinker was poured into the beaker on the scale to measure out the exact amount
5. The stirrer was used to create a homogeneous mixture within the silicone and crosslinker
6. The mixture was then poured into the mold
7. The mold was checked for air bubbles through the fill holes and was set to dry

## 5.3 Vibration Testing

The project team performed vibration testing on the model in an attempt to demonstrate similar trends to the middle ear. This section includes information on calibration, test procedure, and data from the vibration testing.

### 5.3.1 Calibration of Accelerometers

Accelerometers were used to measure vibration on the model. In order to do so, the accelerometers first had to be calibrated. Appendix B outlines the calibration procedure for the Z-axis of two accelerometers. Appendix C includes justification for the calibration methods outlined in Appendix B. Appendix D contains a graph of the appropriate correction factors calculated during calibration.

### 5.3.2 Test Procedure

This section contains the test procedure used to gather data pertaining to the input and output of the middle ear assembly.

- Equipment
  - Laptop with APx and MATLAB software installed
  - 2 - ADXL335 Accelerometer
  - Small Speaker
  - Audio Precision 585 multichannel audio analyzer (DAQ)
  - QSC RMX 850a Professional Amplifier
  - 10 N Force Meter
  - Functional Model of the Middle Ear
  - 5 IMJs, with different stiffnesses
- Assumptions
  - Assumes Accelerometers are aligned perpendicular to respective membranes
- Wiring

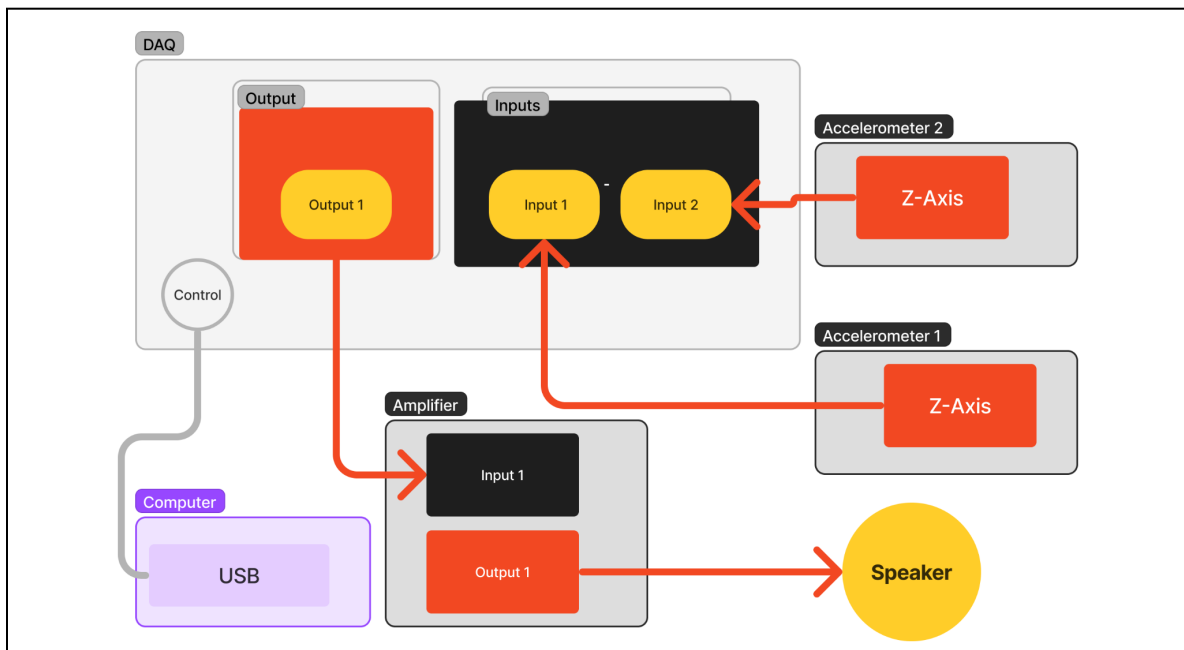


Figure 5.3: Wiring Diagram of Accelerometer Test Setup



- Description of the wiring:
  - With this setup, the software will output a signal to the DAQ, which passes through the amplifier. After going through the amplifier, it goes to the speaker, dictating the magnitude and frequency of its vibrations. Simultaneously, the software displays the measurements from the z-axis of each accelerometer, with the data coming through the DAQ. Figure 5.3 shows this wiring setup.
- Description of the setup shown in Figures 5.4 and 5.5:
  - Use magnets to attach accelerometer 1 to the umbo, with the z-axis aligned in the direction of motion.
  - Use magnets to attach accelerometer 2 to the stapes footplate, with the z-axis aligned in the direction of motion.
  - Attach a small piece of foam to the speaker.
  - Position the speaker so the foam is in contact with accelerometer 1, so when the speaker is actuated it will mechanically stimulate the middle ear assembly.

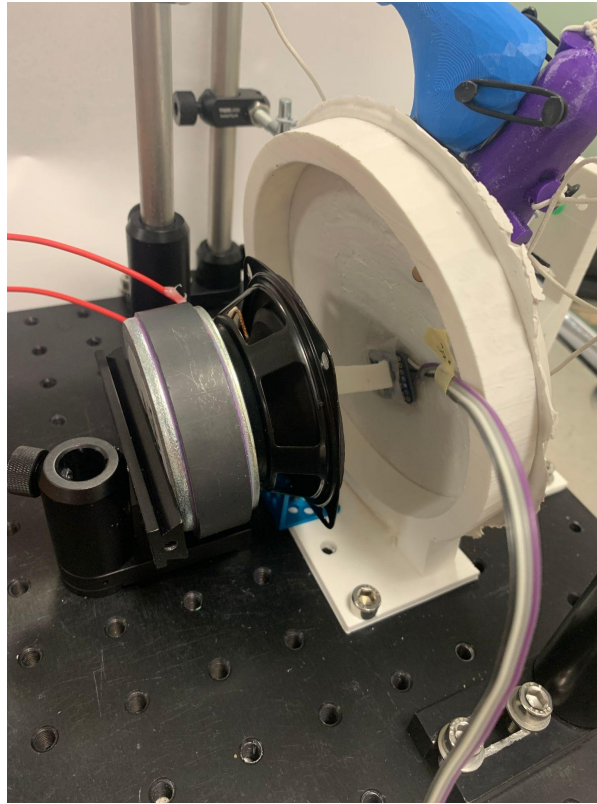


Figure 5.4: Mechanical Actuation of the Model

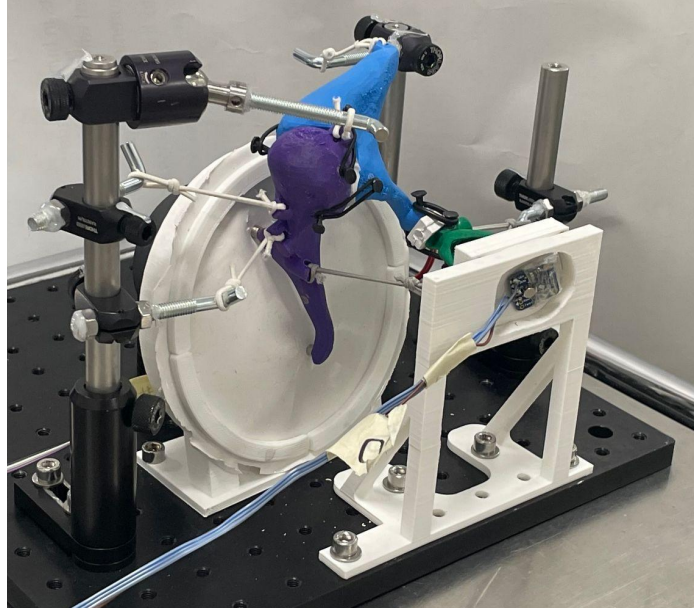
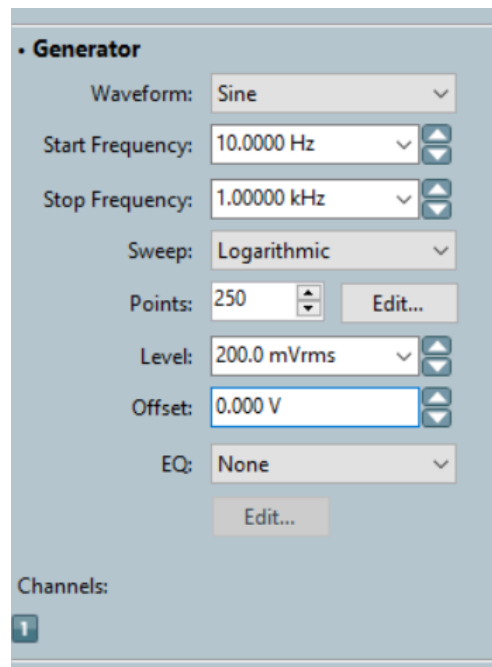
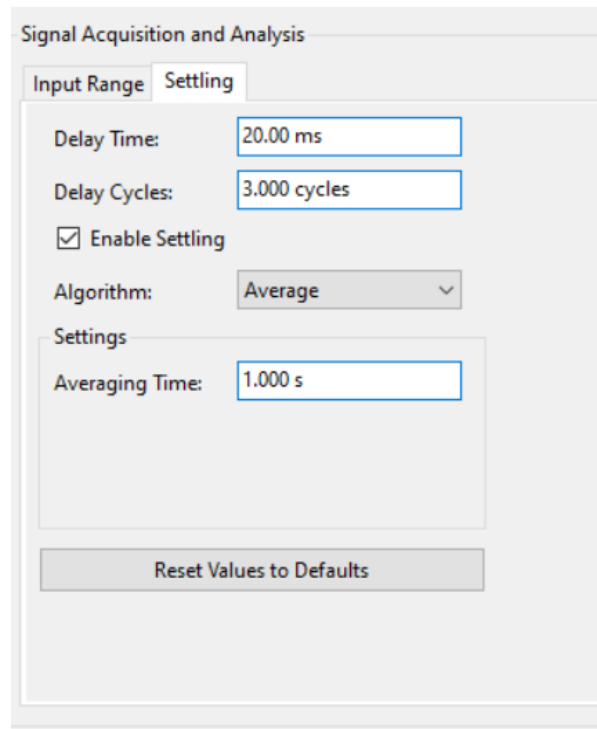


Figure 5.5: Accelerometer Placement on Oval Window

- Figures 5.6 and 5.7 show settings used in the APx software.



- Figure 5.6: APX Settings for Calibration of Accelerometer



○ Figure 5.7: APX Settling Settings for Calibration of Accelerometer

- Data Acquisition
  - Run one sweep with the speaker unplugged, to establish a noise floor.
  - For each of the IMJs:
    - Run 3 identical sweeps at the above settings, using Sequence Mode in the APx Software.
  - Load Testing:
    - Run one sweep with IMJ 1, with no load applied.
    - Run one sweep with IMJ 1, with a 0.5 N force on the Umbo, pulling towards the middle ear.
    - Run one sweep with IMJ 5, with no load applied.
    - Run one sweep with IMJ 5, with a 0.5 N force on the Umbo, pulling towards the middle ear.
- Data Analysis:
  - Download the output data into Excel.
  - Using Matlab, perform the following:
    - If applicable, average the Vrms output at each frequency for each accelerometer.
    - Mask these averaged numbers, by replacing each one that is less than  $3 \times$  the noise at that frequency with “NaN.”
    - Convert the averaged numbers from Vrms to g, and apply the appropriate conversion factors, shown in Appendix B.

- Calculate the ratio of accelerometer 2 acceleration to accelerometer 1 acceleration at each frequency for each IMJ.

Appendix E Contains the Matlab Code Used for this process.

### 5.3.3 Results

This section contains the data collected during testing with the accelerometers. Figures 5.8, 5.9, and 5.10 show the results of the data taken. Figure 5.8 shows a graph where each line represents a different IMJ. The Y-axis is the ratio of accelerometer 2 to accelerometer 1, also considered the transfer function across the model, and the X-axis is frequency. In each case the first natural frequency of the system occurs between 30 and 50 Hz, but no clear trend exists with the stiffening of the IMJ.

Figure 5.9 contains data pertaining to IMJ 1. The blue line represents data taken with no load applied, and the red line represents data taken with a 0.5 Newton force applied on the Umbo in the direction of the middle ear. This force simulates a positive pressure in the ear canal, as discussed in section 2.4.1. Figure 5.10 contains data taken with IMJ 5. The blue and red lines represent the same as in Figure 5.9. Two conclusions can be drawn about the first natural frequency with IMJ 1 in Figure 5.9. The application of a load shifts the first natural frequency slightly higher and marginally reduces its resulting transfer function. Figure 5.10 shows a slight increase in the location of the first natural frequency and a slight increase in transfer function at this new location. Comparing the two shows that both first natural frequencies trend upward with the application of a load while the magnitude of the transfer function at this point decreases for IMJ 1 and increases for IMJ 5.

IMJ 1 can be considered similar to the flexible IMJ discussed in section 2.4.1, and IMJ 5 can be considered similar to the fixed IMJ. Section 2.4.1 describes how a research team discovered that in a human middle ear, the application of a load on the Umbo in the direction of the middle ear has different effects based on the flexibility of the IMJ. The load on a flexible IMJ resulted in a slightly higher first natural frequency, with a slightly lower magnitude. The load on a fixed IMJ resulted in a similarly greater first natural frequency and a larger reduction in magnitude. The trends shown in the functional model partially match the trends seen in the real middle ear. Both IMJ 1 and IMJ 5 show a similar shift upwards in frequency of first natural frequency with the application of the load, but the magnitude differences do not follow the trend set by the human middle ear.

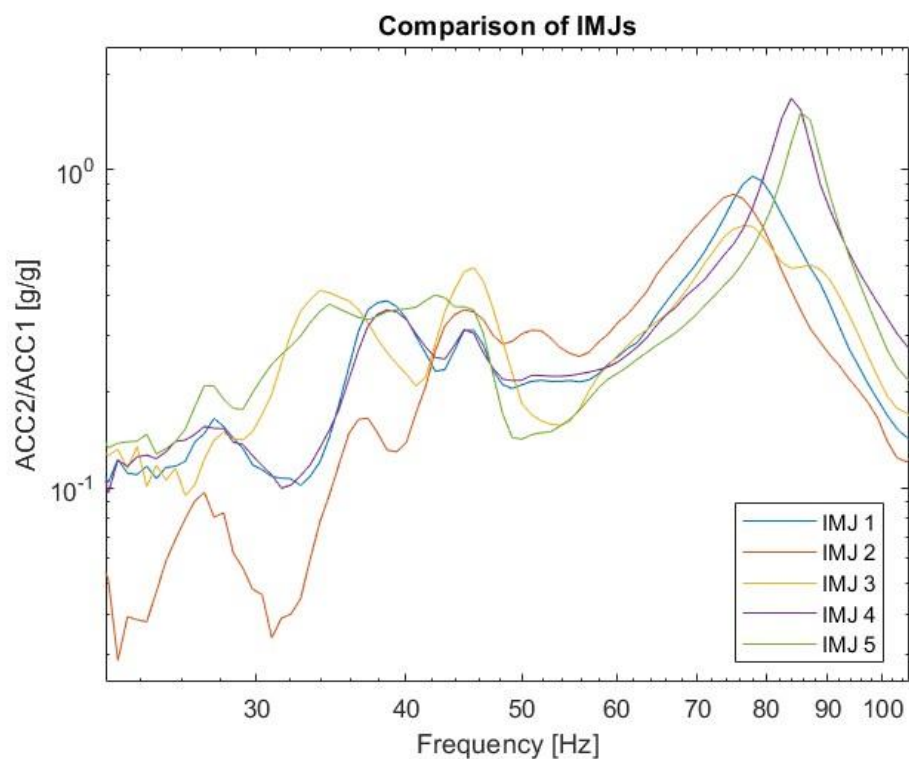


Figure 5.8: Sweeps of each IMJ

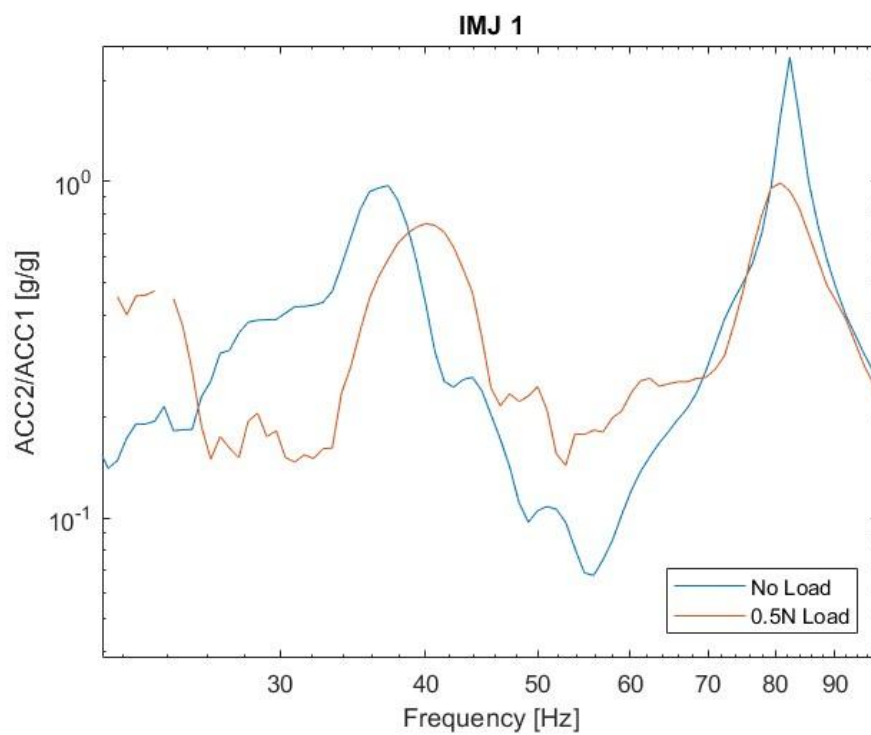


Figure 5.9: IMJ 1 Load Application Results

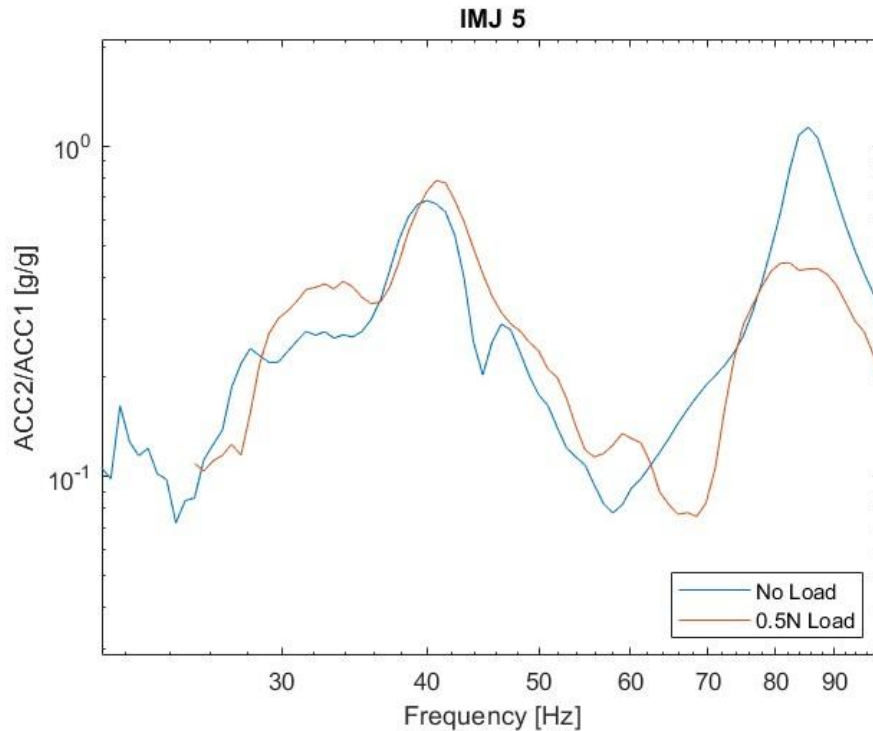


Figure 5.10: IMJ 5 Load Application Results

## 5.4 System Stiffness Testing

Stiffness testing was performed on the system to determine if the model could demonstrate similar trends to the actual middle ear. This section will discuss the camera calibration, test procedure, and resulting data of the stiffness testing.

### 5.4.1 Calibration of Cameras

Two USB cameras were used to track the displacement of the model. The cameras had to be calibrated before testing to ensure that the cameras were both accurate and precise in recording the displacements, which were on the order of millimeters. Appendix F contains the procedure used for calibrating the cameras.

### 5.4.2 Test Procedure

This section contains the test procedure used to gather data pertaining to the stiffness of the middle ear model.

- Equipment
  - Laptop with ISpy and ImageJ software installed
  - 2 USB Cameras
  - 10 Newton Force Meter

- Fluorescent point source microbeads (for point tracking)
- ThorLabs Pieces (for mounting cameras and force meter)
- Functional Model of the Middle Ear
- 5 IMJs, with different stiffnesses
- Assumptions
  - Cameras are aligned perpendicular to direction of displacement.
  - Displacement is occurring in the same direction as the force applied
- Description of the setup:

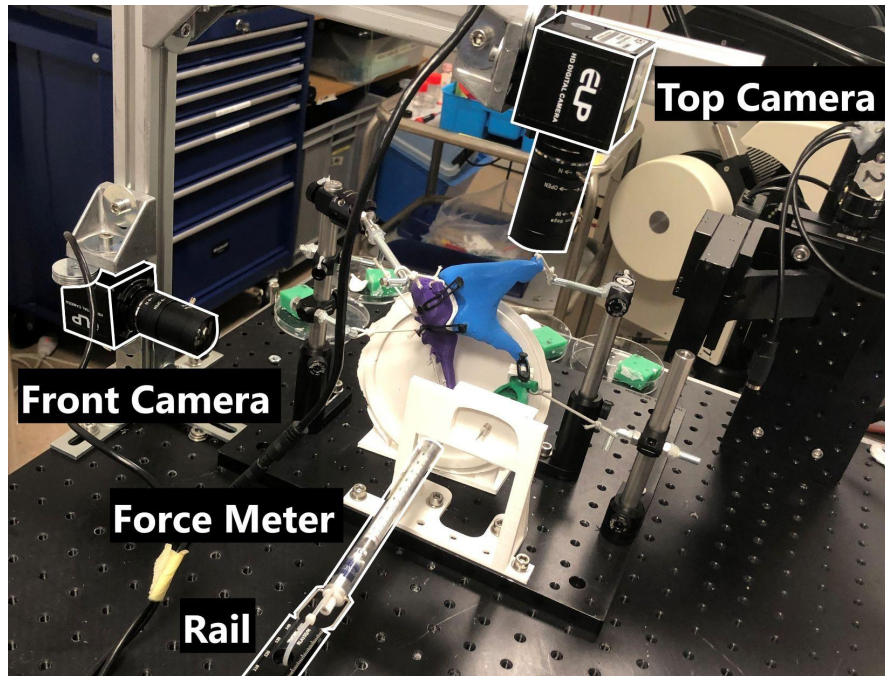


Figure 5.11: Stiffness Testing Setup

- Insert one of the IMJs into the model.
- Hook 10 N force meter to head of malleus with opposite end connected to a thorlabs rail that slides in one direction and can be tightened down.
- Mount cameras at a right angle to each other with a top and side view of the oval window. Cameras should be parallel to the oval window and perpendicular to the movement of the stapes.
- Connect cameras to a laptop, and use ISpy software to view both camera angles.
- Add magnets to the oval window where the stapes is attached, so that the camera view is on the magnets and perpendicular to the movement of the magnets (Figure 5.12).
- Place fluorescent microbeads at the head of the magnet (Figure 5.12). These will be used for point tracking in ImageJ.



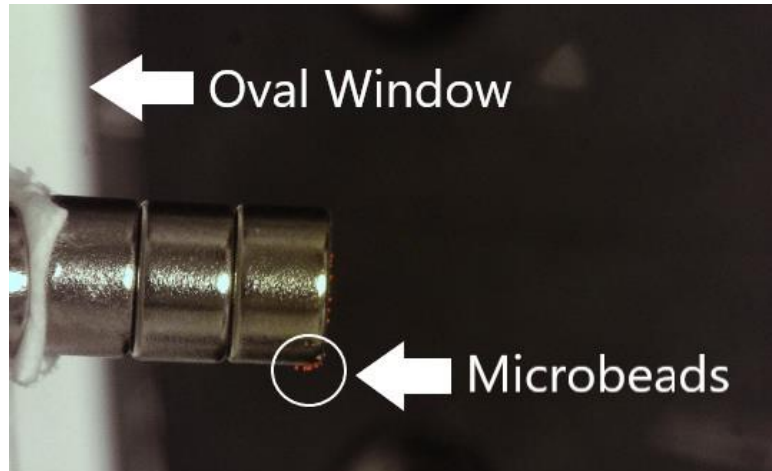


Figure 5.12: Top Camera View of Magnets at Oval Window

- Add a ruler to the frame to act as a frame of reference for data processing in ImageJ (Figure 5.13). One tick mark represents one millimeter.



Figure 5.13: Top Camera View with Ruler

- Data Acquisition
  - Begin by taking a picture of the magnets when no force is being applied.
  - Increase the force being applied to the system by pulling on the force meter with the slide and tightening it down at 0.2 N increments.
  - At each increment, take pictures of the magnets and save as jpg.
  - Change out the IMJ and repeat these steps for each of the five IMJs.
- Data Analysis
  - In ImageJ:



- Start by setting a global scale using the point of reference picture with the ruler (Figure 5.14)



- Use the Straight Line tool to draw a line from one tick mark to another on the ruler.
- Click Analyze > Set Scale... and put in the known distance of the line drawn and unit of length. For example, the line in Figure 5.14 is 0.5 mm based on the ruler and 112.0317 pixels based on the picture, resulting in a scale of 22.428 pixels/mm.
- Check mark global, so that the scale will be used in future pictures that are opened. Note: Make sure to redo these steps for each new trial or camera view.

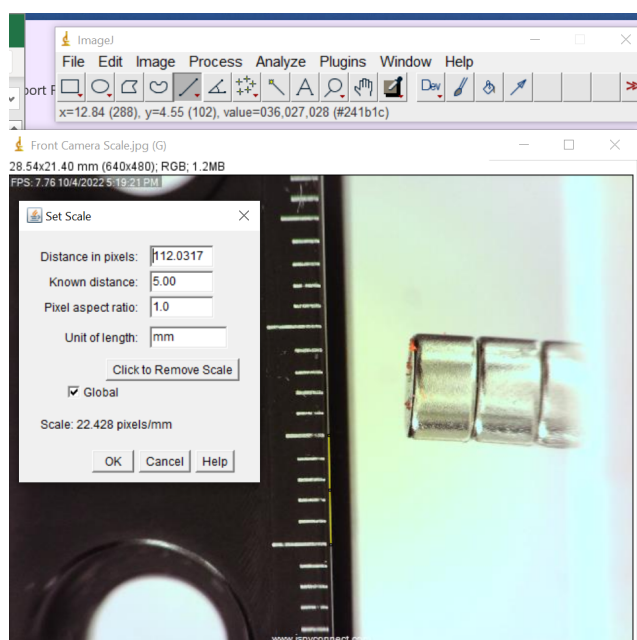


Figure 5.14: Using the Set Scale Tool in ImageJ

- Once scaling is complete, measure the distance between one fluorescent microbead and the end of the frame.  
Note: The end of the frame will not move over the course of one trial since the cameras and model are not adjusted or touched for the duration of the trial. The movement of the magnet at the fluorescent microbeads will then be measured with the end of the frame as the origin.



- Use the Straight Line tool to draw a line from the fluorescent bead to the end of the frame in the direction of the magnet movement (Figure 5.15).

Note: For the purpose of these tests, movement was only measured in the x-direction, so ensure that the angle of the line is at zero or 180 degrees so only movement in one direction is collected.

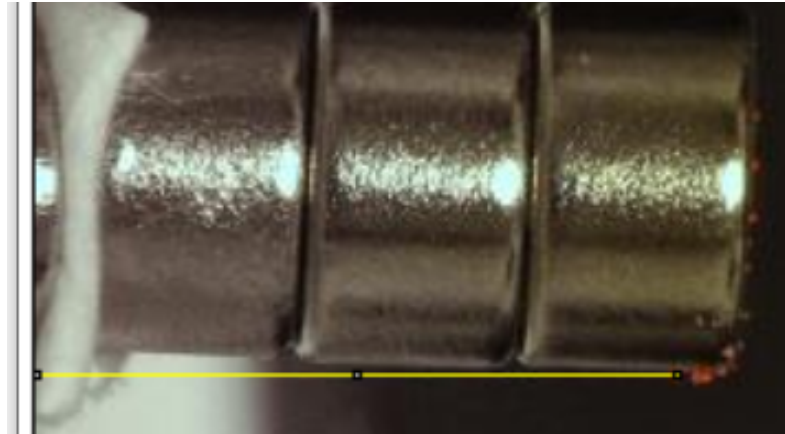


Figure 5.15: Line Measurement From One Microbead to End of Frame

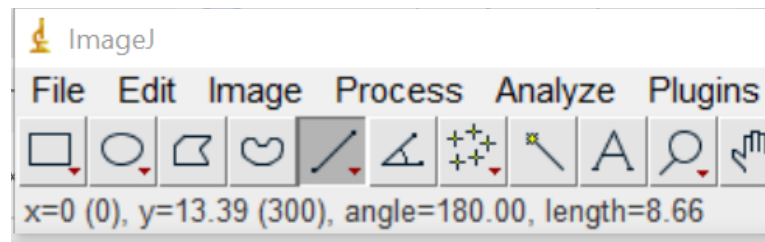


Figure 5.16: Angle (degrees) and Length (mm) of Line

- Repeat these steps for all trials.
- In Excel:
  - Collect all of the lengths for each force increment in Excel (Table 5.3).

Table 5.4: Initial Data Collection

Distance (mm)	Force (N)
9.23	0
9.44	0.2
9.72	0.4
9.92	0.6
10.18	0.8
10.43	1

- To get the displacement of the magnets from starting point to end point, subtract all the values by the distance between the microbead and end of

frame found at 0 N. This will mean that at 0 N there is a displacement of 0 mm.

Table 5.5: Displacement Data in Millimeters

Displacement (mm)	Force (N)
0	0
0.21	0.2
0.49	0.4
0.69	0.6
0.95	0.8
1.2	1

- Convert mm to m, so that when Force V Displacement is graphed the slope of the line, which will represent the stiffness, will be in N/m.

Table 5.6: Displacement Data in Meters

Displacement (m)	Force (N)
0	0
0.00021	0.2
0.00049	0.4
0.00069	0.6
0.00095	0.8
0.0012	1

- Plot Force vs Displacement and apply a linear trendline. Set the intercept to zero and add the equation and  $R^2$  value. The slope of this line represents the stiffness of the model with the given IMJ. For Figure 5.17, the stiffness of the model would be 841.82 N/m.

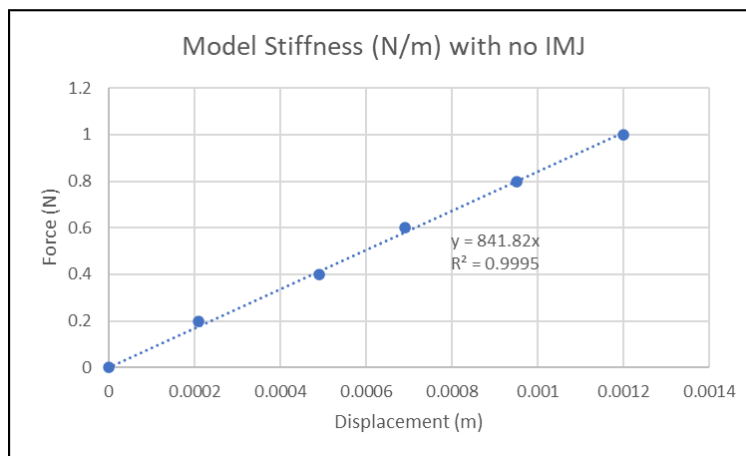


Figure 5.17: Force Displacement Graph of Middle Ear Model with No IMJ Inserted

### 5.4.3 Results

The results of the stiffness testing are split into two parts: the results of the IMJ stiffness testing and results found about the effect that ligament stiffness had on the model's overall stiffness.

#### 5.4.3.1 IMJ Stiffness Results

The average stiffness of the model with no IMJ inserted was 860.65 N/m (Figure 5.18).

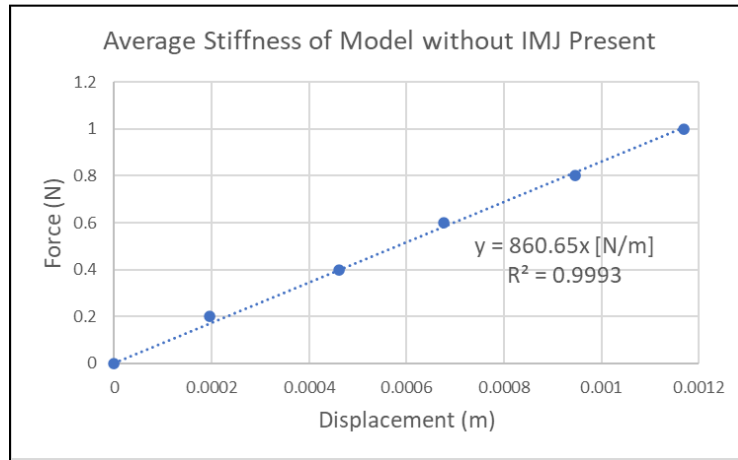


Figure 5.18: Average Stiffness of Model with No IMJ Inserted

The stiffness increased with the addition of an IMJ. However, when the five different IMJs were swapped in and out of the system, the stiffness of the system saw a decrease as the IMJ stiffness increased. When the model had the 1.5% crosslinker IMJ inserted, the average system stiffness was 1458.5 N/m while the 5.5% crosslinker IMJ yielded an average system stiffness of 1228.7 N/m (Figure 5.19).

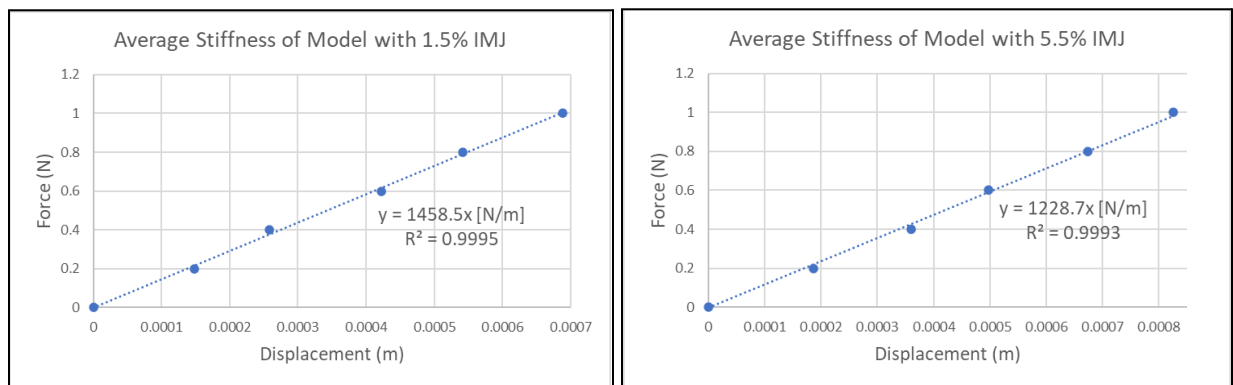


Figure 5.19: a) Average Model Stiffness for IMJ 1, b) Average Stiffness for IMJ 5

Additionally, the 2.5%, 3.5%, and 4.5% crosslinker IMJs yielded model stiffnesses of 1267.6 N/m, 1257.2 N/m, and 1121 N/m, respectively (Figure 5.20).

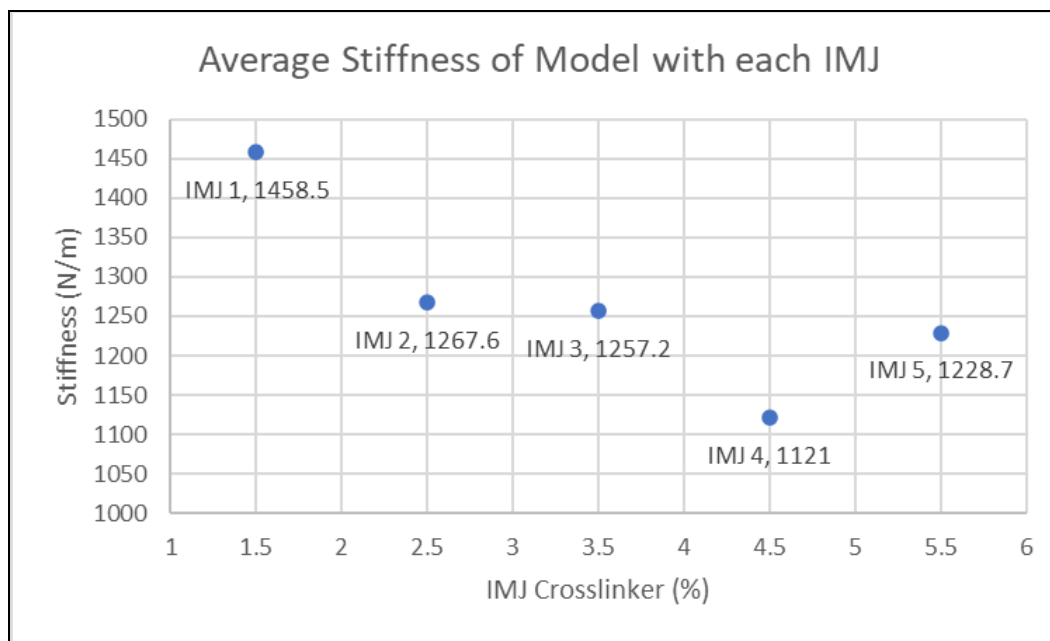


Figure 5.20: Average Model Stiffness per IMJ

There was not much variation seen in the model's stiffness when IMJs 2, 3, 4, and 5 were added. Throughout all the trials, these stiffnesses fell around similar values. For example, depending on the trial, the system stiffness of the model with IMJ 2 would fall both above and below that of the model with IMJ 3. Because of this, it can be assumed that the stiffness of the individual IMJs did not have an effect on the system. Instead, it is more likely that the slight changes occurred in the model when switching out the IMJ since removing and replacing pieces of the model could result in shifting and change in ligament tension.

The higher system stiffness with IMJ 1 added and lack of trend for the following four IMJs suggests saturation, meaning the IMJ stiffness no longer had an effect on the system. Rather, another part of the system was determining the stiffness.

#### 5.4.3.2 Ligament Stiffness Results

The ligaments had a much greater effect on the model's stiffness than the IMJ. The two ligament options chosen in the design process were both tested to see how the stiffness of the model was affected. The model with ligaments made of the 2mm elastic band had a stiffness twice that of the model when the 1mm elastic band was used for the ligaments. The average stiffness of the model with 2mm ligaments was 2349.3 N/m while the stiffness of the model with 1mm ligaments had a stiffness of 1187.4 N/m (Figure 5.21). IMJ 5 was inserted in the model during these tests.

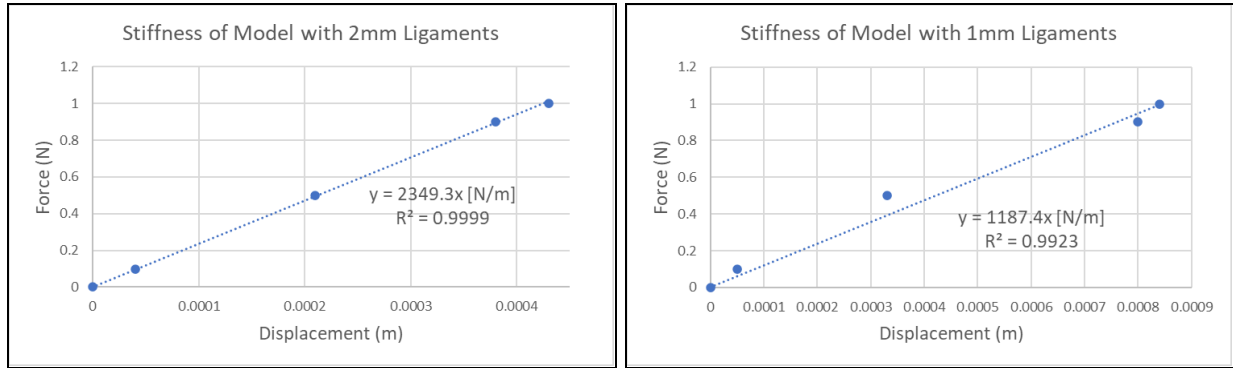


Figure 5.21: a) Model Stiffness with 2mm Elastic Bands as Ligaments,  
b) Model Stiffness with 1mm Elastic Bands as Ligaments.

## 6.0 Final Design Validation

This chapter includes the validation processes for the physical and digital model creation.

### 6.1 Digital Modeling and Design

The first, second and fourth project objectives were completed with digital modeling tools: Geomagic, Blender, and Solidworks. The group first adapted and modified the previous group's Geomagic model in Solidworks in pursuit of the first objective, improving the durability and adjustability of the support structure of the model. Feature recognition on the .stl files' geometry was utilized to add structural support and adapt the bodies to allow for easy integration of hardware, such as the hooks and magnets, into the 3D printed parts. Next, objective four, which was to implement a realistic incudostapedial joint, was completed by creating a mold design that allowed for the molding of an ISJ that implemented a realistic interface for current “bone on bone” contact points. Finally, objective two, to demonstrate varying stages of pathological hearing loss due to the stiffening of the incudomalleolar joint, was furthered by creating a mold design that allowed for the molding of different stiffness IMJs. This was accompanied by force-displacement and vibration testing in order to demonstrate the trends of varying stages of pathological hearing loss due to the stiffening.

The client, Dr. Ivo Dobrev, was able to provide guidance and feedback throughout the digital design process. In the first few weeks of the project's design, the adjustability of the support structure was addressed by integrating in the Thorlabs pieces and eye hooks (Figure 6.1), which improved the interchability of the ligaments. This allowed for easier interchangeability of the five different IMJ models without disturbing other aspects of the structure during testing.

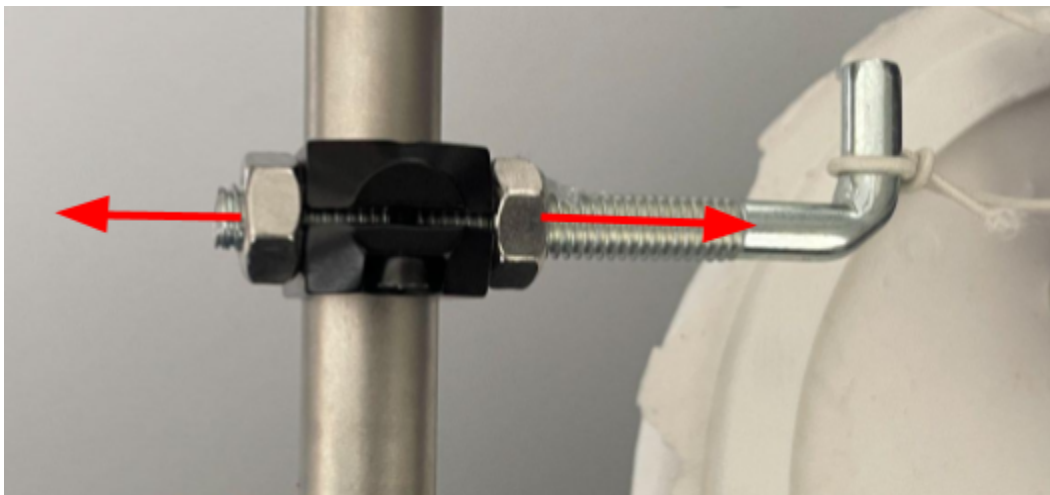


Figure 6.1: Adjustability of Eye Hooks on ThorLabs Pieces

The durability of the support structure was addressed by utilizing a combination of ThorLabs pieces and 3D printed parts. 3D printed support beams were added to the oval window structure (Figure 6.2) , and the outer diameter of the eardrum structure was thickened.

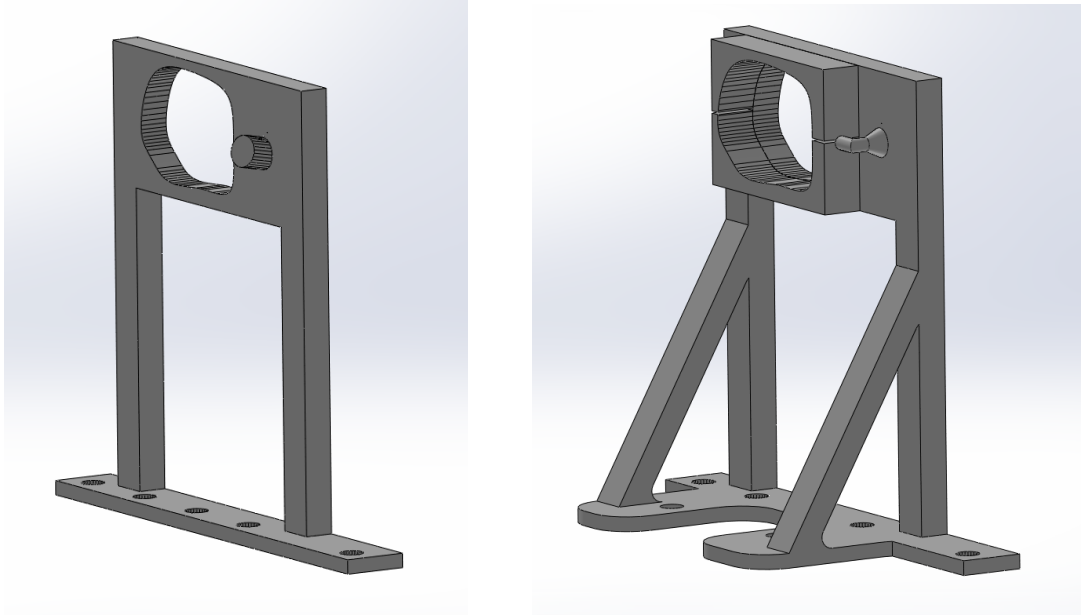


Figure 6.2: Before and After Oval Window 3D Printed Design

The design portion of the second objective consisted of creating a mold design for the IMJs used in the model. This process required multiple iterations of the mold design. Before tackling the design of the IMJ mold, the design for the ISJ was developed first. After an iterative design process testing different molds, a model was chosen that would produce a silicone ISJ (Figure 6.3) that allowed for more realistic anatomical movement.

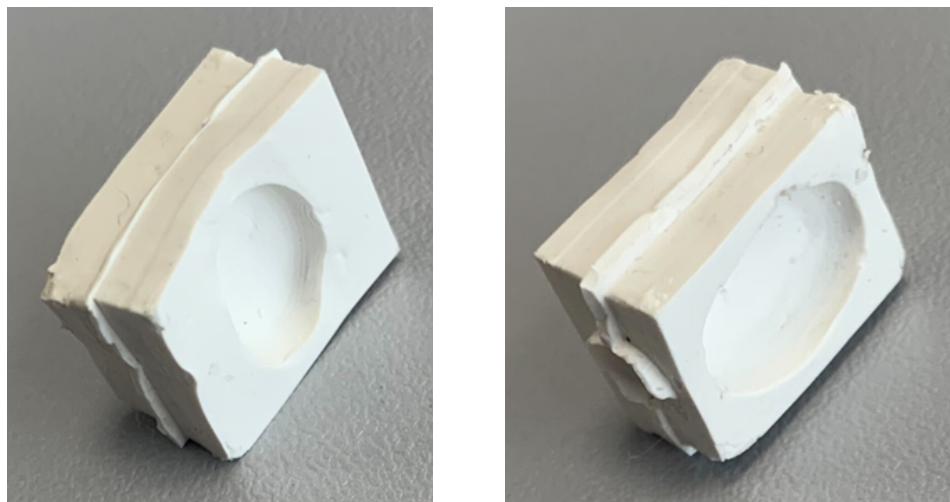


Figure 6.3: Final Molded ISJ



It was necessary to simplify the geometry of the IMJ in order to allow for easy removal of the mold while also retaining anatomical correctness in the design. The final design that could be easily molded with silicone is shown in Figure 6.4. The mold was used to create multiple variations of the silicone IMJ that could demonstrate the stiffening of the incudomalleolar joint through vibration and force-displacement testing.



Figure 6.4: Final Molded IMJ

## 6.2 Physical Modeling and Testing

The second project objective was continued through analysis and trials using the five molded IMJs of different stiffnesses seen in Section 5. The third project objective was met through analysis of different elastic materials that could be used as the ligaments for the model. Through this analysis we were able to select and justify the use of a material modeling the support ligaments and muscles to satisfy the third objective. One of the requirements that Dr. Ivo Dobrev saw needed improvement from the last group was justification on why the ligament material choice was selected. The justification for this was split into two parts. First, materials that would be practical for use in a dynamic model were chosen. These included materials that would resist deformation over time as well as breakage due to regular use. The silicone material used for the previous model's ligaments appeared to have deformed significantly over the time between the previous team completing the model and the start of this project. Additionally, as we began working on the model, the silicone ligaments began to break. Because of this, it was decided it would be best to select a material that would be durable for regular use of the model.

The second part of the justification process was selecting a material that would perform similarly to the actual ligaments of the middle ear. For the purposes of the model, this would mean ligaments that result in a model stiffness within the range of 200 to 2500 N/m. These numbers were selected based on the stiffness of the actual middle ear, with 200 to 500 N/m

representing a healthy ear and 1000 to 2500 N/m representing an ear experiencing conductive hearing loss (Dobrev et al., 2018).

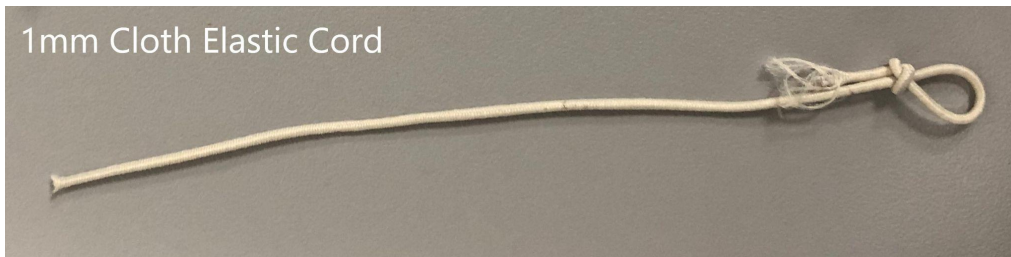


Figure 6.5: Material Used to Replicate Ligament in the Model

The third project objective was met with the use of 1mm cloth elastic cord (Figure 6.5). The cloth elastic cord was significantly more durable than the silicone cord used in the previous iteration of the model. The cord did not snap under the tension required to suspend the model and was easy to tie off without breakage occurring. The cloth covering acts as a protectant for the elastic underneath, preventing drying out or tearing of the elastic material. Additionally, the stiffness of the model with the 1mm cloth elastic cord fell within a realistic range that would be representative of conductive hearing loss.

Figure 6.6 shows the completed model once the physical modeling and testing was complete.

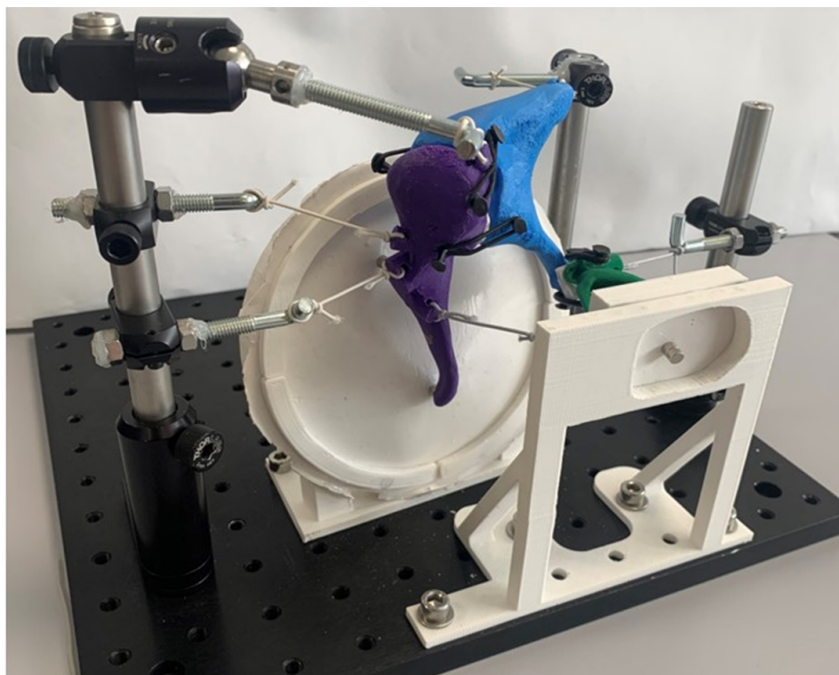


Figure 6.6: The Completed Model

## 7.0 Discussion

This section outlines the results of the design verification in conjunction with the project objectives and in context with primary literature. It also discusses the limitations associated with each objective.

### 7.1 Support Structure Accomplishments and Limitations

The support structure of the model was made both adjustable and durable with the addition of Thorlabs pieces. The Thorlabs pieces made it possible to shift the ligament connection points up and down as well as tighten and loosen the ligaments. The hooks that connected the ligaments to the Thorlabs pieces make it possible to easily remove and store the ossicular chain of the model. One limitation of the structure is that the ThorLabs pieces can be easily moved unintentionally and shifted into anatomically incorrect positions.

### 7.2 Varying Stiffnesses of IMJ Accomplishments and Limitations

The variation of stiffnesses was accomplished by increasing the amount of crosslinker within the silicone mixture by 1% increments. Increasing the crosslinker by 1% increased the silicone's stiffness. These increments indicated a precise difference in the material makeup of each IMJ. One of the main limitations of the varying stiffnesses was not having the time to measure the elastic modulus of each IMJ variation. Testing in order to measure the elastic modulus for each IMJ would provide numerical values to the stiffness, giving the team a greater understanding of the stiffness and vibration testing results.

### 7.3 Stiffness Testing Accomplishments and Limitations

The stiffness testing of the model showed that the ligaments have a significant effect on the stiffness of the system and the presence of the IMJ makes the system stiffer than if no IMJ is present. One of the main limitations of the stiffness testing was that it only measured input and output. Since the force was applied at the tympanic membrane and the displacement measured at the oval window, no measurements of any subsystems were taken.

### 7.4 Ligament and Muscle Material Accomplishments and Limitations

The material selected for the ligaments and muscles was successful in being a durable material which was easy to use. Users of the model are able to easily manipulate the ligaments without worrying about breakage or deformation. One limitation of the ligament and muscle material was that it caused the model to fall on the stiffer end of the 200 to 2500 N/m range set for the model. Because of the material's high stiffness, reducing the stiffness below around 1000 N/m with the IMJ inserted was not possible.

## 7.5 Digital Model Accomplishments and Limitations

One of the deliverables that the project team provided was a 3D model of the current design, in Solidworks. The benefit that this model provides is the ability to easily modify the 3D printed parts for future iterations of the model. This model is an assembly that can be easily interacted with and modified as adjustments are made allowing for easier design adaptations. This also allows for students who don't have direct access to a physical model to be able to easily view and understand the model. Figure 7.1 is a picture of the Solidworks model, identical to the physical model excluding the ligament connections.

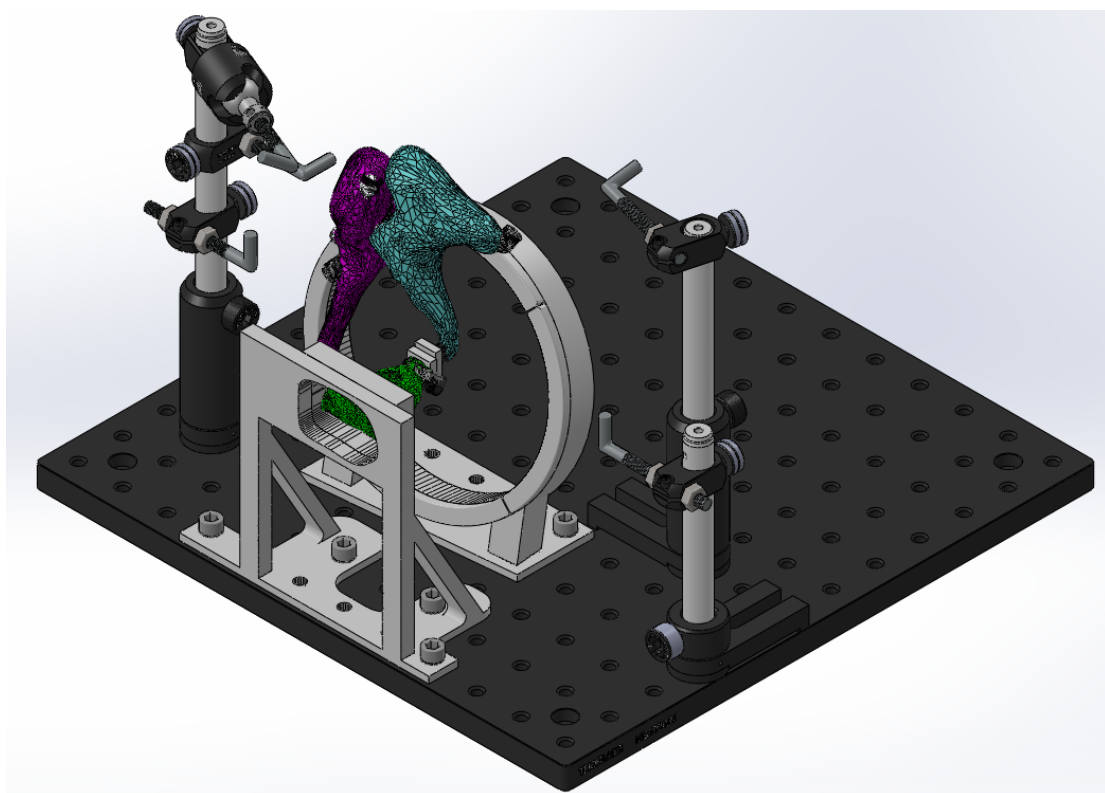


Figure 7.1: Final Solidworks Model Excluding Ligament Connections

One limitation of having this model in Solidworks was the challenges of file conversion. When converting these files from Geomagic, some of the intricate geometric details that were within the Geomagic model were not easily converted into the Solidworks file. In the case of the IMJ the geometry had to be simplified. A more simplified geometry lowers the anatomical accuracy of the joint, but the ability to modify the model through Solidworks in order to create the mold for the joint was a clear benefit.

## 8.0 Conclusions and Recommendations

This section outlines the future recommendations and broader impacts of the project, while providing detail on possible areas of improvement for future iterations of the project.

### 8.1 Future Recommendations

Many ideas of how to improve the model were theorized, but were unable to be included in this project due to time limitations. Below are a few of these ideas that could be helpful for future project teams to look at.

#### 8.1.1 Instructional Page

The model currently lacks a “How to” guide, that would instruct users on important aspects of the model. The project team recommends that future teams create an instructional page to be stored with the model that documents how the model works, the correct ligament lengths when hooked up to the model and when relaxed, and assembly instructions. This would be beneficial for future users to better understand the model. The model could be disassembled when not in use to prevent creep and material degradation.

#### 8.1.2 Functional model capable of showing trends

This project attempted to explore some trends of the middle ear that correspond with the stiffening of the IMJ. During that process, the project team created the necessary IMJs and procedures to explore many other trends. This objective was ultimately not met since no clear trends were discerned when the stiffness of the IMJ was changed. The vibration and force-displacement testing yielded results that suggested trends might be shown with changes to the system. Overall, the model is capable of having an output when an acoustic or mechanical force is applied, and that output changes when the IMJ is removed. Changes were seen when the stiffness of the IMJ was increased, but the change was not significant enough to show a clear trend. The project team recommends that the next group to work on this project select trends of the middle ear, and enhance the model so it can mirror these trends.

#### 8.1.3 3-Axis Accelerometer Data

Throughout vibration testing, the accelerometers only collected data along their Z-axis, which the project team considered the most relevant. The project team recommends that future teams explore the possibility that important information may be lost by ignoring the output on the X and Y axes.

### 8.1.4 Ligament Stiffness

This project attempted to mirror the stiffness of the ligaments supporting the ossicular chain in the middle ear. There were many thought processes incorporated into this decision, but no scientific research. The project team recommends that future teams explore how to properly scale the ligament stiffness, and if necessary choose new materials to model the ossicular chain support ligaments.

## 8.2 Broader Impacts

This section contains an overview of the broader impacts of this project.

### 8.2.1 Environmental Impacts

This project has very little environmental impact. However, the two main environmental impacts would be the fossil fuel consumption to make and ship the required hardware, and the degradability of the materials used such as PLA and silicone. The degradability of the materials is focused on in section 8.2.6.

### 8.2.2 Societal Influence

The goal of this project was to have an impact on academia by providing a physical dynamic model of the middle ear. Ideally this model will spark an interest in the importance of providing learning resources for students studying the middle ear. Also this project may aid the future growth and funding provided to the University Hospital of Zurich middle ear research and experiments.

### 8.2.3 Ethical Concerns

One possible ethical concern of this project would be its impact on the deaf community. Throughout the years, cochlear implants have remained a controversial topic within the deaf community with some believing cochlear implants are made to cure deafness or that it takes away a large part of deaf culture (Jodlowski & 2015, 2015). With this model aiding with future cochlear implant research, it could have a negative impact on those of the deaf community with these beliefs.

### 8.2.4 Health and Safety Issues

The model created in this project has the ability to have a positive impact on the health and safety of middle ear patients. This model will hopefully spark interest in future studies of the middle ear, while providing a pivotal learning resource for future middle ear surgeons and researchers. This will help with successful surgeries and the advancement of new hearing assistance devices.

### 8.2.5 Manufacturability

The manufacturability of the parts of the project are simple with limited 3D printing capabilities. The ossicles and some of the hardware of the project are easily replicable through FDM printing. The molds used to fabricate the joints can be replicated through SLA printing.. The variety of hardware used through the project can also be easily obtained with the only specialized parts being some of the structural support that need to be ordered through ThorLabs.

### 8.2.6 Sustainability

Many of the parts on the model will not degrade with time, including the 3D printed parts and the Thorlabs pieces. The elastics representing ligaments and muscles will last for a long time if the model is disassembled when it is not in use. Additionally, all parts can easily be reprinted, remolded, or repurchased.

## References

- 50 SHA VMQ Silicone O-ring cord Ø3.00 mm.* (n.d.). Retrieved October 6, 2022, from <https://www.gteek.com/50-SHA-VMQ-Silicone-O-ring-cord-3.00-mm>
- Candle gel.* (n.d.-a). Retrieved October 4, 2022, from <https://www.rayher.com/en/candle-gel-3130000>
- Carlota V., C. (2019, July 23). *Is PLA filament actually biodegradable?* 3Dnatives. <https://www.3dnatives.com/en/pla-filament-230720194/>
- Casting powder Raysin 200.* (n.d.-b). Retrieved October 4, 2022, from <https://www.rayher.com/en/casting-powder-raysin-200-34405102>
- Creative cement.* (n.d.-c). Retrieved October 4, 2022, from <https://www.rayher.com/en/creative-cement-34152000>
- Daily Go Mini-Haargummi.* (n.d.). Retrieved October 6, 2022, from [https://www.manor.ch/de/p/10001312522?gclid=Cj0KCQjw-fmZBhDtARIsAH6H8qjyU9o\\_JID2RroV2l5dTY5v6TDQpzY2JYl3ZAlrbTWQmN66zfRmg5oaAgX6EALw\\_wcB](https://www.manor.ch/de/p/10001312522?gclid=Cj0KCQjw-fmZBhDtARIsAH6H8qjyU9o_JID2RroV2l5dTY5v6TDQpzY2JYl3ZAlrbTWQmN66zfRmg5oaAgX6EALw_wcB)
- DailyGo Mini (Hair tie).* (n.d.). Retrieved October 6, 2022, from [https://www.galaxus.ch/en/s6/product/dailygo-mini-hair-tie-hair-ties-9802035?dbq=1&gclid=Cj0KCQjw-fmZBhDtARIsAH6H8qi-nKzjBsdprxvL3IOtiXOFw8QwSahLh-P5zVMahqvHzmjGTVbjjw0aAm8nEALw\\_wcB&gclsrc=aw.ds](https://www.galaxus.ch/en/s6/product/dailygo-mini-hair-tie-hair-ties-9802035?dbq=1&gclid=Cj0KCQjw-fmZBhDtARIsAH6H8qi-nKzjBsdprxvL3IOtiXOFw8QwSahLh-P5zVMahqvHzmjGTVbjjw0aAm8nEALw_wcB&gclsrc=aw.ds)
- Dancer, A., & Rebillard, G. (2018, January 16). *Middle ear.* Journey into the World of Hearing. <http://www.cochlea.eu/en/ear/middle-ear>
- Dobrev, I. (2022, August 31). *Personal Communication* [Online].
- Dobrev, I., Sim, J. H., Aqtashi, B., Huber, A. M., Linder, T., & Rösli, C. (2018). Effects of middle ear quasi-static stiffness on sound transmission quantified by a novel 3-axis



optical force sensor. *Hearing Research*, 357, 1–9.

<https://doi.org/10.1016/j.heares.2017.11.002>

*ELASTISCHE KORDEL kaufen bei JUMBO*. (n.d.). BauundHobby. Retrieved October 6, 2022,

from

<https://www.jumbo.ch/de/maschinen-werkstatt/beschlaege-briefkaesten/ketten-seile/seile-schnuere/elastische-kordel/p/6224083>

Gassler, J. (2019, April 5). *Anatomy of the Ear, Nasal Cavity, Pharynx and Larynx*.

Gerig, R. (2015). *Acousto-Vibratory function of the incudo-malleal joint* [University of Zurich].

[https://www.zora.uzh.ch/id/eprint/122206/6/Diss\\_Gerig\\_Rahel\\_ohne\\_CV.pdf](https://www.zora.uzh.ch/id/eprint/122206/6/Diss_Gerig_Rahel_ohne_CV.pdf)

Gil-Loyzaga, P. (2016, November 18). *Superior olivary complex*. Journey into the World of

Hearing. <http://www.cochlea.eu/en>

*Glorex Gummibänder, 4x3m; Ø 1mm beige/grau/braun/schwarz*. (n.d.). Retrieved October 6,

2022, from

[https://www.galaxus.ch/de/s5/product/glorex-gummibaender-4x3m-1mm-beigegraubraun-schwarz-basteln-12449295?dbq=1&gclid=Cj0KCQjw-fmZBhDtARIsAH6H8qjuR-BQQTK9il0PEtevWVG-zKoaMxswXVOyVct1KrldbXDETi6T3GEaAhsfEALw\\_wcB&gclsrc=aw.ds](https://www.galaxus.ch/de/s5/product/glorex-gummibaender-4x3m-1mm-beigegraubraun-schwarz-basteln-12449295?dbq=1&gclid=Cj0KCQjw-fmZBhDtARIsAH6H8qjuR-BQQTK9il0PEtevWVG-zKoaMxswXVOyVct1KrldbXDETi6T3GEaAhsfEALw_wcB&gclsrc=aw.ds)

*Glorex Gummibänder, 4x3m; Ø 2mm beige/grau/braun/schwarz*. (n.d.). Retrieved October 6,

2022, from

[https://www.galaxus.ch/de/s5/product/glorex-gummibaender-4x3m-2mm-beigegraubraun-schwarz-basteln-12449293?gclid=Cj0KCQjw-fmZBhDtARIsAH6H8qgG3w2jgeoK-clFfMnvQNnTWqLtzzCwoJleKuvy1i9aICc2Ouwvvrq0aAroHEALw\\_wcB&gclsrc=aw.ds](https://www.galaxus.ch/de/s5/product/glorex-gummibaender-4x3m-2mm-beigegraubraun-schwarz-basteln-12449293?gclid=Cj0KCQjw-fmZBhDtARIsAH6H8qgG3w2jgeoK-clFfMnvQNnTWqLtzzCwoJleKuvy1i9aICc2Ouwvvrq0aAroHEALw_wcB&gclsrc=aw.ds)

*Hillman Steel Screw Eye Hook in the Hooks department at Lowes.com*. (n.d.). Retrieved October

6, 2022, from <https://www.lowes.com/pd/Hillman-Steel-Screw-Eye-Hook/3036088>

*How Do We Hear?* (2022, March 16). How Do We Hear?

<https://www.nidcd.nih.gov/health/how-do-we-hear>

Jodlowski, N. J. & 2015. (2015, October 5). *Cochlear Implants and Deaf Identity*. Reporter.

<https://reporter.rit.edu/views/cochlear-implants-and-deaf-identity#:~:text=Throughout%20the%20years%2C%20cochlear%20implants%20have%20remained%20a,that%20it%20is%20a%20way%20to%20cure%20deafness>

*Kinzo—O-Ringe*. (n.d.). Beyti. Retrieved October 6, 2022, from

<https://beytihome.com/products/kinzo-o-ringe>

*Latex emulsion*. (n.d.-d). Retrieved October 4, 2022, from

<https://www.rayher.com/en/latex-emulsion-3412900>

*MakerBeam Starter Kit Black Premium*. (n.d.). MakerBeam. Retrieved October 4, 2022, from

<https://www.makerbeam.com/makerbeam-makerbeam-starter-kit-black-premium.html?source=facebook>

*Modelling clay air-drying*. (n.d.-e). Retrieved October 4, 2022, from

<https://www.rayher.com/en/modelling-clay-air-drying-34502>

Mudhol, R. S., Naragund, A. I., & Shruthi, V. S. (2013). Ossiculoplasty: Revisited. *Indian*

*Journal of Otolaryngology and Head & Neck Surgery*, 65(S3), 451–454.

<https://doi.org/10.1007/s12070-011-0472-7>

Osika, A. (2022, June 15). *Auditory ossicles*. Kenhub.

<https://www.kenhub.com/en/library/anatomy/auditory-ossicles>

Ossicular Fixation. (n.d.). *Dallas Ear Institute*. Retrieved September 1, 2022, from

<https://www.dallasear.com/education/ear-disease/ossicular-fixation/>

- Otosclerosis*. (2019, May 23). Nhs.Uk. <https://www.nhs.uk/conditions/otosclerosis/>
- Otosclerosis*. (2022, March 16). NIDCD. <https://www.nidcd.nih.gov/health/otosclerosis>
- Overstock.com: Online Shopping—Bedding, Furniture, Electronics, Jewelry, Clothing & more*. (n.d.). Retrieved October 4, 2022, from <https://www.overstock.com/Home-Garden/1.3-Ceiling-Hooks-Cup-Hook-Screw-in-Hanger-for-Indoor-and-Outdoor-Use-50pcs/28848075/product.html>
- Porzella—Papier-mâché, fine*. (n.d.-f). Retrieved October 4, 2022, from <https://www.rayher.com/en/porzella-papier-mache-fine-3450000>
- Properties of Silicones*. (n.d.). Retrieved October 8, 2022, from <https://polymerdatabase.com/polymer%20classes/Silicone%20type.html>
- Puria, S., Fay, R. R., & Popper, A. N. (2013a). In *The Middle Ear: Science, otosurgery, and Technology* (Vols. 9 & 10).
- Puria, S., Fay, R. R., & Popper, A. N. (Eds.). (2013b). *The Middle Ear: Science, Otosurgery, and Technology*. Springer New York. <https://doi.org/10.1007/978-1-4614-6591-1>
- Rensink, M. J. (2011). Anatomy of open ear. *The Hearing Journal*, 64(8), 10. <https://doi.org/10.1097/01.HJ.0000403505.49971.84>
- Scrivanich, M., DeLorie, S., Gunnison, M., O'Connor, S., & Piela, S. (2022). *Functional Middle Ear Model—Zurich C-term 2022*. Worcester Polytechnic Institute.
- Silicone caoutchouc, HB with catalyst*. (n.d.-g). Retrieved October 4, 2022, from <https://www.rayher.com/en/silicone-caoutchouc-hb-with-catalyst-3411600>
- Silicone caoutchouc, NV with catalyst*. (n.d.-h). Retrieved October 4, 2022, from <https://www.rayher.com/en/silicone-caoutchouc-nv-with-catalyst-3411100>
- Sound and Hearing. (2019). In H. Young & R. Freedman, *University Physics with Modern*

*Physics* (15th ed.). Pearson.

*Suki Fliesenlenergummischnur kaufen bei JUMBO*. (n.d.). BauundHobby. Retrieved October 6, 2022, from

<https://www.jumbo.ch/de/maschinen-werkstatt/handwerkzeug/bau-messwerkzeug/baumeisswerkzeug/suki-fliesenlenergummischnur/p/6941826>

Sunil Puria, Jae Hoon Sim, & Charles R. Steele. (2007). Calculation of Inertial Properties of the Malleus-Incus Complex from Micro CT-Imaging. *Journal of Mechanics of Materials and Structures*, 2.

[https://www.zora.uzh.ch/id/eprint/53974/1/Sim\\_etal\\_JMechMatStruc\\_0710.pdf](https://www.zora.uzh.ch/id/eprint/53974/1/Sim_etal_JMechMatStruc_0710.pdf)

Swartz, J. D., Wolfson, R. J., Marlowe, F. I., & Popky, G. L. (1985). Postinflammatory ossicular fixation: CT analysis with surgical correlation. *Radiology*, 154(3), 697–700.

<https://doi.org/10.1148/radiology.154.3.3918333>

*SYLGARD™ 184 Silicone Elastomer Kit*. (n.d.). Retrieved October 4, 2022, from

<https://www.dow.com/en-us/pdp.sylgard-184-silicone-elastomer-kit.01064291z.html>

Tanner, A., Kane, S., Paradise, E., & Torraca, T. (2021). *Design and Stimulation of a Middle Ear Model to Aid with Otological Studies* [Tanner, Arden R.]. Worcester Polytechnic Institute.

*Thomann Silicone Cord Ø=5mm x L=100mm*. (n.d.). Musikhaus Thomann. Retrieved October 6, 2022, from

[https://www.thomannmusic.ch/intl/thomann\\_silicone\\_cord\\_5mm\\_x\\_1100mm.htm](https://www.thomannmusic.ch/intl/thomann_silicone_cord_5mm_x_1100mm.htm)

*Thorlabs—PH2 Ø1/2" Post Holder, Spring-Loaded Hex-Locking Thumbscrew, L = 2"*. (n.d.).

Thorlabs. Retrieved October 4, 2022, from

<https://www.thorlabs.com/thorProduct.cfm?partNumber=PH2#ad-image-0>

*Tympanosclerosis*. (n.d.). Otorhinolaryngology - Head & Neck Surgery. Retrieved September 1,

2022, from

<https://med.uth.edu/orl/online-ear-disease-photo-book/chapter-15-miscellaneous/tympanosclerosis/>

Types, Causes and Treatments of Hearing Loss—The Basics. (n.d.). *Hearing Loss Association of America*. Retrieved September 1, 2022, from

<https://www.hearingloss.org/hearing-help/hearing-loss-basics/types-causes-and-treatment/>

Vrachovska, M. (n.d.). *Is Silicone Biodegradable Or Recyclable? Almost Zero Waste*. Retrieved October 10, 2022, from <https://www.almostzerowaste.com/does-silicone-break-down/>

Wang, Z., Volinsky, A. A., & Gallant, N. D. (2014). Crosslinking effect on polydimethylsiloxane elastic modulus measured by custom-built compression instrument. *Journal of Applied Polymer Science*, 131(22). <https://doi.org/10.1002/app.41050>

Warnholtz, B., Schär, M., Sackmann, B., Lauxmann, M., Chatzimichalis, M., Prochazka, L., Dobrev, I., Huber, A. M., & Sim, J. H. (2021). Contribution of the flexible incudo-malleal joint to middle-ear sound transmission under static pressure loads. *Hearing Research*, 406. <https://doi.org/10.1016/j.heares.2021.108272>

*Wax lenses*. (n.d.-i). Retrieved October 4, 2022, from

<https://www.rayher.com/en/wax-lenses-3107202>

*What Noises Cause Hearing Loss? | NCEH | CDC*. (2019, October 7).

[https://www.cdc.gov/nceh/hearing\\_loss/what\\_noises\\_cause\\_hearing\\_loss.html](https://www.cdc.gov/nceh/hearing_loss/what_noises_cause_hearing_loss.html)

Yilmaz-Bayraktar, S., Foremny, K., Kreienmeyer, M., Warnecke, A., & Doll, T. (2022).

Medical-Grade Silicone Rubber-Hydrogel-Composites for Modiolar Hugging Cochlear Implants. *Polymers*, 14(9), 1766. <https://doi.org/10.3390/polym14091766>

Zare, M., Ghomi, E. R., Venkatraman, P. D., & Ramakrishna, S. (2021). Silicone-based biomaterials for biomedical applications: Antimicrobial strategies and 3D printing technologies. *Journal of Applied Polymer Science*, 138(38), 50969. <https://doi.org/10.1002/app.50969>

## Appendix A – Weeks 1-3 of Team Gantt Chart

				WEEK 1					WEEK 2					WEEK 3				
				M	T	W	R	F	M	T	W	R	F	M	T	W	R	F
				08/15	08/16	08/17	08/18	08/19	08/22	08/23	08/24	08/25	08/26	08/29	08/30	08/31	09/01	09/02
	Task	Notes	% Complete															
1	Project Conception and Definition																	
1.1	Review of Past Literature		50															
1.2	Preliminary Research		50															
1.3	Generate Client Statement		100															
1.3.1	Reevaluate Client Statement		100															
1.3.2	Finalize Client Statement		75															
1.4	Generate Goal and Objectives		100															
1.4.1	Reevaluate Goal and Objectives		100															
1.4.2	Finalize Goal and Objectives		100															
2	Project Prep & Planning																	
2.1	Familiarize with Instrumentation Devices		75															
2.2	Familiarize with Existing Code		15															
2.3	Familiarize with Data Collection and Processing		15															
2.4	Determine Joint Materials	pdms, FDM, SLA	0															
2.5	Determine Number and Type of Joint Pieces		0															
2.6	Determine Muscle/Ligament Materials		0															
2.7	Determine Changes for Current Model		50															
2.8	Purchase Materials		15															
2.9	Purchase Model Copy Materials	not received	100															
3	Purchase Hardware Materials		0															
3.1	Purchase Joint/Muscle/Ligament Materials		0															
3.2	Final Order Date for all CAD pieces		0															

## Appendix B – Calibration of Accelerometers

This appendix specifies the procedure to calibrate the ADXL335 Accelerometers the client provided for instrumentation in this project. The procedure below explains how the Z-axis of one accelerometer was calibrated, and the process was repeated for the Z-axis of a second accelerometer.

- Equipment
  - Laptop with APx and MATLAB software installed
  - ADXL335 Accelerometer
  - Mini Mechanical shaker
  - Audio Precision 585 multichannel audio analyzer (DAQ)
  - QSC RMX 850a Professional Amplifier
  - Polytec CLV-2534 Laser Vibrometer
  - Polytec Laser
- Assumptions
  - The accelerometer is already wired
  - Assumes Accelerometer is fully in the XY Plane
- DAQ Wiring
  - Connect the DAQ to the computer via USB Cable
  - Connect the amplifier Coax cable output to input 1 on the DAQ
  - Connect the reference laser Coax cable to input 2 on the DAQ
  - Connect the accelerometer Z-1 Coax cable to input 3 on the DAQ
  - Connect the amplifier input Coax cable to output 1 on the DAQ
  - Connect the amplifier output to the mechanical shaker
- Description of the wiring:
  - With this setup, the software will output a signal to the DAQ, which passes through the amplifier. After going through the amplifier, it goes to the mechanical shaker, dictating the magnitude and frequency of its vibrations. The same signal goes back through the DAQ to the computer, and the software displays what the amplifier is outputting. Simultaneously, the software displays the measurements from the laser and the accelerometer, with the data coming through the DAQ.
- Description of the setup:
  - Put Scotch tape around the accelerometer in a loop, sticky side towards the accelerometer
  - Use Hot glue to adhere the tape-accelerometer assembly to the mechanical shaker
  - Place a small piece of reflective tape on top of the accelerometer
  - Focus the laser onto the reflective tape
- Settings:
  - Laser Setting: 20 mm/s/V



- APx Settings

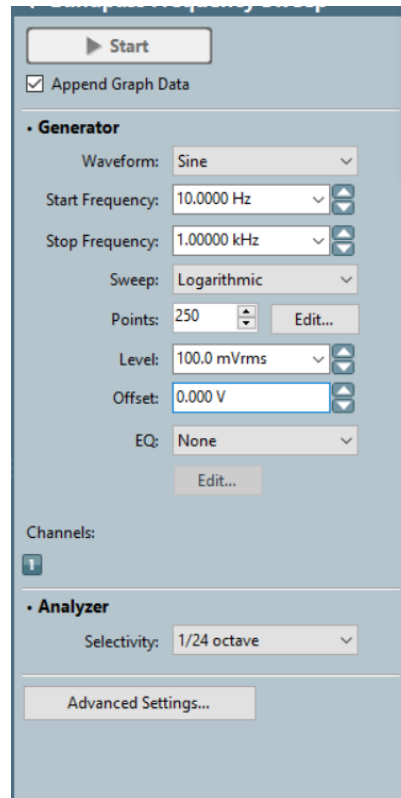


Figure B.1: APX Settings for Calibration of Accelerometer

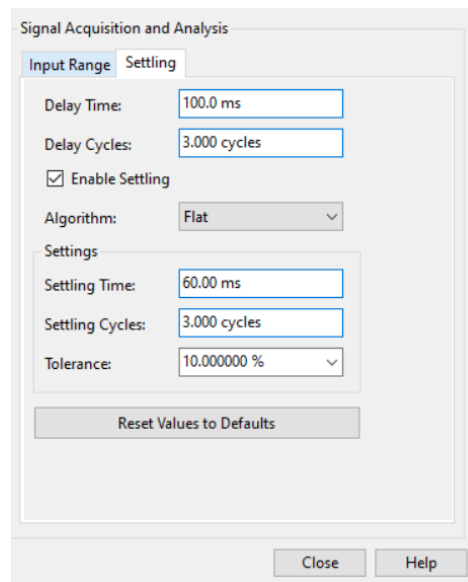


Figure B.2: APx Settling Settings for Calibration of Accelerometers

- Data Acquisition

- Run 50 sweeps at the above settings, using Sequence Mode in the APx Software

- Data Analysis
  - Download the output data into Excel
  - Using Matlab, analyze the data to have a matrix that outputs the mean, coefficient of variation, and standard error of the mean of the correction factor at each frequency tested. The code performs the following operations:
    - For Laser output
      - Multiply the Vrms output by 20 mm/s/V
      - Multiply this new velocity by  $2\pi \times \text{frequency}$ , getting an acceleration in mm/s<sup>2</sup>
      - Multiply this acceleration by 0.000101971621297792 to convert to g
    - For accelerometer output
      - Multiply the Vrms value by 3.03030303 to convert it to g
      - Divide the laser output by the accelerometer output, both in g. This new value is the Correction Factor.
    - Analyze the correction factor for data at the same frequencies
      - Calculate the mean and coefficient of variation at each frequency

MATLAB Code Used:

% Take Excel Data and Get Mean and Standard Error of the Mean

clc; clear all;

%% Inputs

%Folder housing the file

data\_dir = 'C:\Users\Tommy\Desktop\MQP Stuff';

%File name

data\_file = 'Accelerometer1 Z Calibration Data.xlsx';

%Number of sweeps done in APX

n\_sweeps = 50;

%"Points" Specified in the APX Sweep

datapoints\_per\_sweep = 250;

%Number of analog inputs on the DAQ

num\_APX\_Inputs = 3;

%These inputs specify which columns have the data for the acc, ldv, and

%frequency. Later on in the code will use these variables instead of actual

%numbers, so all of the inputs stay in the same place

ldv\_reading\_column = 2;

acc\_reading\_column = 4;

Freq\_reading\_column = 1;

%Conversions used to bring acc to g

%Multiply acc by this number to convert it from Volts to g

acc\_V\_to\_g = 3.03030303;

```

%Conversions used to bring ldv to g
% The laser setting in mm/s/V
ldv_mm_per_s_per_V = 20;
% After converting the laser to acceleration in mm/s^2, use this to convert
% the acceleration to g
mm_s_squared_to_g = 0.000101971621297792;
%% Setting up meas_data_all matrix
num_excel_col = 2*num_APX_Inputs;
%meas_data_all needs to match the dimensions of the input data or it falls
% This creates a zero matrix the same dimensions of the final data, which
% will then be replaced in each sweep
meas_data_all = zeros(datapoints_per_sweep,num_excel_col,n_sweeps);
%% Scrape the Data from excel into a 3D matrix
% columns = data points
% Rows = measurements at each data point
% Note that Odd rows will all be the same, showing Frequency at that data point
% Slices (3rd Dim) = Independent Sweeps
%For loop runs from 1 up to the number of sweeps exported from APX
%This is also the number of relevant sheets in the excel file
for meas_ID = 1:n_sweeps
    meas_ID_xls = meas_ID - 1;
    %Naming convention of the sheets that APX exports to excel
    if meas_ID<2
        meas_ID_xls_txt = 'RMS Level';
    else
        meas_ID_xls_txt = ['RMS Level (' ,num2str(meas_ID_xls),')'];
    end
    %Takes 1 Sweep of data and puts it into the meas_data_all matrix
    [meas_data_singlesweep, ~, ~] = xlsread( [data_dir,'\',data_file],meas_ID_xls_txt);
    %Replaces the appropriate slice of the meas_data_all matrix with the
    %corresponding singlesweep data
    meas_data_all(:, :, meas_ID) = meas_data_singlesweep ;
end
%% Calculations to convert the accelerometer reading to g
%acc_g is the g values from the accelerometer
acc_g = meas_data_all(:,acc_reading_column,:) * acc_V_to_g;
%% Calculations to convert the ldv Reading to g
%Convert the ldv reading [Volts] to a velocity by multiplying by the laser
%setting, which has units of [mm/s/V]
ldv_mm_per_s = meas_data_all(:,ldv_reading_column,:) * ldv_mm_per_s_per_V;

```

```

%Convert the ldv value into acceleration in units of [mm/s^2] by
%multiplying by 2*pi*Frequency
% The first calculation multiplies by the frequency, and the second
% calculation multiplies by 2*pi
ldv_mm_per_s_squared = ldv_mm_per_s(:,,:) .* meas_data_all(:,Freq_reading_column,:);
ldv_mm_per_s_squared = ldv_mm_per_s_squared * 2 * pi;
%Convert the ldv value from mm/s^2 to g, using the conversion factor
%specified in the input section of this code
ldv_g = ldv_mm_per_s_squared * mm_s_squared_to_g;
%% Calculate the Correction Factor at each Frequency (ldv/acc)
correction_factor = ldv_g ./ acc_g;
%% Find the Mean and the Standard Error of the Mean for the Correction Factors at each
Frequency
%This creates a vector that is 100 x 1, with each value being the mean of
%the correction factors for the corresponding frequencies
mean_correction_factor = mean(correction_factor,3);
% This creates a 100 x 1 vector with each value being the standard
% deviation of the correction factors for the corresponding frequencies
stddev_correction_factor = std(correction_factor, 0, 3);
% Calculations for coefficient of variation
coefficient_Variation = stddev_correction_factor ./ mean_correction_factor
%Calculations for Standard Error of the Mean
standard_error_mean = stddev_correction_factor ./ sqrt(n_sweeps);
%Here, make a matrix that has column 1 = Frequency, 2 = mean, 3 =
%coefficient of variation, 4 = standard error of the mean
output_matrix =
[meas_data_all(:,Freq_reading_column,1),mean_correction_factor(:),coefficient_Variation(:),sta
ndard_error_mean(:)];
%% Data Display
% This section adds a sheet on the excel file, and puts the output matrix
% in it. It also plots the output matrix.
close all;
writematrix(output_matrix,[data_dir,'\',data_file],'Sheet','Correction Factors');
%Plots Correction Factor vs Frequency, with CoV for Error Bars
figure;
errorbar(output_matrix(:,1),output_matrix(:,2),output_matrix(:,3))
set(gca,'xscale','log');
title('Correction Factor vs Frequency, CoV Error Bars');
xlabel('Frequency [Hz]');
ylabel('Correction Factor [g/g]');

```

```
%Plots Correction Factor vs Frequency, with Standard Deviation for Error Bars
```

```
figure;
errorbar(output_matrix(:,1),output_matrix(:,2),stddev_correction_factor)
set(gca,'xscale','log');
title('Correction Factor vs Frequency, StdDev Error Bars');
xlabel('Frequency [Hz]');
ylabel('Correction Factor [g/g]');
```

```
%Plots Correction Factor vs Frequency, with Standard Error for Error Bars
```

```
figure;
errorbar(output_matrix(:,1),output_matrix(:,2),output_matrix(:,4))
set(gca,'xscale','log');
title('Correction Factor vs Frequency, SE of M Error Bars');
xlabel('Frequency [Hz]');
ylabel('Correction Factor [g/g]');
```

```
%Plots CofV, Standard Error, and Standard Deviation vs Frequency
```

```
figure;
plot(output_matrix(:,1),output_matrix(:,3),output_matrix(:,1),output_matrix(:,4),output_matrix(:,1),stddev_correction_factor)
set(gca,'xscale','log');
set(gca,'yscale','log');
title('Error vs Frequency');
xlabel('Frequency [Hz]');
ylabel('Error');
legend('Coefficient of Variation', 'standard error of the mean', 'Standard Deviation' );
```

## Appendix C – Justification of Accelerometer Calibration Methods

Figures C.1 through C.3 demonstrate the repeatability of the ADXL 335 accelerometers used in this project. Figure C.1 shows that the correction factor does not have an amplitude dependence above a stimulus level of 0.02 Vrms and below 0.2 Vrms. The calibrations were done at a stimulus level of 0.1 Vrms, making them valid for the entire range of 0.02-0.2 Vrms. Figure C.2 displays the repeatability of data taken with the accelerometers. It shows three sweeps done right after the other, with very little variation between the sweeps. Figure C.3 shows that the correction factor is not dependent on how the data was taken. Whether the sweep began at a low frequency or began at a high frequency, the results were similar. Also, when a stimulus with a constant frequency was present, the correction factor matched the sweeps at that frequency.

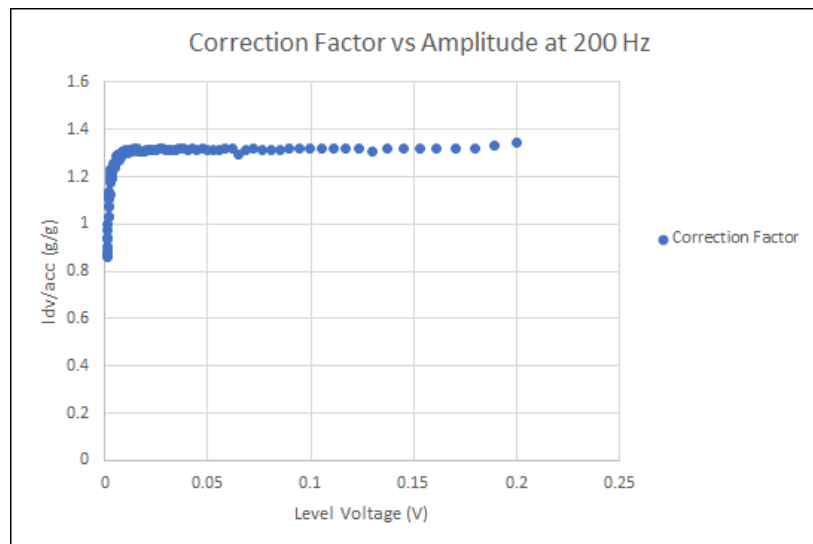


Figure C.1: Correction Factor vs Amplitude at 200 Hz

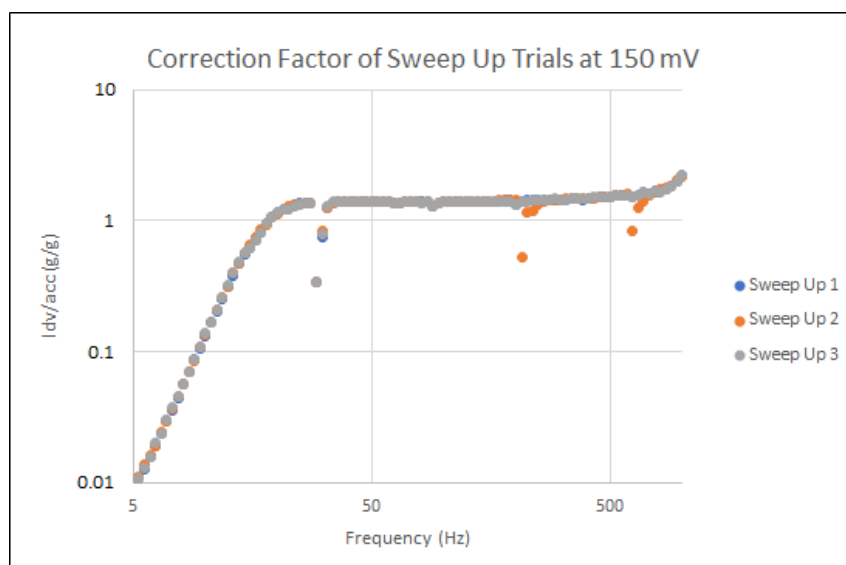


Figure C.2 Correction Factor of Sweep Up Trials at 150 mV

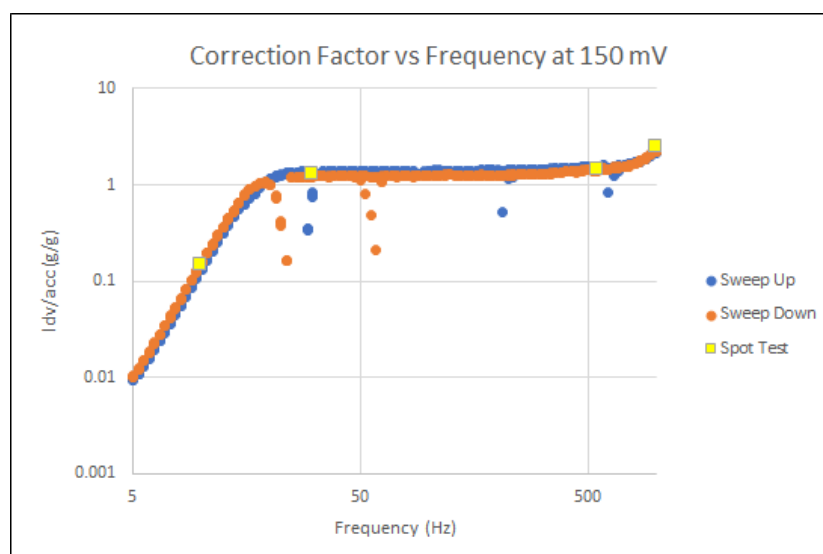


Figure C.3: Correction Factor vs Frequency at 150 mV

## Appendix D - Graph of Accelerometer Correction Factors

Graphs of accelerometer correction factors versus frequency for both accelerometers (Figures D.1 and D.2). The error bars represent standard error of the mean.

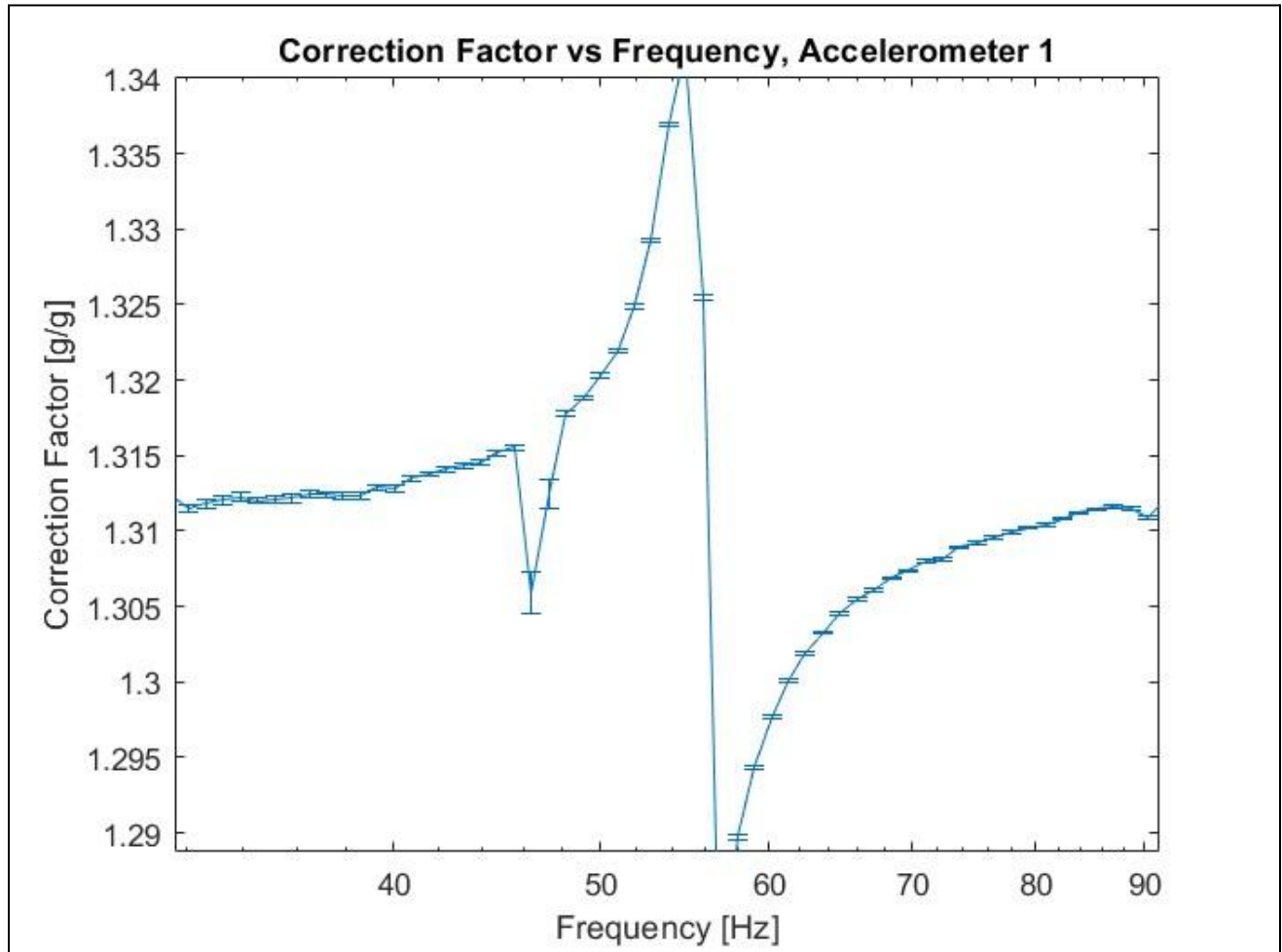


Figure D.1: Correction Factor vs Frequency, Accelerometer 1



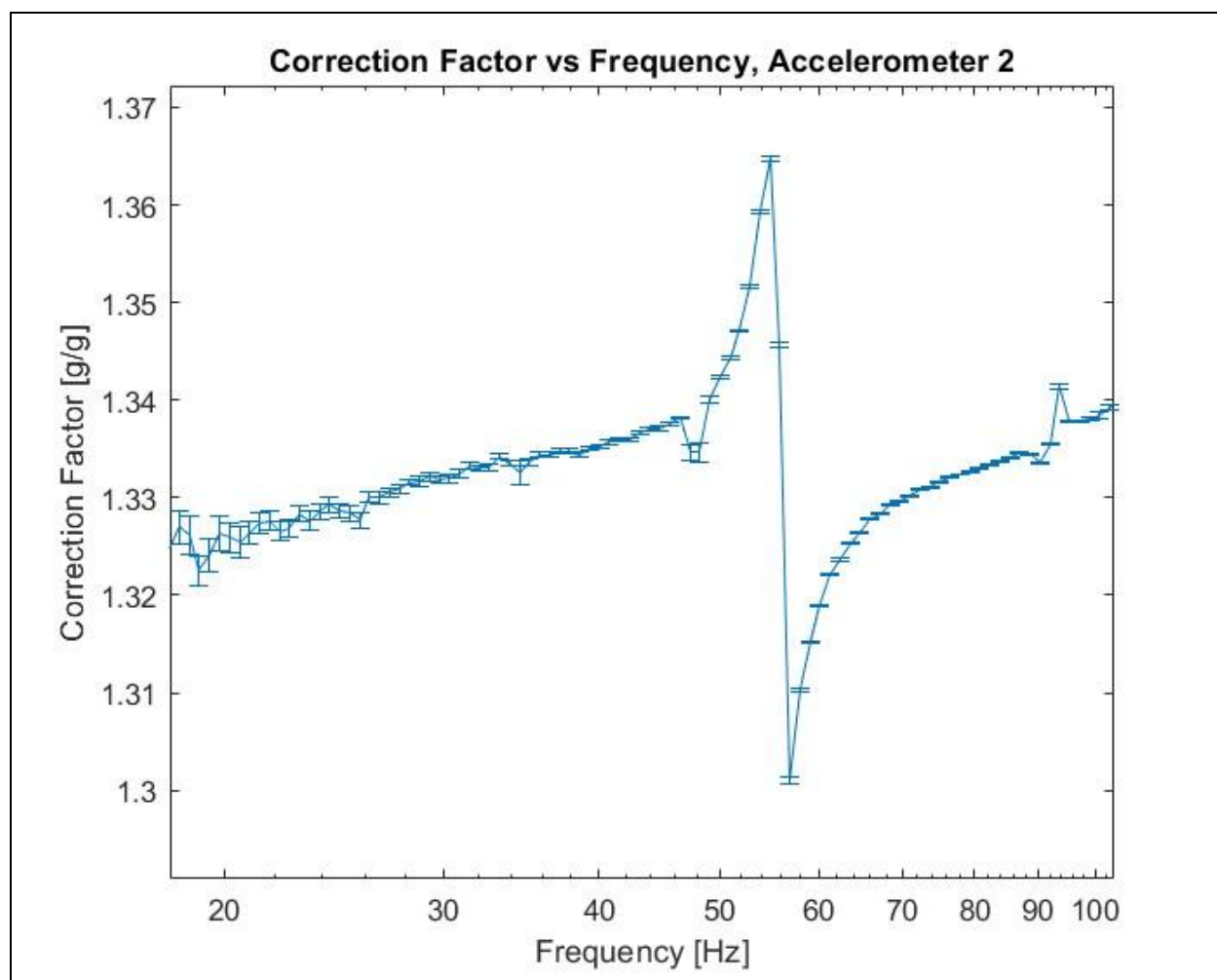


Figure D.2: Correction Factor vs Frequency, Accelerometer 2

## Appendix E - Matlab Code for Data Acquisition and Analysis

### IMJ Comparison Code

```

%% Inputs
clc; clear all; close all;
%Folder housing the file
data_dir = 'C:\Users\Tommy\Desktop\MQP Stuff\Oct 5';
%File name
data_file = '1 Sweep Per IMJ.xlsx';
%combine full file name
file = [data_dir, '\', data_file];
%"Points" Specified in the APX Sweep
datapoints_per_sweep = 250;
%Number of analog inputs on the DAQ, and corresponding number of excel columns
num_APX_Inputs = 2;
excel_col = 2*num_APX_Inputs;
%Number of sweeps done in APX, and the number of sweeps not including the
%noise sweep
n_sweeps = 6;
trialsPerIMJ = 1;
n_sweeps_minusNoise = n_sweeps-1;
n_IMJ = n_sweeps_minusNoise/trialsPerIMJ;
%The sheet of the excel file that contains the Noise data
noise_sheet = 1; %THERE IS AN ASSUMPTION LATER ON THAT THIS IS 1!!!
%STN Ratio Floor
STN_ratio = 10;
%These inputs specify which columns have the data for acc1, acc2, and
%frequency. Later on in the code will use these variables instead of actual
%numbers, so all of the inputs stay in the same place
acc1_reading_column = 2;
acc2_reading_column = 4;
Freq_reading_column = 1;
%Conversions used to bring acc to g
%Multiply acc by this number to convert it from Volts to g
acc_V_to_g = 3.03030303;
%Make a matrix now for efficiency
maskedANDcorrected_all = ones(datapoints_per_sweep, excel_col, n_IMJ);
average_data = ones(datapoints_per_sweep, excel_col, n_IMJ + 1);
%% Note that these sweep from 10 to 1000 Hz, so data should be taken in the

```

```

%%same direction.
%Conversion Factors used to calibrate acc1 in g
acc1_cf = load('CorrectionFactor_for_ACC1.mat');
acc1_cf_matrix = acc1_cf.output_matrix;
%Conversion Factors used to calibrate acc2 in g
acc2_cf = load('CorrectionFactor_for_ACC2.mat');
acc2_cf_matrix = acc2_cf.output_matrix;
%% Scrape the Data from excel into a 3D matrix
[meas_data_all] = scrapeExcel(file,n_sweeps,datapoints_per_sweep,num_APX_Inputs);
%% Calculations to convert the Volt readings to g, and use conversion factors
%First: masks data. Second: converts data
% This for loop masks data too close to the noise floor using the maskNoise
% function, and then multiplies each V reading by acc_V_to_g, then by its
% corresponding correction factor
for meas_ID2 = 1:[n_sweeps_minusNoise]
    %Use maskNoise to get a 2 D matrix
    [masked_meas_data_singlesweep] =
maskNoise(meas_data_all(:,acc1_reading_column,noise_sheet),meas_data_all(:,acc2_reading_c
olumn,noise_sheet),meas_data_all(:,meas_ID2+1),STN_ratio,acc1_reading_column,acc2_readi
ng_column);

    %Apply the conversion factors to the 2D matrix
    masked_meas_data_singlesweep(:,acc1_reading_column) =
(masked_meas_data_singlesweep(:,acc1_reading_column) .* acc1_cf_matrix(:,2)) *
acc_V_to_g;
    masked_meas_data_singlesweep(:,acc2_reading_column) =
(masked_meas_data_singlesweep(:,acc2_reading_column) .* acc2_cf_matrix(:,2)) *
acc_V_to_g;
    %Put the 2D matrix in the correct slot of the 3D matrix
    maskedANDcorrected_all(:,meas_ID2) = masked_meas_data_singlesweep;
end
%% Calculate the ratio of accelerometer readings
%Has n_sweeps -1 columns
acc2_over_acc1 =
maskedANDcorrected_all(:,acc2_reading_column,[1:n_sweeps_minusNoise])./(maskedANDcorr
ected_all(:,acc1_reading_column,[1:n_sweeps_minusNoise]));
%% Data Display
% This section plots
% close all;
% writematrix(output_matrix,[data_dir,'\',data_file],'Sheet','Correction Factors');

```

```

%
figure;
for line_index = 1:n_sweeps_minusNoise;
plot(maskedANDcorrected_all(:,1,line_index),acc2_over_acc1(:,line_index))
hold on;
end
set(gca,'xscale','log');
set(gca,'yscale','log');
title('Comparison of IMJs');
xlabel('Frequency [Hz]');
ylabel('ACC2/ACC1 [g/g]');
legend('IMJ 1','IMJ 2', 'IMJ 3', 'IMJ 4', 'IMJ 5');
hold off;

```

### Applied Load Code

```

%% Inputs
clc; clear all; close all;
%Folder housing the file
data_dir = 'C:\Users\Tommy\Desktop\MQP Stuff\Oct 5';
%File name
data_file = 'Oct 5 Load and No Load Sweeps.xlsx';
%combine full file name
file = [data_dir,'\',data_file];
%"Points" Specified in the APX Sweep
datapoints_per_sweep = 250;
%Number of analog inputs on the DAQ, and corresponding number of excel columns
num_APX_Inputs = 2;
excel_col = 2*num_APX_Inputs;
%Number of sweeps done in APX, and the number of sweeps not including the
%noise sweep
n_sweeps = 9;
trialsPerIMJ = 1;
n_sweeps_minusNoise = n_sweeps-1;
%The sheet of the excel file that contains the Noise data
noise_sheet = 1; %THERE IS AN ASSUMPTION LATER ON THAT THIS IS 1!!!
%STN Ratio Floor
STN_ratio = 10;
%These inputs specify which columns have the data for acc1, acc2, and
%frequency. Later on in the code will use these variables instead of actual
%numbers, so all of the inputs stay in the same place

```

```

acc1_reading_column = 2;
acc2_reading_column = 4;
Freq_reading_column = 1;
%Conversions used to bring acc to g
%Multiply acc by this number to convert it from Volts to g
acc_V_to_g = 3.03030303;
%Make a matrix now for efficiency
maskedANDcorrected_all = ones(datapoints_per_sweep,excel_col,n_sweeps_minusNoise);
%average_data = ones(datapoints_per_sweep,excel_col,n_IMJ + 1);
%% Note that these sweep from 10 to 1000 Hz, so data should be taken in the
%%same direction.
%Conversion Factors used to calibrate acc1 in g
acc1_cf = load('CorrectionFactor_for_ACC1.mat');
acc1_cf_matrix = acc1_cf.output_matrix;
%Conversion Factors used to calibrate acc2 in g
acc2_cf = load('CorrectionFactor_for_ACC2.mat');
acc2_cf_matrix = acc2_cf.output_matrix;
%% Scrape the Data from excel into a 3D matrix
[meas_data_all] = scrapeExcel(file,n_sweeps,datapoints_per_sweep,num_APX_Inputs);
%% Calculations to convert the Volt readings to g, and use conversion factors
%First: masks data. Second: converts data
% This for loop masks data too close to the noise floor using the maskNoise
% function, and then multiplies each V reading by acc_V_to_g, then by its
% corresponding correction factor
for meas_ID2 = 1:[n_sweeps_minusNoise]
    %Use maskNoise to get a 2 D matrix
    [masked_meas_data_singlesweep] =
maskNoise(meas_data_all(:,acc1_reading_column,noise_sheet),meas_data_all(:,acc2_reading_c
olumn,noise_sheet),meas_data_all(:,meas_ID2+1),STN_ratio,acc1_reading_column,acc2_readi
ng_column);

    %Apply the conversion factors to the 2D matrix
    masked_meas_data_singlesweep(:,acc1_reading_column) =
(masked_meas_data_singlesweep(:,acc1_reading_column) .* acc1_cf_matrix(:,2)) *
acc_V_to_g;
    masked_meas_data_singlesweep(:,acc2_reading_column) =
(masked_meas_data_singlesweep(:,acc2_reading_column) .* acc2_cf_matrix(:,2)) *
acc_V_to_g;
    %Put the 2D matrix in the correct slot of the 3D matrix
    maskedANDcorrected_all(:,meas_ID2) = masked_meas_data_singlesweep;

```

```

end
%%% Calculate the ratio of accelerometer readings
%Has n_sweeps -1 columns
acc2_over_acc1 =
maskedANDcorrected_all(:,acc2_reading_column,[1:n_sweeps_minusNoise])../maskedANDcorrected_all(:,acc1_reading_column,[1:n_sweeps_minusNoise]);
%%% Data Display
% This section plots
% close all;
% writematrix(output_matrix,[data_dir,'\',data_file],'Sheet','Correction Factors');
%
close all;
figure;
for line_index = 1:n_sweeps_minusNoise;
plot(maskedANDcorrected_all(:,1,line_index),acc2_over_acc1(:,line_index))
hold on;
end
set(gca,'xscale','log');
set(gca,'yscale','log');
title('Output/Input, in g');
xlabel('Frequency [Hz]');
ylabel('ACC2/ACC1 [g/g]');
legend();
hold off;
figure;
for line_index = 1:4;
plot(maskedANDcorrected_all(:,1,line_index),acc2_over_acc1(:,line_index))
hold on;
end
set(gca,'xscale','log');
set(gca,'yscale','log');
title('Output/Input, in g');
xlabel('Frequency [Hz]');
ylabel('ACC2/ACC1 [g/g]');
legend();
hold off;
figure
plot(maskedANDcorrected_all(:,1,1),acc2_over_acc1(:,1),maskedANDcorrected_all(:,1,1),acc2_over_acc1(:,2))
set(gca,'xscale','log');

```

```

set(gca,'yscale','log');
title('IMJ 1');
xlabel('Frequency [Hz]');
ylabel('ACC2/ACC1 [g/g]');
legend('No Load', '0.5N Load');
figure

```

```

plot(maskedANDcorrected_all(:,1,1),acc2_over_acc1(:,4),maskedANDcorrected_all(:,1,1),acc2_
over_acc1(:,3))

```

```

    set(gca,'xscale','log');
set(gca,'yscale','log');
title('IMJ 5');
xlabel('Frequency [Hz]');
ylabel('ACC2/ACC1 [g/g]');
legend('No Load', '0.5N Load');
figure

```

```

plot(maskedANDcorrected_all(:,1,1),acc2_over_acc1(:,5),maskedANDcorrected_all(:,1,1),acc2_
over_acc1(:,6))

```

```

    set(gca,'xscale','log');
set(gca,'yscale','log');
title('IMJ 1');
xlabel('Frequency [Hz]');
ylabel('ACC2/ACC1 [g/g]');
legend('No Load', '0.5N Load');
figure

```

```

plot(maskedANDcorrected_all(:,1,1),acc2_over_acc1(:,8),maskedANDcorrected_all(:,1,1),acc2_
over_acc1(:,7))

```

```

    set(gca,'xscale','log');
set(gca,'yscale','log');
title('IMJ 5');
xlabel('Frequency [Hz]');
ylabel('ACC2/ACC1 [g/g]');
legend('No Load', '0.5N Load');

```

## Appendix F - Calibration of Camera System

The two cameras in the camera system used in the stiffness testing were calibrated with three tests. The first test compared known lengths to lengths measured from the camera using a calibration grid (Figure F.1). The calibration grid contains squares with a width of 200 microns.

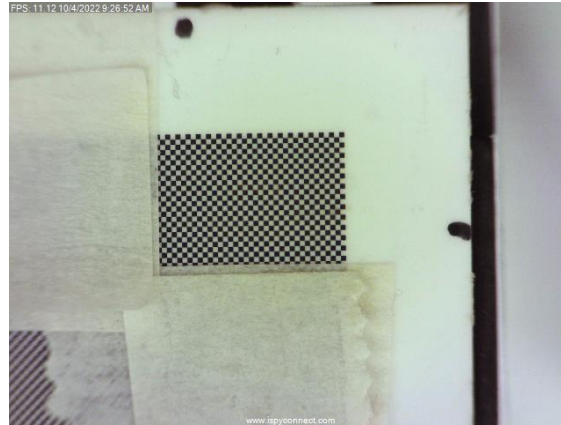


Figure F.1 Calibration Grid Photo Using USB Camera

In ImageJ, multiple boxes were measured to create a calibration curve that would compare the measured length to the actual length of the boxes. Table F.1 shows the data collection process for Test 1.

Table F.1: Data Collection for Test 1: Calibration Curve

Measure 1 ( $\mu\text{m}$ )	Measure 2 ( $\mu\text{m}$ )	Measure 3 ( $\mu\text{m}$ )	Measured Length ( $\mu\text{m}$ )	Actual Length ( $\mu\text{m}$ )
994.14	1002.55	998.36	998.35	1000
1195.47	1199.67	1203.88	1199.673333	1200
1396.83	1390.52	1400.51	1395.953333	1400
1597.89	1602.09	1593.83	1597.936667	1600
1795.24	1803.66	1799.47	1799.456667	1800
1996.36	2000.81	1994.53	1997.233333	2000



The results were plotted to create the calibration curve, which showed a slope of 1.0012 and  $R^2$  value of 1 (Figure F.2). This meant that the camera and ImageJ were yielding both accurate and precise lengths.

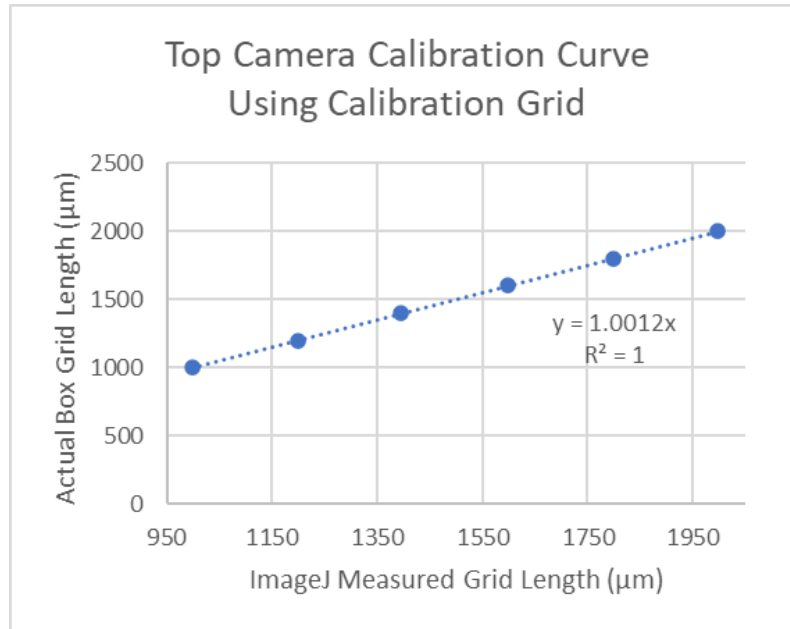


Figure F.2: Calibration Curve of Top Camera in Stiffness Testing System

The second test was a repetition test to determine human error in the camera and ImageJ measurements. One box was randomly selected from the center of the calibration grid, and measured multiple times. Each measurement was recorded, and then the average and standard deviation were calculated (Table F.2).

Table A.2: Data Collection for Test 2: Repetition

Box Width (μm) *one box selected randomly from center of grid	201.35
	199.24
	201.35
	202.09
	200.3
Avg.	200.866
St. Dev.	1.110283748

Margin of error was also calculated for this test using the equation:

$$\text{Margin of error} = z * \frac{\sigma}{\sqrt{n}}$$

where,

$z = 1.96$  (the z-score for a 95% confidence level)

$\sigma = \text{standard deviation}$

$n = \text{sample size}$

The resulting margin of error was:

$$\text{Margin of error} = 1.96 * \frac{1.11}{\sqrt{5}} = 0.964 \text{ microns}$$

The third test done was a variation test to see if the length of the boxes in the calibration grid changed depending on the location in the frame. This is because the edges of images sometimes stretch or distort due to the camera. Boxes in nine different locations on the calibration grid were measured and recorded (Table F.3). The average and standard deviation were also calculated.

Table F.3: Data Collection for Test 3: Location Variation

Box Location (x,y)	Box Width ( $\mu\text{m}$ )
Top Left	202.44
Top Middle	200.3
Top Right	201.34
Middle Left	199.26
Middle Middle	198.2
Middle Right	200.29
Bottom Left	200.29
Bottom Middle	198.2
Bottom Right	200.03
Avg. Width	200.0388889
St. Dev.	1.37032336